UNIVERSITÀ DI PAVIA

UNIVERSITÀ DEGLI STUDI DI BERGAMO

Doctoral Research in Economics and Management of Technology (DREAMT)

Innovation and Technology Management-XXXI cycle

μEDM sustainability: economical optimization and machinability of advanced materials

Supervisor: Prof. Giancarlo Maccarini

Co-Supervisor: Prof. Gianluca D'Urso

PhD. Student: Mariangela Quarto

Università di Pavia

Department of Economics and Management

Università degli Studi di Bergamo

Department of Management, Information and Production Engineering

DOCTORAL RESEARCH IN ECONOMICS AND MANAGEMENT OF TECHNOLOGY (DREAMT)

INNOVATION AND TECHNOLOGY MANAGEMENT

XXXI CYCLE

μEDM SUSTAINABILITY: ECONOMICAL OPTIMIZATION AND MACHINABILITY OF ADVANCED MATERIALS

School Director: Ch.mo Prof. GIANMARIA MARTINI

Tracks Coordinators: Ch.mo Prof. PAOLO GAIARDELLI
Ch.mo Prof. TOMMASO MINOLA

Supervisor: Ch.mo Prof. GIANCARLO MACCARINI

Co-Supervisor: Ch.mo Prof. GIANLUCA D'URSO

PhD Student: MARIAGELA QUARTO

If you knew what you were doing it wouldn't be called research

Einstein

AKNOWLEDGMENT

I want to thank my supervisor Prof. Giancarlo Maccarini, who played a central role in encouraging me to start the journey as PhD student. I am grateful because he believed in me and involved me in teaching and research activities of the Department. His trust in my competences as academic has been a great incentive that pushed to give my best in all what I did.

I express my gratitude to Prof. Gianluca D'Urso and Prof. Claudio Giardini, whom have represented a role model during these three years. More importantly, they transmitted to me the passion for research and were constantly available for feedbacks and brainstorming.

My sincere gratitude to Prof. Giuliano Bissacco and to the entire Section of Manufacturing Engineering for having hosted me and for the opportunity to increase my knowledge and expertise at the Technical University of Denmark.

I want to thank Prof. Chiara Ravasio, Doc. Sara Bocchi and all my co-authors from which I had the opportunity to learn and become a better researcher.

Many thanks also to the reviewers of this dissertation, Prof. Bigot and Ing. Fassi, who spent their time to read my research and provide me valuable feedbacks that helped me in improving the value of this work.

Prof Gianmaria Martini, coordinator of the Doctoral School is acknowledged for the help and advice.

Special thanks to all the UniBg laboratories staff I have worked with, and to all those with whom I have shared these three years. In general, I am grateful to the nice people met and with whom I shared these three years, in particular, to Chiara and Alice, who always gave me precious advice.

I would like to dedicate this work to my parents, for helping to make my higher education possible; furthermore, thanks to my sister Daniela. I would like, in conclusion, to express my thanks to Manuel for the strong motivation that he gave to me to always do my best.

ABSTRACT

The micro electrical discharge machining has a set of advantages that makes it commercially interesting, with potential for further developments in the future. In this sense, its application to new kind of materials and its optimization has been the focus of many researches. In this work, the micro-electrical discharge machining sustainability, from the economic point of view, related to the technological performances and its new application fields were analysed, focusing on both the challenges and limitations in high-quality products and the relationship between the economic aspects and the performances.

This research was divided into two parts. In the first one, a model and an index for the economic evaluation of the technologies and the process performance optimization were developed, correlating the process parameters to the process performances and the production costs. Specifically, a model cost completely dedicated to the estimation cost for μEDM was developed and its capability was verified by its application to two case studies. The cost index takes into account the performances and the costs correlating both of them to the process parameters and their optimization, minimizing the costs and maximizing the performances.

The second part of the research took into account the application of this process on a new promising class of advanced materials which are characterized by a huge range of applications in several fields and in critical environments. In particular, the ZrB2 – based composites doped with different SiC fractions were considered for this set of experiments. Once the machinability was verified, the model cost developed in the first part was applied.

The present work contributes to cover a literature gap about the economic aspects of this technology, and at the same time, to extend the state-of-the-art knowledge about the □EDM process and its application on advanced materials.

CONTENTS

LIST OF FIGURES

LIST OF TABLES

CHAPTER 1

Introduction to Micro Electrical Discharge Machining

1.1 Micro-manufacturing

The demand for products (macro and micro) and parts made of difficult to machine materials has been rapidly increasing; in particular, micro-components and parts are almost everywhere in our lives. During the last years, the applications of micro-parts have covered huge and differentiated application fields. The most relevant fields are related to the IT components such as inkjet printers and reading caps for hard disk, as well as medical and biomedical devices (pacemakers, analysis equipment, and sensors), aerospace, automotive, optics, electronics and communications applications. On the technological side, the development has moved very fast, led by the need of the electronic industries to produce still smaller chips characterized by still larger capacity. The miniaturization of parts could represent the next technological revolution [1,2], specifically, micro and nano-manufacturing technologies connected with silicon are relatively highly developed compared to the technologies used to manufacture metals, polymers, and ceramics [3]. Micro-manufacturing includes technologies, processes, equipment and organizational strategies for developing products characterized by at least two dimensions within sub-millimetre ranges. The term micro-manufacturing engineering includes relevant activities such as the chain of manufacturing micro-components, design, analysis, materials selection, processes, tools, machinery, and operational management methods. For all mechanical processes, to create an operational basis for mass production of micro-parts is a continuously increasing challenge. Product development and design of new parts are the core business of the companies and this includes the ability to understand and apply the capabilities

of micro and nano-technologies. These aspects enclose the ability to integrate, into the component development process, considerations regarding processes and materials, involving the development of new design principles and methodologies integrating the necessary skills. Micro and nano-components fabrication steps must be dealt with different approaches and these generate new challenges in design, production, handling, assembling, control and measurement phases. In fact, the main issues are not just about the downscaling of the existing production technologies and procedures but, in some cases, the development of a completely new process or the replacement of conventional technology is necessary. Since the micro-parts are introduced to large markets and mass production, the development and improvement of materials and processes are necessary, since some micro and nano-technologies still lack maturity.

1.1.1 Micro – products definitions

In some works, about the micro-technology, different definitions of the micro concept were applied. In 2000, Masuzawa T. [4] provided an overview of the state-of-the-art in micro-machining, the paper aimed to discuss micro-machining of structures with dimensions less than 500 pm; Corbett J. et al. [5] defined nano-technology and thereby the goal of the investigation to be "the study, development and processing of materials, devices, and systems in which structures on a dimension of less than 100 nm is essential to obtain the required functional performance". In 2001, Geiger M. et al. [6] described forming technologies applied to "the production of parts or structures with at least two dimensions in the submillimetre range". Other works do not focus on the definition of micro-technologies, but use the fabrication of micro-electromechanical systems (MEMS) to describe different problems connected to the technologies; in fact, Van Brussel H. et al. [7] in 2000 described the micro-assembly and MacGeough J.A. et al [8] in 2001 introduced the use of electroforming processes for the production of micro-products. In all the above-mentioned papers the discipline of "moving borders" in terms of achievable dimensions, accuracy or surface texture is emphasized. All of them deal with the issues emerging from downscaling conventional processes and

materials and they discuss possible solutions to these problems. It is difficult to give an exact definition of micro-component which seems to be related only to the size in a rapidly changing environment. Of course, micro-products are characterized by small dimensions, either of the product itself or of functional features or structures on the product. This viewpoint makes a clear-cut definition hard since features by nature can be one or more orders of magnitude smaller than the dimensions of the products. In this respect the obtainable manufacturing accuracy is important and often this is the limiting factor. It is often only possible to move this limit downwards by choosing alternative manufacturing strategies.

1.1.2 Micro – products characteristics

From a geometrical point of view micro-products can be organised into two groups based on the number of dimensions (Figure 1.1):

- 2½D structures. For example, fluid sensors;
- 3D structures. For example, components for hearing aids.

Figure 1.1. Example of parts with different dimensions number.

The geometry affects the possible manufacturing processes and the associated production support activity such as handling, quality check, and assembly. Another important characteristic of micro-products is related to different shades of the integration concept: integration of functions, integration of different operation principles (physical, chemical, biological) and integration of intelligence into products in terms of information processing and control (sensors and actuators). A look into the reason of miniaturization has to be considered, in particular for the functionality of the products, to identify products that need to be small for reaching a more compact volume and those products whose functionality is achievable only

in virtue of their small dimensions. Micro-products are usually composed of several components assembled in order to obtain the required functionality: it is simple to distinguish between micro-product and micro-component. The realization of a micro-product requires miniaturization of the constituting components creating challenges in terms of handling and assembly of components into a product and therefore the integration of different functions is desirable to fulfil different goals by the same product. For this purpose, specific mechanical, electrical, thermal, and chemical material properties are required in order to achieve the required performances.

1.1.3 Micro – products processes

In micro-product development, principles and methodologies considering functionality as well as manufacturability for designing is the key area of interest, and at the same time, the micro-engineering aims to develop and manufacture micro-products in general. The industrial mass production of micro-products is a key goal; many micro-products have successfully been developed as prototypes using expensive techniques suitable only for prototyping, but most of the times the mass production is delayed due to the difficulty in developing a sustainable manufacturing process. In fact, developing a micro-product is not only a matter of downscaling a macro product and/or process, but it is a question of a different way of thinking using different principles and methodologies, then the relationship between product design and production system design must be properly considered. Discuss the entire process chain for the development and manufacture of micro-products can be very useful because it considers all the aspects of the industrialization of a product. Masuzawa T. [4] introduced a description of the relationship among technologies and objects in production (Figure 1.2) showing the process chain for the development and manufacture of products. Materials, components, and products are defined as physical objects whereas design, processing, assembly, and control measurement are defined as technologies. The process chain opens up the possibility to discuss specific characteristics of each

technology and each physical object. The connection of each step of the process chain into a continuous flow is one of the main challenges in micro-engineering.

There is a huge diversity in micro-products, the main types being micro-electronics products, micro-optical electronics systems (MOES), micro-electronic mechanical systems (MEMS) and micro-optical electronics mechanical systems (MOEMS), correlated to the combination of product functionalities and applications. There are different technologies and strategies which could be used to manufacture micro-parts and the increased demand for micro-products has led to rapid development of other technologies for micro-manufacturing of individual parts, following the paths of downscale existing manufacturing processes or develop new processes in the cross field of existing technologies. Although on the technological side the development has moved very fast, it is a continuous challenge to create the operational basis for industrial production of micro-products; in particular process reliability and stability must be targeted for the design for micro-manufacturing.

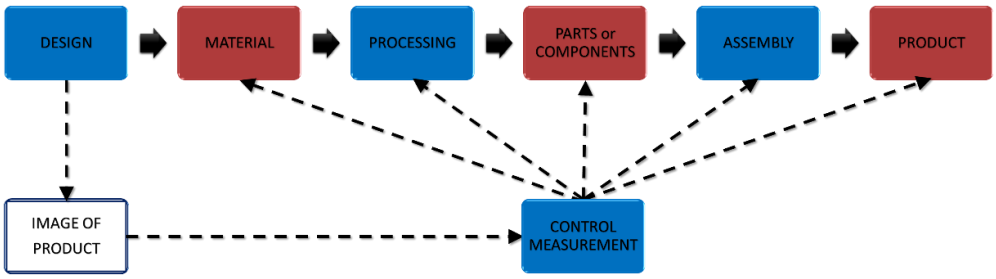

Figure 1.2. The relationship between technologies and objects [4].

1.1.4 Micro-processes gap

The current market requirements, both in terms of advanced materials and high performances, represent a challenge for both the industries and the manufacturing processes. To meet these challenges new processes with advanced methodologies and tooling need to be developed. The conventional machining of such advanced requirements is often difficult due to the improved of material characteristics, the downsizing of the components and of the products and the high quality. Conventional machining such as turning, milling and drilling show inefficiencies,

since it results in poor material removal rate, excessive tool wear, poor product quality and increased surface roughness. On the other side, non-conventional machining processes can be an optimal solution for the manufacturing of complex micro-parts and advanced materials. These processes are classified according to the type of energy used for removing material from the workpiece (Figure 1.3). Among these non-conventional processes, the Electrical Discharge Machining (EDM), classified as a thermal material removal process, has firmly established its use in the production of forming tools, dies, mould and devices characterized by complex shapes.

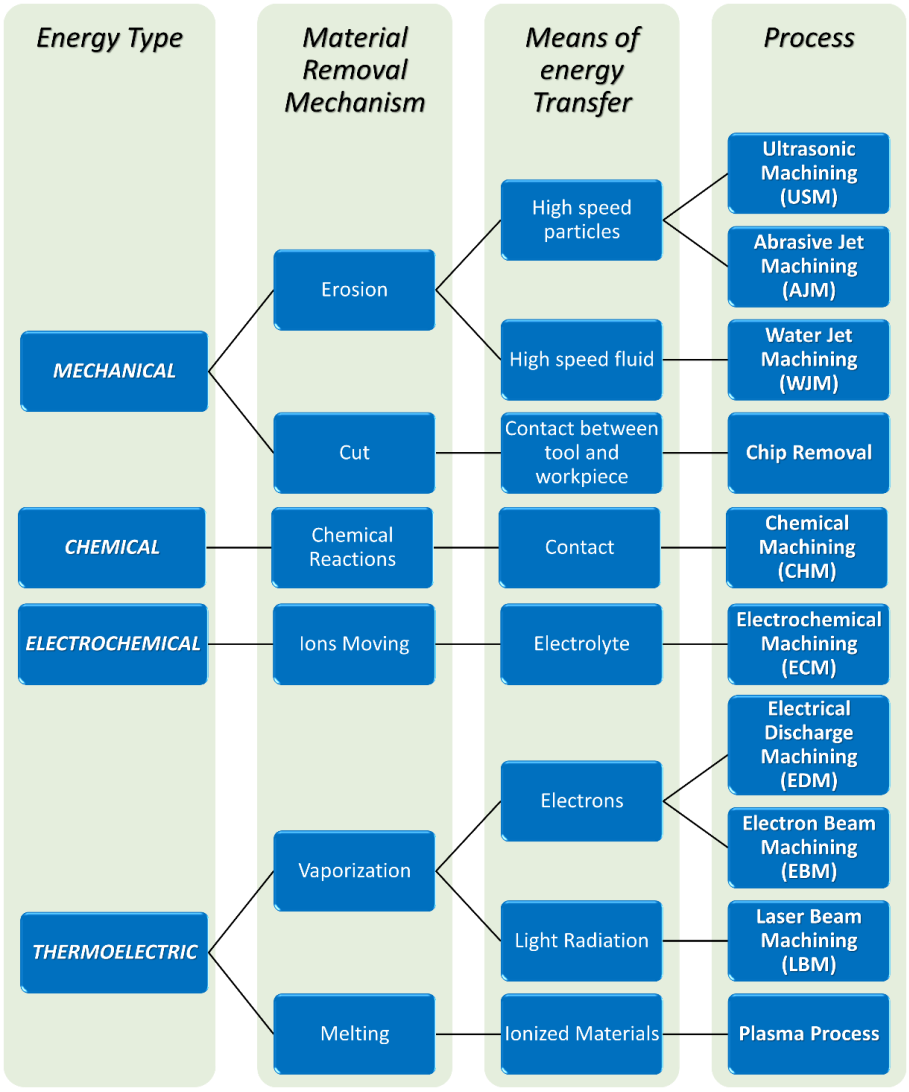

Figure 1.3. Classification of machining processes according to the energy type.

1.1.5 Issues of design and fabrication

High volume production of micro-components should be a target for micro-manufacturing design. Designing these products, not only functional requirements need to be considered but also micro- manufacturing related factors will have to be taken into account. Typical issues at the design stage are summarized as follow:

- Overall dimensions of the parts (e.g. diameters, widths, lengths and thicknesses): are very much constrained by the overall capabilities of the processes and manufacturing facilities (machines, handling devices, tool, etc.). Both maximum and minimum dimensions are parameters that need to be checked with reference to the manufacturing system capabilities. Complexity around dimensional scale issues is a dominant factor in micro-manufacturing.

- Design of local features (e.g. hole, pocket, dimensions of channels, wall thickness, area reductions, density of the local features): are largely constrained by the processing, especially those relying on the use of tools such as replicating processes. Manufacture of local features spread over a large area also renders challenges to many micro-manufacturing processes and equipment.

- Shape capability: considers the capability/limitation of a manufacturing process in dealing with the shapes to be produced. Conventional rules on shape capability of manufacturing may not be applicable to micro-manufacturing largely due to the sizes to be considered and limitation of the tool shapes that could be produced.

- Tolerance and surface quality capability: data about the manufacturing tolerances for design for micro-manufacturing are not defined by standards but most of the data is inhouse determined.

- Material capability: material for micro-manufacturing will be constrained largely by the availability of the material for volume

production, due to the limited number of the suppliers currently operating in this field. New studies about the material properties may be needed if the material suppliers are not able to provide the material data relevant to micro-manufacturing, such as size effects and material property descriptions. The properties will have to be qualified for design uses, with consideration of size effects, and these have to be available with the inclusion of mechanical, thermal, electrical and magnetic properties.

The design of micro-products is still a challenging task due to lack of sufficient standards, design and manufacturing rules and understanding of the manufacturing process themselves. Compared to the manufacture of macro-products, manufacturing methods and strategies in micro-manufacturing may be different. Macro-products may be carried out by manufacturing individual parts by removing and/or deforming and/or adding materials and then assembling them. These can be carried out either at a single industrial site or at different sites. Manufacturing micro-products may be carried out with patterning, deposition and layering methods within a single manufacturing platform (e.g. integrating components/parts fabrication with assembly/packaging is often used in MEMS and micro-systems manufacturing). Micro-manufacturing largely uses non-conventional manufacturing methods or scaling down or modifying the traditional methods, as appropriate, to fully address issues related to micro-manufacturing. Moreover, the increased demand for micro-products has led to rapid development of other technologies for micro-manufacturing of individual parts and systems, following the paths of downscale existing manufacturing processes or develop new processes in the cross field of existing technologies. Although on the technological side the development has moved very fast, it is a continuous challenge to create the operational basis for industrial production of micro products, process reliability and stability must be targeted for the design for micro-manufacturing. In recent years non-conventional techniques, such as electrical discharge machining, have been adapted for the necessities of micro-components fabrication. Electrical discharge

machining is a process technology that has been well established in the production of complex shape parts in the macro dimensional range. Parts fabricated by μEDM are characterized by high value added.

1.2 Electrical Discharge Machining

Electrical Discharge Machining (EDM) is one of the widely used non-conventional material removal processes. Precise machining can be done on electrically conductive and semiconductive materials using this contactless process. EDM is used to drill circular and non-circular holes, to mill profiles and make complex shapes dies. It is an electro-thermal process where the material is removed from the workpiece by means of a series of periodic electrical discharges, created by electric pulse generators in micro-seconds, generated in the gap between two electrodes. One electrode represents the electrode-tool while the second one is the workpiece [9]. The gap is filled by dielectric fluid, usually formed by hydrocarbon oil, which becomes locally ionised at the point where the spark gap is the narrowest [10]. The basis of EDM can be traced back to 1770 when the English chemist Josep Priestly discovered the erosive effect of the electrical discharges. However, the process was developed only by the end of the 1940s by Russian scientists Boris and Natalya Lazarenko at the Moscow University. The Soviet government assigned to them an investigation about the wear caused by sparking between tungsten electrical contacts, a very critical problem for maintenance of automotive engines during the Second World War. Putting electrodes in the oil, they found that the sparks were more uniform and predictable than in the air. In this way, they had the idea to reverse the phenomenon and use controlled discharges as an erosion method [11]. They developed a controlled process for machining difficult-to-cut metals by vaporizing the material itself from the workpiece surface. In the 1950s, progress was made in understanding the erosion method and industries produced the first EDM machine. At that time, the poor quality of electronic components represented a limitation for the application of this kind of machine and process. In the 1960s, the great development of semiconductor industry, the advent of computer numerical

control (CNC) and more powerful and sophisticated generators based on transistors, allowed to increase the interest toward this technology improving the efficiency of the machining operation. CNC has facilitated the development and the use of EDM permitting automatic and unattended processes. These growing merits of EDM have since then been intensely sought by manufacturing industries, yielding enormous economic benefits, generating keen research interests and allowing to consider it an attractive solution for the manufacturing of several types of products [12,13].

1.3 Material Removal Mechanism

The erosion mechanism in EDM is a very complex phenomenon and involves many physical processes; for this reason, the exact physical phenomenon taking place in the gap between the electrode-tool and the workpiece continues to be a topic of research [9,14]. In general, simulation of the process reveals that the material removal mechanism can be explained in two ways: one by vaporization of material and the other by the bubble explosion of superheated material. A more accurate description of the removal process asserts that, first of all, the material removal mechanism makes use of electrical energy and turns it into thermal energy through a series of discrete discharges occurring inside the small gap between the electrode-tool and the workpiece immersed in a dielectric medium (Figure 1.4).

The thermal energy generates a plasma channel between the cathode and the anode at a temperature in the range of 8,000°C to 12,000°C. When the current supply occurring with a frequency approximately equal to 15 – 30 kHz is turned off and the plasma channel breaks down. This phenomenon causes a rapid reduction of the temperature allowing the dielectric fluid to flush away the molten material from the machined area in form of small particles named debris. Modification of the main process parameters (voltage, peak current, frequency and duty cycle) of the generator, connected to anode and cathode to rule the process, allows controlling the process performances such as the surface roughness, the erosion speed and the general accuracy of the machining [11,15]. The gap between the electrode-tool and the workpiece is filled by a dielectric fluid which, during the removal process,

achieves stable performance, ensuring a constant dielectric resistance, reducing the temperature near the worked areas and washing away the debris [16,17].

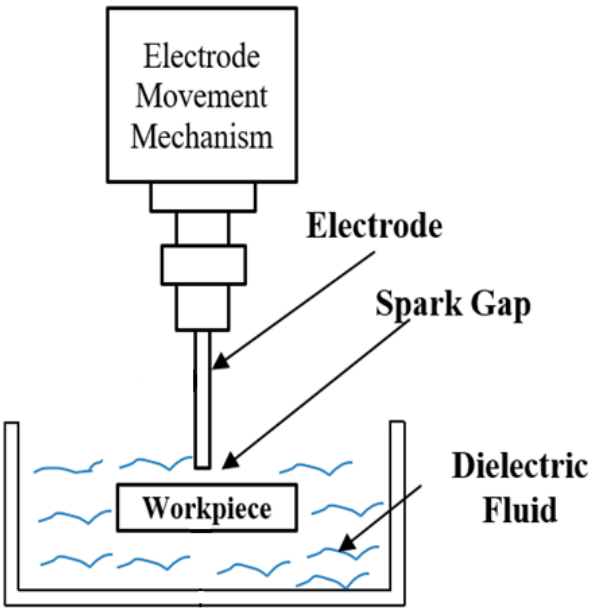

Figure 1.4. Schematic representation of EDM technology.

The electrical discharges material removal process (Figure 1.5) can be divided into three main phases [14]:

- Preparation phase for discharge;
- Phase of discharge;
- Interval phase between discharges.

The potential difference applied between the electrodes by the generator induces an electromagnetic field inside the gap and it reaches the highest strength in the area, where electrode-tool and workpiece surfaces are closest. The high speed of the debris generated during the machining is enough to form numerous particles that bridge continuously the gap between the electrode-tool and the workpiece [18]. The presence of debris in this area increases the probability of dielectric breakdown [19], so ionization begins and small particles start to evaporate. This phase

anticipates the discharge. At this point, the sparks occur and plasma channel increases its intensity until it reaches an equilibrium.

The first plasma channel has to become developed in the position where the electrode is closer to the workpiece. The result is a great increment of the pressure inside the channel creating also a shock wave distribution within the liquid. The electrical energy transferred from the anode to the cathode through the sparking gap is converted into thermal energy, causing a great increment of temperature to both parts, then the material of both electrodes melts and vaporizes.

As the electron-processes show quicker reaction, the anode material is most affected. This effect causes minimum wear to the electrode-tool and becomes of importance under finishing operations (short pulses). When the discharge is ended by switching off the generator, the plasma channel de-ionises quickly; in this phase pressure and temperature decrease in the plasma channel. The gas bubble, however, stays a quite long time in position and the pressure on the molten material decreases, so it starts to boil and particles are ejected from the machined area; these, once in contact with the dielectric, are shocked hardened. Once the concentration of debris particles around the previous discharge crater and the dielectric breakdown strength are recovered, the generator can be turned on and the discharge procedure is repeated in a different location. The driving force that promotes the discharge movement outside the previously discharged channel, all around the sparking gap, is essential for precision EDM and is defined as spark mobility [14]. In general, high sparks mobility allows obtaining uniform surfaces and high process performance, while low sparks mobility generates surface deterioration and unstable process performances. Surface roughness, concentration of debris, gap, dielectric strength and pulse-off time influence the sparks mobility. On both electrode-tool and workpiece surface, each spark generates discharge craters typical characteristic of this mechanical process. The final shape of the crater is characterized by a depression with edges that are elevated above the raw surface. Protruding borders are formed when the molten material is kept in place under plasma pressure and re-solidifying immediately until the plasma collapses and the

molten metal is violently expelled from the crater [20]. The disposition and dimensions of these craters can be used, to define the resulting surface roughness by calculation derived from the crater shape and distance.

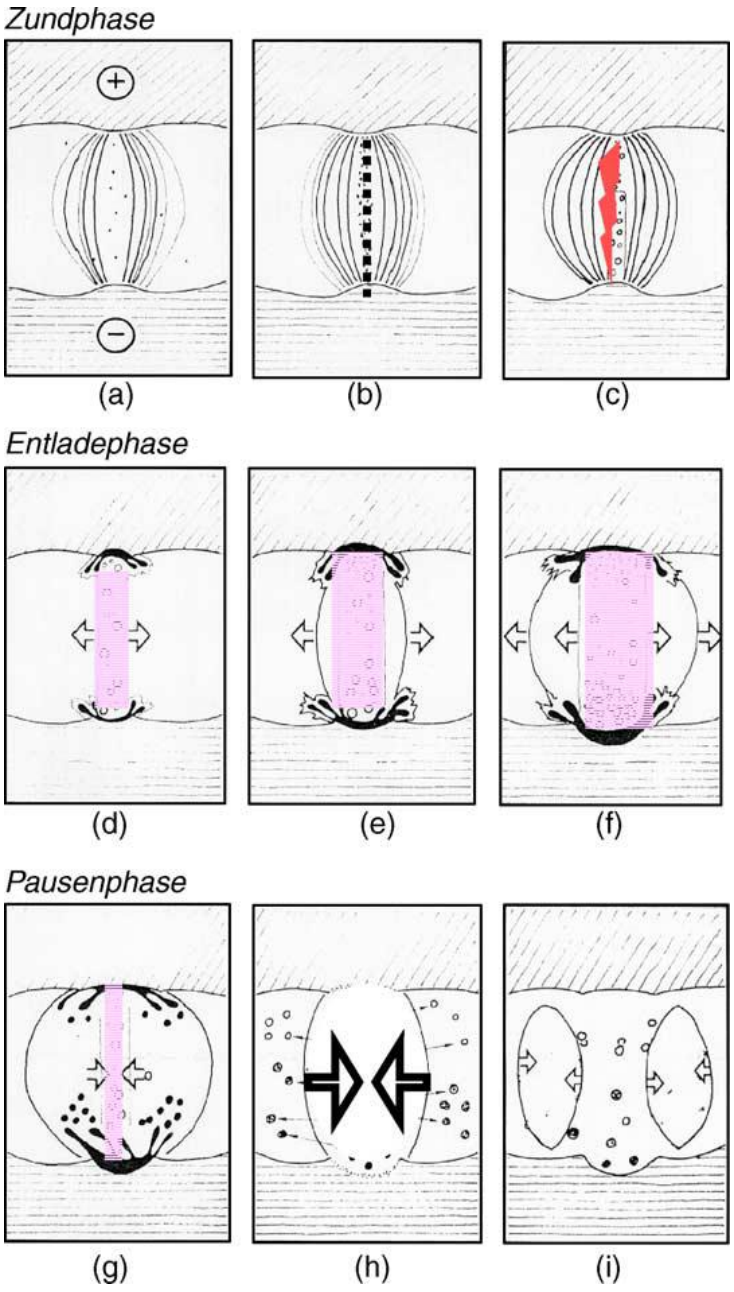

Figure 1.5. Phases of electrical discharges [14].

1.4 Main configurations

Micro-EDM and Macro-EDM are characterized by the same complex physical phenomenon responsible for material removal. The main difference between these configurations is the dimension of the plasma channel generated while discharges occur. In macro-EDM, the plasma channel dimension is several orders of magnitude higher than the one developed in μEDM; then there is a great difference in the value of energy [21,22]. Another important difference between these two configurations is the electrode dimension: for μEDM the electrode diameter range is between 0.5 mm and 0.005 mm. Both Micro and Macro-EDM can be performed in different configurations [23,24].

- Wire-EDM [25]. A thin wire with a diameter typically between 0.3 mm and 0.2 mm is tensed between two spoons and it is used as electrode-tool to remove the material from the workpiece. The wire is continuously regenerated; thus, the effects of tool wear are negligible. This technique allows to machine complex profiles with a high aspect ratio.

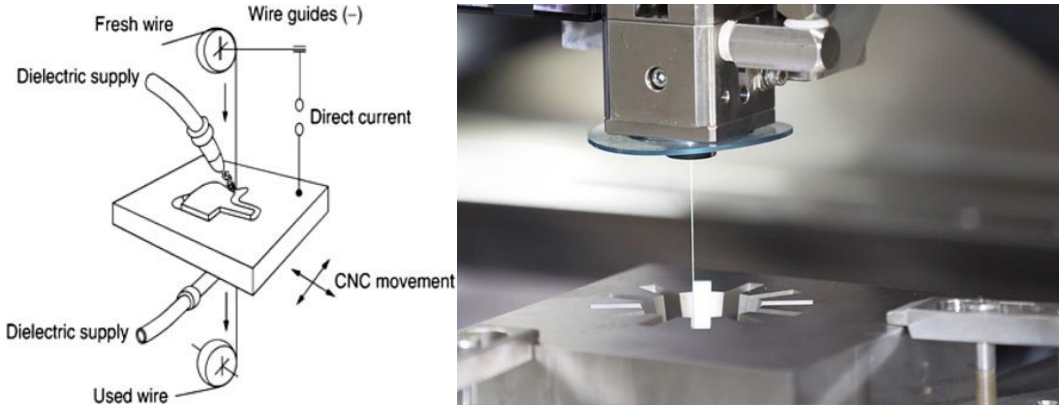

Figure 1.6. Schematic representation of Wire EDM and a machining example.

- Die-Sinking EDM [26]. The electrode-tool is characterized by the negative shape of the feature to be carried out. It is moved towards the workpiece surface immersed in a dielectric fluid along the Z axis. In the

end, the shape of the electrode-tool is replicated on the workpiece. In this case, the electrode-tool can be produced by LIGA process or by laser ablation machining, usually in copper or graphite. If the geometry is not too complex another solution for the production is the Wire-EDM. Sinking EDM is widely used to produce mould and the countering of simple shapes.

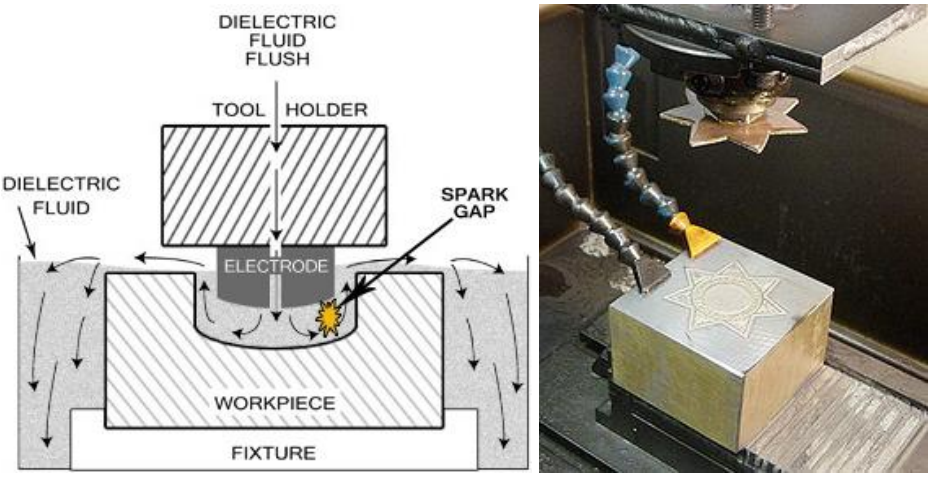

Figure 1.7. Schematic representation of EDM drilling and an example of a machined feature.

- EDM Drilling. [27]. It is performed by means of a rod electrode-tool that is rotating and moving along the Z-axis in order to produce a hole in the workpiece. High aspect ratio micro-holes can be machined by flushing the high-pressure dielectric fluid through a tubular electrode to remove the debris from the internal of the cavity.

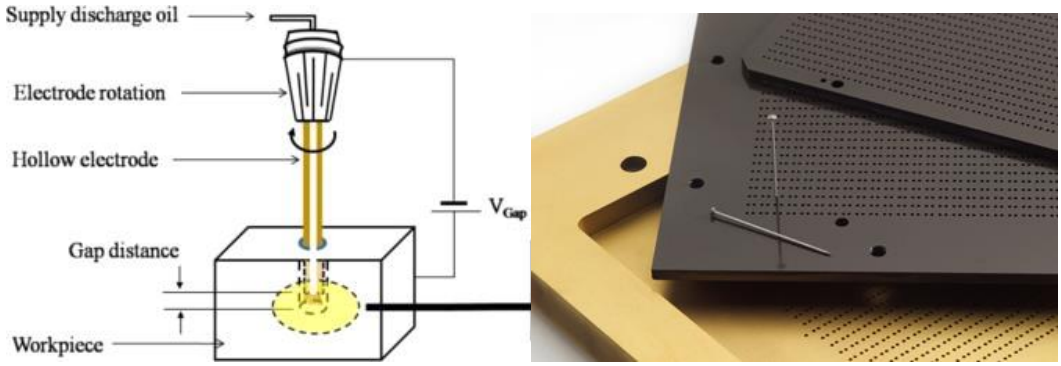

Figure 1.8. Schematic representation of EDM drilling and an example of machined holes.

- EDM Milling [28,29]. It is used to machine features on the workpiece surface such as pocket, channel, 3D complex shape and to improve surface finishing. It uses a single electrode with a variable diameter ranging from few microns (μEDM) to dozens of millimetres and a standardized cylindrical configuration characterized by a constant rotation to generate axisymmetric electrode wear. The material is removed layer-by-layer with a layer thickness as low as 0.1 μm. This method is based on the stabilization of the tool wear phenomenon after the machining of a few layers. Micro features having complex 3D shape and high accuracy machining can be achieved by implementing tool wear compensation strategies.

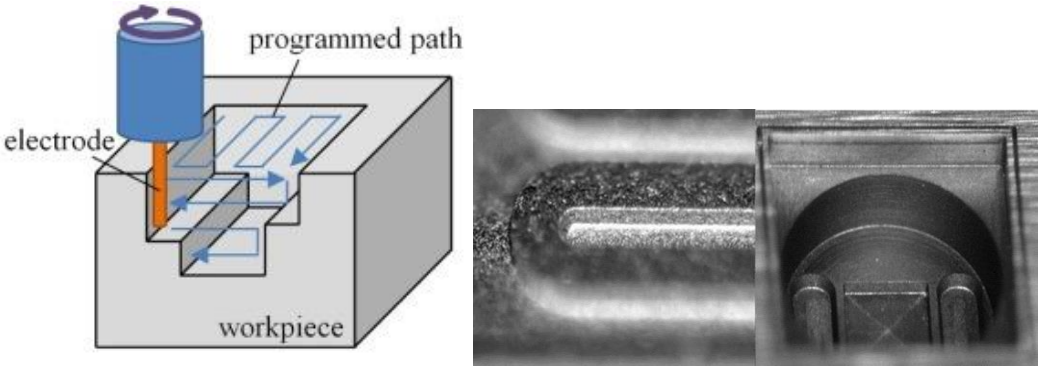

Figure 1.9. Schematic representation of EDM milling and an example of machined features.

1.5 Micro-EDM

The trend in reducing the size of products has given to μEDM a significant amount of research attention, it is an example of the adaptation of an existent technology to the new requirements of the market. μEDM is a contactless process representing a valid alternative machining process for the production of micro-components [12].

Given the lack of contact between the electrode and the workpiece, there are no mechanical vibrations and the forces exerted during the material removal process on the two parts are very small and these aspects allow to produce 3D complex

shapes micro-feature [23,30,31]. This is different from mechanical drilling, which allows producing holes just up to 70 μm, or the micro-laser machining, which can only create holes as small as 1 μm [4]. In some works [28,32,33], several attempts producing micro-parts such as micro-pins, micro-nozzles and micro-cavities using μEDM were performed. In addition, a feasibility study of applying μEDM as an alternative method for producing photo-masks for integrated circuit (IC) industry has been conducted [34].

In order to machine micro-components by μEDM process, it is necessary to increase the accuracy and the resolution of the process in terms of surface roughness and minimum machinable feature size. To achieve this purpose, it is necessary to reduce the minimum amount of material removed per single electrical discharge, which is proportional to the discharge energy [1,21]. To improve the efficiency of the machining, Han et al. applied to the machine a transistor type iso-pulse generator and demonstrated that further improvements can be achieved by implementing a servo feed control [23]. However, iso-energetic generators are still under development, and in commercial μEDM machines relaxation type generators based on RC circuits are used to provide very short and low energy discharge pulses.

Main process parameters applied in μEDM are the same as macro-EDM because the μEDM process characteristics are very similar to that of the macro process. The main difference between macro and micro EDM is the plasma channel radius which can be controlled by the pulse duration. In μEDM, the process is complicated by the electrode-tool heating; in fact, the electrode is very small, thus it has not a large mass which allows dispersing the heat from the location of the electrical discharge. This limits the amount of energy that can be supplied to a single discharge, and consequently, the material removal rate. This aspect must not be absolutely considered a process restriction, rather it is considered an advantage because it allows improving the results in terms of surface finishing and precision of the machined parts. The effect of the dielectric flush force on the electrode is more significant in the μEDM process since the electrode is much more susceptible

to deflection. Somehow, all these aspects are affected by the process parameters and their optimization is one of the main issues investigated in the last years, in particular, because of the complexity of physical and chemical phenomena taking place during the removal process.

1.5.1 Main process parameters

In general, the electrical discharges generated during the material removal process can be classified based on their duration and this time interval is directly correlated to the main electrical process parameters.

- Gap. It represents the distance between the electrode-tool and workpiece during the removal process. To obtain good performance and gap stability a suitable gap should be maintained. For the reaction speed, it must obtain a high speed so that it can respond to short circuits or even open gap circuits. Gap width is not measured directly but can be inferred from the average gap voltage [35].

- Voltage (V). It is related to the electrode materials, the working gap (distance between electrode-tool and workpiece) and the stiffness of the dielectric medium.

- Peak current (I). It is proportional to the energy index selected on the machine, and it represents the most influent parameter. With the other parameters kept constant, the variation in the current affects the quantity of material removed from the workpiece. Increasing the peak current generates an increment in the energy transferred per discharge, so the dimensions of the crater generated on the surface increases.

- Width (t_{on}). It is the pulse duration of time (measured in micro-seconds). In this time period, the generator allows the transfer of power from the electrode-tool to the workpiece within a short gap called spark gap. The material removal is directly proportional to the amount of energy applied during the discharge. Material removal rate depends on the

longer or shorter pulse on time period. Longer pulse duration improves debris removal rate from the area affected by the machining which also effects on the electrode-tool wear. The resulting crater produced will be broader as a comparison to the shorter pulse on time. But, in some experimental research work, it has been proved that optimal pulse duration gives higher performance measures [36].

- Frequency (F). It represents the number of complete cycles in 1s. Together with the width regulates the numbers of pulses and the aggressiveness of the process.

1.5.2 Characterization of the process

Process performances optimization as a function of process parameters is one of the most investigated issues. In literature, many studies aim to identify which and how the process parameters influenced the process performances indicators. The typical indicators taken into account for the performance evaluation are related to the machining speed and the tool wear. In general, these two indicators increase when high energy is transferred to the surfaces by a single discharge, developing greater and wider craters. The process performances are evaluated by two main quantitative indicators:

- Material Removal Rate (MRR). It indicates the machining speed in terms of material removed from the workpiece in a unit of time. It is defined as the volume [mm^3] of material removed from the workpiece, divided by the machining time [min or s]. The volume of material removed from the workpiece can be estimated on the base of the difference in weight (or volume) of the workpiece measured before and after the machining.

$$MRR = \frac{Volume\ removed\ from\ workpiece}{Machining\ time} \qquad \text{Eq. 1.1}$$

In general, MRR is influenced by the process parameters set up for the machining, in particular, it is strictly related to the width of peak current and its intensity because of the characteristics of the discharges affect the quantity of energy transferred the surface. Increasing the duration and the intensity of the current, the MRR increase its value. The same effect is generated by the increment of the frequency of discharges and the voltage. Usually in μEDM the value of MRR very in a range of tens of μm^3.

In 2007 Son S.M. et al. [37] investigated the influences of pulse condition on the μEDM properties. Voltage, peak current, and width of the pulse were selected as experimental parameters based on a simple equation for the material removal rate. The analysis of experimental results was attempted on the basis of the principal electric theories. The pulse condition is particularly focused on the pulse duration and the ratio of off-time to on-time and the machining properties are reported on tool wear, material removal rate, and machining accuracy. The experimental results show that the process parameters considered in that investigation are the main parameters to make a decision about the material removal rate. In particular, the voltage and current of the pulse exert strongly to the machining properties and the shorter EDM pulse is more efficient to make a precision part with a higher material removal rate. Comparatively, shorter width of the discharges facilitates the accuracy of the machining with a lower tool wear ratio. Sundaram M. et al. [38] presented an investigation on the optimization of machining parameters on MRR and tool wear in ultrasonic assisted μEDM by using Taguchi's design of experiments. The significance of selected parameters (capacitance, percentage of peak power vibration, feed rate and machining time) on MRR and tool wear is determined by using analysis of variance. Based on this analysis, the combination of the percentage of peak power vibration and capacitance was found to be significant for

improving MRR. In general, the integration within the ultrasonic vibration generates a significant increment in MRR. In 2009, Jahan M.P. et al. [39] conducted an investigation aimed for obtaining fine surface finish of WC using tungsten (W), copper tungsten (CuW) and silver tungsten (AgW) electrodes. The effect of different operating parameters in addition to electrode material properties on the finishing μEDM of WC, and a comparative study on the performance of W, CuW and AgW electrodes for the finishing of WC were investigated. It was found that the surface characteristics are dependent mostly on the discharge energy during machining. The fine-finish requires minimization of the pulse energy supplied into the gap. In addition, the surface finish was found to be influenced greatly by the electrical and thermal properties of the electrode material. The performance of the electrodes for the finishing was evaluated based on the achieved surface roughness and surface characteristics with respect to material removal rate (MRR) and electrode wear ratio (EWR). It was found that AgW electrode produces smoother and defect-free nano-surface with the higher surface quality among the three electrodes. Besides, a minimum amount of material migrates from the AgW electrode to the WC workpiece during the finishing. On the other hand, CuW electrodes achieved the highest MRR followed by AgW. In 2010, Jahan et al. M.P. [40] investigated the feasibility of machining deep micro-holes on two difficult-to-cut materials (cemented carbide WC-Co and austenitic stainless steel SUS 304) by μEDM drilling considering also the effect of discharge energy and electro-thermal material properties on the performance. The μEDM drilling performance of two materials has been assessed based on the quality and accuracy of the produced micro-holes, machining stability, material removal rate (MRR), and electrode wear ratio. The results show that deep-hole μEDM drilling is technically more feasible in WC-Co as it offers micro-holes with smooth and burr-free surfaces at the edge in

addition to improved circularity and lowers overcut than those provided by SUS 304. The results of this work show that the WC-Co is preferable to SUS 304.

- Tool Wear Ratio (TWR). It represents the tool wear compared to the material removed from the workpiece. It is defined as the ratio of the amount of electrode-tool wear to the amount of material removed from the workpiece. There are four methods usually used to measure the electrode-tool wear, by means of measuring length, total volume, weight, and shape.

$$TWR = \frac{Volume\ of\ tool\ wear}{Volume\ removed\ from\ workpiece} \qquad \text{Eq. 1.2}$$

As has been previously reported for the MRR, also the TWR is affected in the same way by the main process parameters. So long pulses generate higher wear for the tool during the machining. The difference is that the electrode wear is also strictly related to the materials applied for the workpiece and the electrode, in particular to their electro-thermal characteristics, in fact, in general, the brass electrode is characterized by very high wear in comparison to the tungsten carbide one.

Yu Z.Y. et al. [41] in 2004 developed a uniform wear method integrated with CAD/CAM software to generate 3D microcavities. They found that this method compensates the electrode-tool wear and helps in regaining the electrode-tool shape during the machining and maintaining the desired spark gap. Uhlmann E. et al. [42] investigated the reduction of electrode-tool wear in μEDM using new electrode materials. the results showed that new materials such as electrically conductive boron doped CVD diamond (B-CVD) and polycrystalline diamond (PCD) can be used looking for the diamond stability with electrical discharge

environment. Pham D. et. al. [43] in 2007 studied the influence of factors contributing to electrode wear during the process, proposing a method for calculating the volumetric wear ratio based only on geometrical information obtained from the process. The aim of the work is the investigation of the suitability for μEDM electrode wear compensation methods. Electrode shape deformation and random variations in the volumetric wear were studied as two main factors affecting the applicability of wear compensation methods as well as indicating the accuracy achievable with μEDM. The results show that variations of the wear ratio due to uncontrolled factors are not negligible, and this does not allow the use of compensation methods relying on the ratio staying fixed. When machining soft materials like brass and aluminium, machining strategies that ensure good flushing, should be adopted to avoid side sparking on the electrode. In cases where flushing becomes an issue, such as for drilling small holes, steel is a preferred material because it is less affected by the flushing conditions. In 2011, G. Bissacco et al. [44] proposed and investigated the applicability of real-time wear compensation in μEDM milling based on the possibility of characterizing the EDM discharges in terms of the statistical distribution of the population rather than individually. Experiments were performed involving discharge counting and electrode wear measurement in a wide range of process parameters settings involving different current pulse shapes. Based on the experimental evidence, it was demonstrated that the tool electrode wear can be effectively compensated on the basis of discharge counting without the implementation of a pulse discrimination system. In 2016 Surleraux A. et al. [45] developed a geometrical simulation method with the final objective of optimizing the initial shape of the tool by adding material on it to counteract the effects of tool wear. In order to do so, the simulation must be fast considering that the optimization method is likely to require at least several iterations.

Actually, in a later stage, this method will take part in a shape optimization process where tens of simulations will be performed. Tsai Y. and Masuzawa T. in 2004 [46] and then D'Urso G. and Ravasio C. in 2017 [47] experimentally investigated the electrode-tool wears of various materials in μEDM and developed an index to correlate the process performances and the process parameters taking into account electrode-tool and workpiece materials characteristics. They found that the volumetric wear ratio of the electrode-tool becomes small for the electrode-tool material with a high boiling point, melting point, and thermal conductivity. This tendency is independent of the workpiece materials. Corner wear of electrode relates to diffusion of heat. The corner rounding is more obvious when the thermal conductivity of the electrode-tool is low. Another important aspect in wear mechanism is related to the role of the boiling point of the electrode-tool material. Since high surface temperature and high energy density correspond to small discharge spot.

The previous indicators refer only to machining time and volume removed from the workpiece and tool, but it is possible to evaluate the performances of the machining taking into account the material removed from the workpiece and the tool wear to the single discharge. In this way, it is possible to perform a better comparison between different machining. This kind of evaluation is possible only knowing the number of discharges occurred during the single machining, which is evaluable by means of a discharge counter connected to the machine. Using only the counter, all the variety of discharges. As a consequence, also short circuits and arches have been recorded. The machine applied for the experiments is a SARIX® SX-200, that is a 3D high precision and high capacity Micro Erosion machine. It is characterized by a precision of +/-0.002 (mm) and travels X=350 Y=200 Z=200 (mm) and presents the multi-axis CNC which allows the indexing of complex work pieces. It allows machining with solid and tube electrodes with a diameter ranging from 45 μm to 3.0 mm obtaining for the milling configuration, but it can also

machine high precision micro holes and shape holes down to 20 μm. μEDM generates surfaces characterized by a high level of surface quality with a finishing capability equal to Ra = 0.05 ÷ 0.1 with a high precision positioning accuracy up to ±1 μm. Other important characteristics of this machine are the automatic axis positioning control with depth control which is very useful for the depth error and the tool wear monitoring, and the refeeding spindle with dielectric or air clamping control for continuous production. It is managed through an easy and user-friendly unlimited programming and editing software. The limitation of this machine is the autoregulating system which avoids setting the instantaneous value of some process parameters that are expressed as indexes; for this reason, it is very difficult to know the correct values of some process parameters (e.g. peak current) and also recording the signals there is not a direct relationship between the indexes selected during the machining and the effective values of, for example, peak current.

For these reasons, for evaluating the machinability and the stability of the process, the characterization of discharges occurring during a generic μEDM process with different sets of process parameters is very important.

Considering these two aspects, for a correct evaluation of the process, it is necessary to measure and evaluate the electric current and the electrical potential which are delivered to the workpiece and electrode-tool by the generator during the machining operations. The distribution of peak current and the real values of energy per discharges have been evaluated through a signal collection and its analysis performed by a software tool programmed in MATLAB language. In particular, it is important to verify that the statistical distribution of the discharge energy, sampled during a generic process, is constant over a reasonable amount of time. As a matter of fact, assuming that the material removed from the workpiece by a given discharge is dependent on the energy supplied by the generator [48], it is reasonable to suppose that if the mean energy per discharge is constant then it will be constant also the material removal per discharge [44,49,50].

Characterizing and counting the discharges population occurred during the machining, it is possible to consider others two process performances indicators

correlated to the machining speed and electrode-tool wear for each discharge. In this case, they are called Material Removal per Discharge (MRD - Eq. 1.3) and Tool Wear per Discharge (TWD - Eq. 1.4) calculated as follows:

$$MRD = \frac{Volume\ removed\ from\ workpiece}{Number\ of\ Discharges} \quad \text{Eq. 1.3}$$

$$TWD = \frac{Volume\ of\ tool\ wear}{Number\ of\ Discharges} \quad \text{Eq. 1.4}$$

Another important aspect for the evaluation of process performances is the surface roughness obtained with the machining. In particular when the features are realized by the milling approach. In this case, does not exist a standard procedure for its estimation only by a mathematical formula, but the evaluation of surface roughness and its parameters are defined by an international standard about the Geometrical Product Specification (GPS) ISO 25178 [51]. Surface roughness is formed by fluctuations in the surface of short wavelengths, characterized by peaks and valleys of varying amplitudes and spacings (Figure 1.10); it most commonly refers to the variations in the height of the surface relative to the reference plane; it can be measured either along a single line profile or along a set of parallel line profiles defined as surface maps. Considering the surface map, this is usually characterized by two statistical height descriptors:

- Sa. Arithmetic mean of the absolute of the ordinate values within a defined area (A).

$$Sa = \frac{1}{A}\int\int_A |z(x,y)|\,dx\,dy \quad \text{Eq. 1.5}$$

- Sq. Root mean square value of the ordinate values within a defined area (A).

$$Sq = \sqrt{\frac{1}{A}\iint_A |z^2(x,y)|\, dx\, dy} \qquad \text{Eq. 1.6}$$

Two others rarely used statistical height descriptors are the skewness (Ssk) and the kurtosis (Sku).

$$Ssk = \frac{1}{Sq^3}\left[\frac{1}{A}\int\int_A z^3(x,y)\, dx\, dy\right] \qquad \text{Eq. 1.7}$$

$$Sku = \frac{1}{Sq^4}\left[\frac{1}{A}\int\int_A z^4(x,y)\, dx\, dy\right] \qquad \text{Eq. 1.8}$$

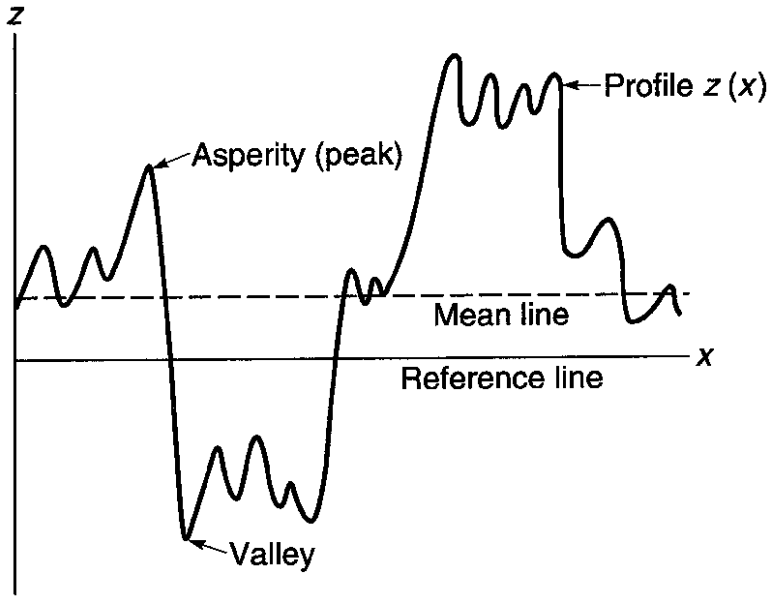

Figure 1.10. Schematic of a surface profile z(x) [52].

The surface finishing influences the parts or components functionality and performances. In μEDM, the machined surface is covered by a multitude of overlapping craters, micro-cracks and small heat affected zone (HAZ), generated by electrical discharges, whose geometry and characteristics depend on the process parameters, the type of dielectric and the characteristics of electrodes materials [53].

In 2007 a model to evaluate the surface roughness based on a configuration of a single-spark cavity formed as a function of process parameters has been developed. The model extends the microscopic phenomenon of spark formation to predict the surface roughness in μEDM [54]. Jahan M.P. in 2011 [55] investigated the feasibility of improving surface characteristics of carbide in fine-finish sinking and milling μEDM using graphite nano-powder-mixed dielectric. The experimental results proved that the fine-finish powder-mixed of WC–Co, the addition of semi-conductive graphite nano-powder in dielectric oil provides smooth and defect-free nano-surface in both sinking and milling μEDM. Arising from a uniform distribution of sparking among powder particles, relatively shallower craters with improved crater distribution are produced on the workpiece surface to result in a smooth and glossy surface finish.

Some methodologies were developed to evaluate the surface texture of metals and ceramic surfaces machined by μEDM. In particular, experimental investigations to define the influence of process parameters setting on machining performance were performed to determine the quality of the produced surface. This methodology helps to determine the best possible parametric setting for electrical discharge machining of the ceramic composite. In other cases, methods to evaluate the entire surface texture were developed and applied to experimental data to evaluate its capability and feasibility [56–58].

1.6 Research Issues

This work aims to study and assess the sustainability of μEDM from the economical point of view and study in the deep new application of this technology.

Specifically, such it will describe in Chapter 2; the literature review represents a gap in the economic investigation about the μEDM process. Many efforts have been accomplished to deepen the technical aspects and the literature is rich of contribution in this sense, on the contrary, literature is poor from the economic evaluation point of view; in fact, no specific model or specific evaluation of μEDM process cost were developed. For this reason, the first part of this study is related to the estimation of productivity costs and the definition of a method to correlate the economic and technological aspects. Another gap in the literature is a limited study about the application of electro discharges process to a particular kind of advanced materials widely used for example in critical environments. An example of these materials is represented by the advanced ceramic which are one of the most interesting issues for the industries that want to innovate and improve the characteristics and the performances of the machined parts. μEDM has all the characteristics to be applied for processing these materials with great results. As reported in the following chapter, some advanced ceramics are the object of many studies, but in general, from the point of view of characteristics and material properties, not as a workpiece of manufacturing processes. The improvement in the application of these materials results to be very interesting not only from the technologies and process point of view but maybe they can help to reduce the economical efforts and emissions during the machining.

CHAPTER 2

Literature Review

This PhD research project takes into account three main aspects and open issues in the literature about μEDM technology. Specifically, in the first period the economic aspects, in terms of optimization and sustainability, were investigated then, the focus moved towards the application of the μEDM process to new advanced materials, with particular attention on the diboride-based composite. In general, this project is aimed to answer three main research questions:

- How is it possible to evaluate the production cost of the μEDM process?
- Does exist a method to correlate the technological and economic aspects of this technology?
- Is it possible to effectively apply this process to ZrB_2-based ceramic materials doped with a different fraction of additive?

2.1 Production cost estimation

μEDM is one of the most extensive technologies used to reach the component miniaturization, but, despite this great development, today there is a limited research activity about the cost of its use. The production cost evaluation is very important for the industries because it has a direct bearing on the performance and effectiveness of a business enterprise. Despite the great development of this particular non-conventional technology, today there is a very limited research activity about the costs of its use: a specific model for the EDM technology which involved all the utilities and resources involved during the machining process still miss in literature. This is a very important gap in the research field, in fact, the lack of a model/algorithm to perform a good cost evaluation could be a problem. The

overestimation can result in loss of business and goodwill in the market, whereas underestimation may lead to financial losses to the enterprise.

Because of this crucial role in an organization, cost estimation has been a focal point for design, operational strategies and a key agenda for business decisions and managerial policies. As a result, a considerable research effort has been made in exploring design implications, new techniques, and methods for producing accurate and consistent cost estimates, not only to generate optimum design solutions but also to achieve the maximum customer satisfaction in terms of low-cost, high-quality, and on-time product delivery [59,60].

Papers published on the product cost estimation investigate many issues ranging from manufacturing cost estimation of standard mechanical components to the analysis of the cost of highly customized products, from cost optimization techniques to specific methods for overhead costs. In the literature, many categorizations of these methods already exist [59]. In 2001, Shehab and Abdalla [61] observed that literature showed that a number of cost model have been developed for several kinds of applications. But little effort has been made in cost modelling at an early stage of the entire product development cycle. They lacked material selection capability. They did not consider non-productive times such as set-up, loading and unloading, and tool changing times. It is also apparent that all aspects of the product life cycle, such as the assembly stage, were not considered in these systems. To overcome the above shortcomings, an integrated framework PC-based system for product cost modelling is developed. The development process is through two major steps: firstly, constructing a knowledge-based system (KBS) for cost modelling, secondly, integrating the KBS with both material selection database and a CAD system has been implemented. The proposed system is composed of a CAD (Computer Aided Design) solid modelling system, user interface, various knowledge bases, process optimisation, databases, and cost estimation technique module. The system is integrated with a CAD system and material selection software (Figure 2.1 and Figure 2.2), to facilitate the product representation and the material selection processes. A user-friendly interface

(menus, active images and buttons) is developed for providing the designers with easily input data to the system and complete results of the analysis. Hybrid knowledge representation techniques, such as production rules, frame and object-oriented are employed to represent manufacturing knowledge in this research. Fuzzy logic-based knowledge representation is applied to deal with uncertainty in the knowledge of cost model. The system has the capability:

- To recommend the most economical assembly technique;
- To select material as well as the manufacturing process based on a set of design and production parameters;
- To estimate the total product cost, ranging from material cost to assembly cost.

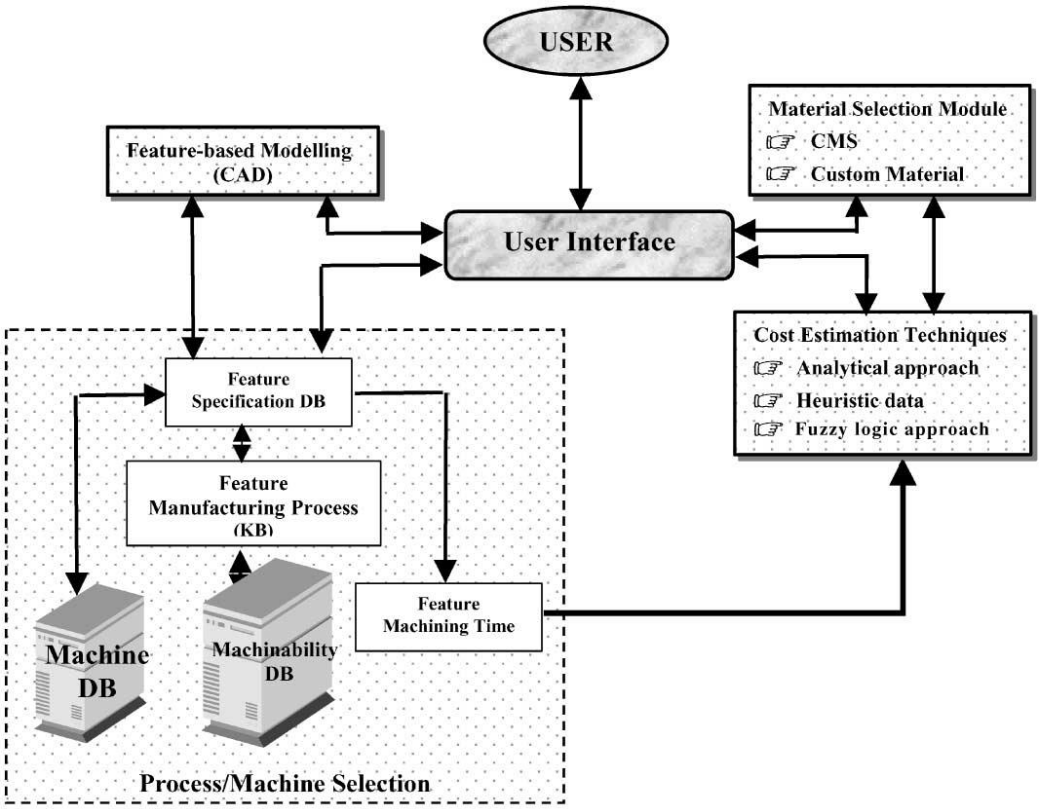

Figure 2.1. The architecture of cost estimation for machining process paradigm [61].

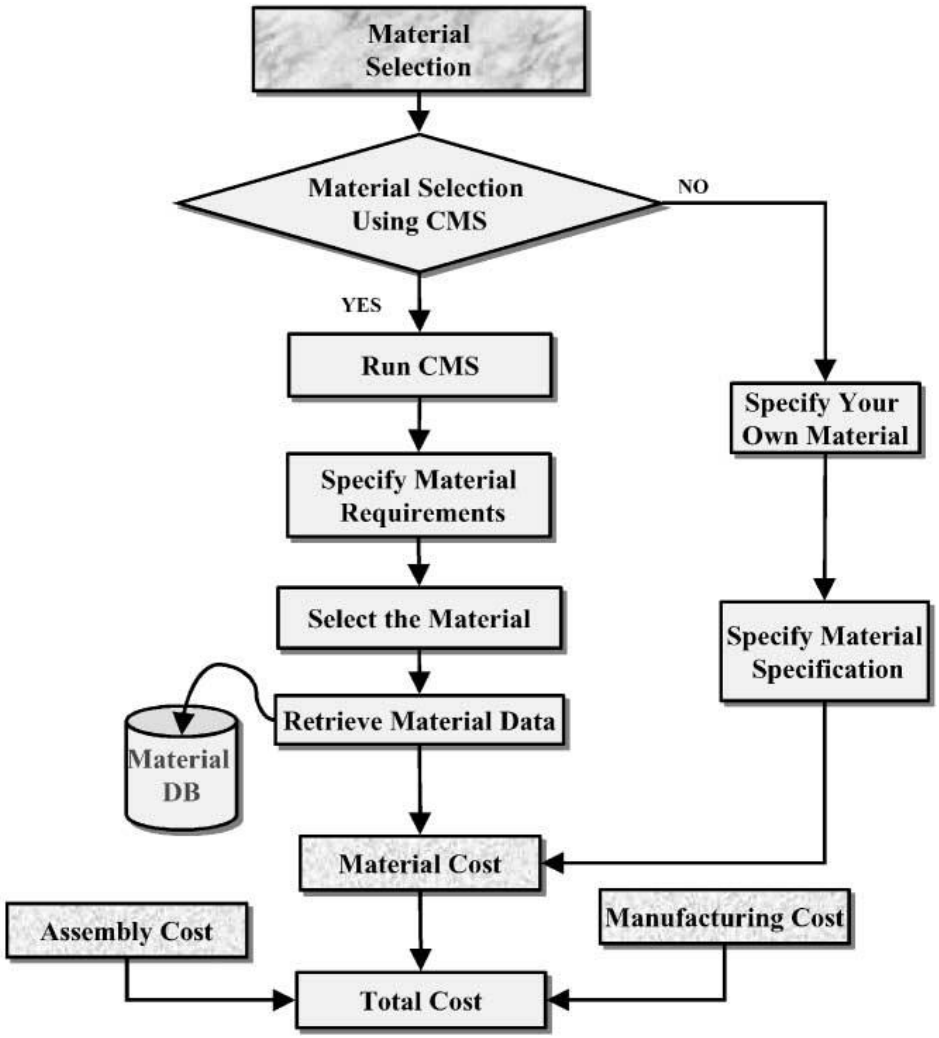

Figure 2.2. Material selection mode [61].

This work mentioned intuitive, variant-based, parametric and generative cost estimating process without giving a real definition, but in 2002 [62] they improved this method and classified cost modelling approaches at the design stage into feature, knowledge, function and operations-based approaches. These works cover the lack of material selection and the CAD design of the parts but do not consider the evaluation of non-machining time (set-up time, damage…). Zhang et al. [63] categorized cost evaluation techniques into traditional detailed-breakdown, simplified-breakdown, group-technology-based, regression-based and activity-based cost. Specifically, in the traditional detailed-breakdown approach, the total product cost is the sum of all the cost occurred during the production cycle of the

goods, such as the raw material, manufacturing, labour and overhead costs. The calculation, however, requires detailed information on product design, process routing, machining time, etc. The accuracy of the cost estimation depends on the availability of the required information and the variance of the actual activities. The simplified breakdown methods are mainly developed for cost estimation in the early design stage when a process plan is not available. The method assumes that the manufacturing process takes place under ideal processing conditions. A limitation of this approach is the difficulty to update the cost estimate based on actual cost information. The group-technology-based approach is founded on the similarity principle. It typically uses a basic cost value while considering the effects of variable cost factors such as size and complexity. Linear relationships between the final cost and the variable cost factors are assumed. The last category, represented by the regression approach, tries to find the dependence relationships between costs and product characteristics such as size and material. The coefficients and exponents are derived through the regression analysis of historical cost data. The limitation of this approach is that the nature of the non-linearity relationship between the cost and the product's characteristics is not known and hence has to be assumed. In this work, the authors presented an algorithm using back-propagation neural networks with a system developed for cost estimation of packaging products. The neural network model is trained using historical cost data and the testing results suggest that the neural network approach can support good product cost estimation. Then performance comparison between the neural network and a linear regression analysis based on the training, validating, and testing samples are performed and the results show that the neural network model outperformed the linear regression model.

Niazi A. et al. [59] proposed a hierarchical classification of all these techniques, considering two main categories: qualitative and quantitative techniques (Figure 2.3). The first category considers the techniques based on a comparative analysis of a new product with products manufactured previously in order to identify the similarities in the new one. The identified similarities help to incorporate the past

data into the new product so that the need to obtain the cost estimate from scratch is greatly reduced. This category includes intuitive cost estimation techniques which are based on using the past experience.

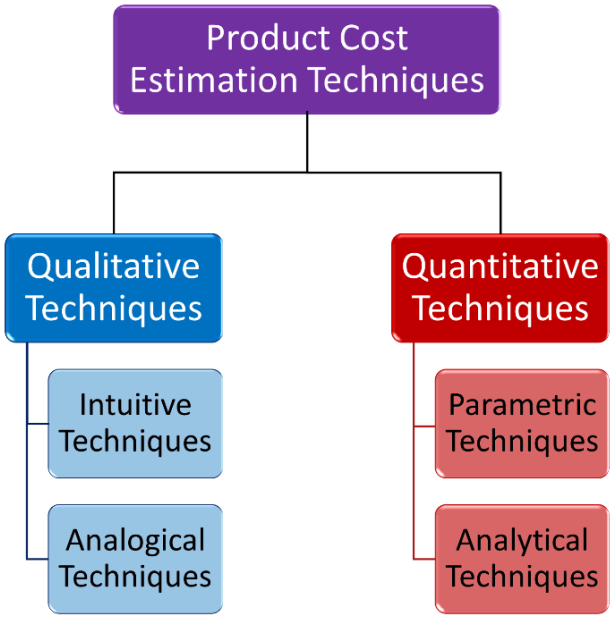

Figure 2.3. Main classification of the product cost estimation techniques.

A domain expert's knowledge is systematically used to generate cost estimates for parts and assemblies. The knowledge may be stored in the form of rules, decision trees and judgements at a specific location. For example, a database helps the end-user to improve the decision-making process and prepare cost estimates for a new product based on certain input information. The other sub-group of qualitative techniques is represented by the analogical cost estimation techniques which employ similarity criteria based on historical cost data for products with known costs, such as regression analysis models or back propagation methods. The second category is represented by the quantitative techniques, which are based on a detailed analysis of product design, its features, and corresponding manufacturing processes instead of simply relying on the past data or knowledge of an estimator. This class includes the parametric models, which are derived by applying the statistical methodologies and by expressing cost as a function of its constituent

variables. These techniques could be effective in those situations where the parameters, sometimes known as cost drivers, could be easily identified. Parametric models are generally used to quantify the unit cost of a given product. Other quantitative approaches are represented by the analytical cost estimation techniques, which requires decomposing a product into elementary units, operations, and activities that represent different resources consumed during the production cycle and expressing the cost as a summation of all these components. Costs are either calculated using an analytical function of certain variables representing different product parameters or as the sum of elementary units (Figure 2.4).

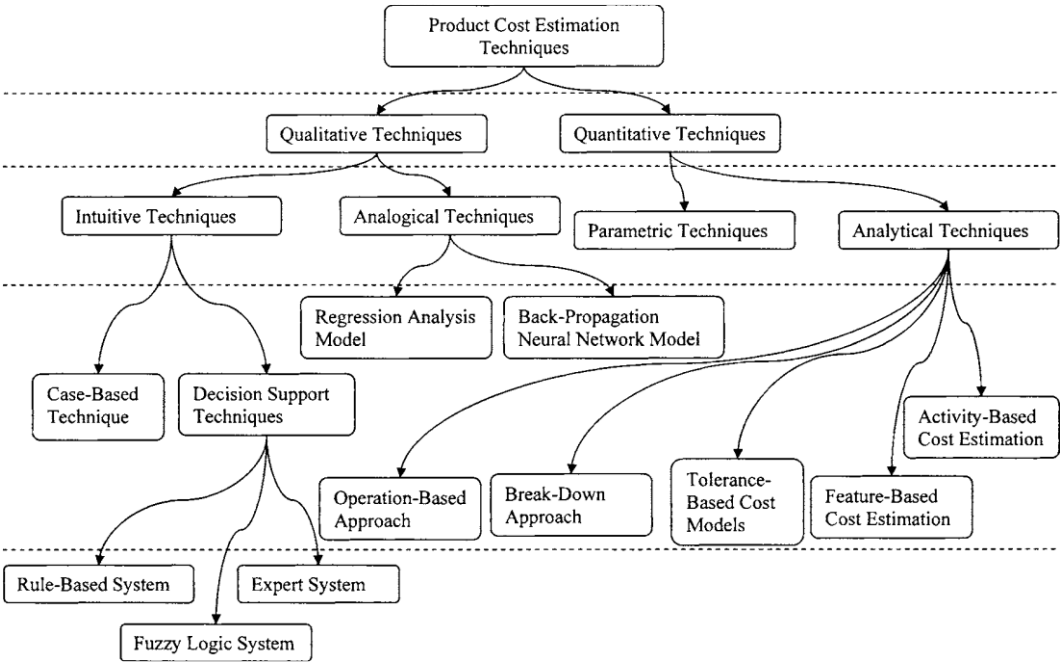

Figure 2.4. Classification of the product cost estimation techniques [59].

D. Ben-Arieh et al. [64] presented a method to evaluate the cost of the design and development activities for machined parts implementing Activity Based Cost (ABC) using the steps reported in Figure 2.5. The methodology is demonstrated on a sample part being produced in a controlled manufacturing facility, follows some steps. First of all, the resource centres directly used for the design and development and the cost associated with these resource centres were identified. The cost centres

include human resources and major equipment. Then, the resources were assigned to each cost centre and their driver rates were determined. In this step, the cost of indirect resources is allocated to cost centres, based on the resource cost drivers. The total cost for each cost centre is estimated; then, for each cost centre, one cost driver is identified. For example, the driver for a machining centre is the machining time, while the driver for the material handling centre is the number of trips. Lastly, in this step, one driver rate is obtained for each cost centre. This method is based on a detailed analysis of the activities involved in the design and development phase, so these activities are modelled using the IDEF0 convention, where major activities, such as design, and CNC prototype machining are decomposed into more detailed activities. At this point, each activity is analysed and the respective total cost was calculated by using the cost-centre drivers' rates multiplied by the amount of the drivers consumed by each activity.

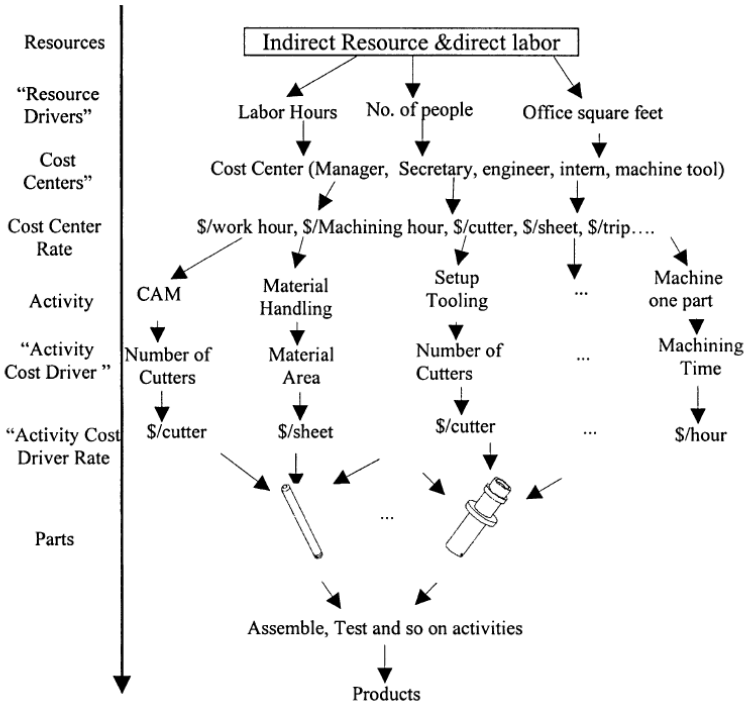

Figure 2.5. ABC implementation: Flow of expenses from resources to activities to products [64].

The cost of the product is found using activity cost drivers consumed by the product. The methodology was demonstrated and verified using sample rotational

parts developed in a controlled manufacturing environment. The method appears to be more accurate than the traditional cost estimation provided by the shop accountant. An additional advantage of the presented method is the ability to expand the costly activities and look in more detail at the causes of the cost. This can provide valuable insight into the factors that cause the cost, helping to better manage the activities. This methodology can be extended by using feature-based cost estimation in coordination with the ABC. This allows evaluating the product cost very early during the design stage based on committed geometrical properties. The limitation, in this case, is related to the complexity of the model; in fact, many drivers are taken into account and some of them are not immediate to be defined. The simplicity of the model is very important because a too complex model would not be introduced in a company for the cost evaluation because high complexity can generate a high waste of time for finding information.

L. H. S. Luong at al. [65] described the development and implementation of a generic knowledge-based system which offers a completely integrated facility for process planning, selection of machining parameters and cost estimation in the hole making process. This system helps to overcome many practical problems associated with the use of group technology for process planning, such as the interpretation of classification codes by users. This system is also flexible and allows users to customize the knowledge stored in the knowledge bases in order to meet the requirements of individual companies. The main function of the system, besides estimating the cost of production, is to recommend appropriate processes, their sequence and their respective machining conditions in order to obtain the required product specifications. Another feature of this system is its ability to cater to a variety of machinability data formats commonly used in industry. It has provided a practical and economic solution, for small companies, by the more efficient performing the task of process planning and cost estimation tasks, in the hole making process.

S. Rehman et al. [66] described a method for modelling costs during all the design phase of a product's life-cycle, from concept to detail design. The

quantitative evaluation of designs through a cost function is facilitated by the timely provision of cost data. This approach to design evaluation has the advantages of allowing management to make a more accurate bid estimates, encouraging designers “to design to cost” and reducing the amount of design rework, hence reducing the product's time to market and controlling product cost. The cost modelling strategy adopted integrates the use of knowledge-based and case-based approaches (Figure 2.6). With this work, for the first time, a hybrid approach integrating the use of knowledge-based adaptation and case-based reasoning is applied to cost estimation at conceptual design. The method is aimed at innovative design and allows the evaluation of such designs through a cost function. Some research has been done in case-based reasoning for innovative design simulation but none has been reported on innovative design evaluation at conceptual design.

The works just presented show that there are many studies about the estimation of production costs taking into account different approaches and level of the production chain. Several cost models have been developed for various kinds of applications, but little effort was made in cost modelling at an early stage of the entire product development cycle and no one is specifically developed for the evaluation of μEDM process. They lacked material selection capability. They did not consider non-productive times such as set-up, loading and unloading, and tool changing times. It is also apparent that all aspects of the product life cycle such as the assembly stage were not considered in these systems. In some cases, the qualitative approaches were introduced improving the complexity of the model and the estimation cost. Easier is the application of the model, more possibilities that the companies try to apply these improvements there are. The model may be simple to apply but involve all the core driver. But most of all, in literature there are no papers specifically focused on the evaluation cost in the μEDM process.

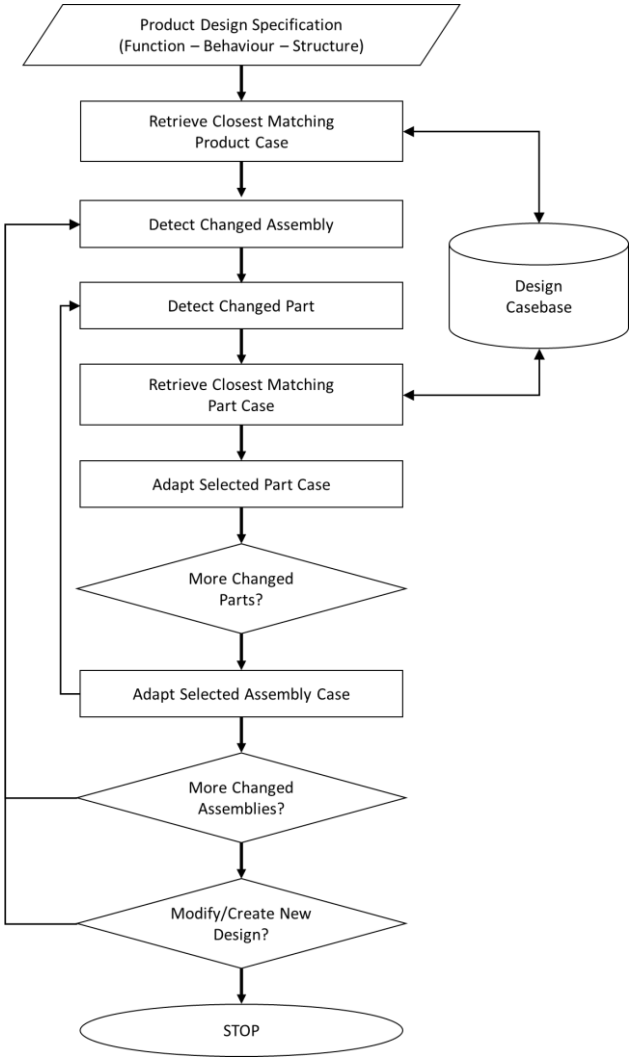

Figure 2.6. Cost estimation process model [66].

2.2 Correlation between economic and technological aspects

Complex electrothermal phenomena, surface irregularities, the interaction between successive discharges and the presence of debris make the μEDM a very complex process; for this reason, a complete and accurate physical modelling of the process is very difficult to be developed. To achieve the best machining performances and to increase the production while reducing machining time, the correct selection of the process parameters is required. Usually, the process parameters are fixed based on experience or on handbook values, but this approach does not ensure that the chosen process parameters accomplish optimal or near-

optimal machining performances and nobody can guarantee that the process parameters selected represented the best solution from the economic point of view. The selected process parameters mainly influenced the machining duration and the tool wear, which are strictly related to the process performance indicators. In some cases, Taguchi method and similar techniques, have been applied to carry out parametric design even though they are limited to the optimization of only one response at a time and in case of multiple responses, these methods do not work [67,68]. Therefore, a multiple response optimization method is necessary to obtain the best parametric combination for the μEDM process [23].

The most used models are based on natural rules. For example, in the Genetic Algorithm (GA), the genetic laws are turned into a mathematical model used to optimize the tool, in the Artificial Neural Network (ANN), the study of neurons and their functionality is involved. In the same way, in the Ant Colony Optimization (ACO) and in the Artificial Bee Colony (ABC) algorithms, the social behaviour of ant and bee are imitated. Similarly, the Biogeography-Based Optimization (BBO) algorithm considers the mathematics of biological distribution of different species to work out complex optimization problems [69].

Somashekhar et al. [70] applied the ANN trying to model and optimize the μEDM process. Artificial intelligence application, in the last years, has great development in virtually all engineering fields. Modelling and optimization are necessary for the understanding and control of any process and precise control is a prerequisite to achieve improved quality and productivity. ANN plays an important role in studying the linear and non-linear problems, thus, many researchers attempted to develop models from experimental data using statistical techniques. As the μEDM is a complex and stochastic process, it is very difficult to predict the output characteristics accurately by mathematical equations; at the same time, it is difficult to obtain an analytical model based on physics of the process because of the high number of phenomena occurred. Therefore, an attempt is made to model such stochastic processes by the ANN approach based on error back-propagation. One of the advantages of using a neural network approach is that a model can be

constructed very easily based on the given input, and the output is trained to accurately predict process dynamics. In the first step of the work, experimentation considering the machining of aluminium varying some process parameters (gap, feed rate, speed and voltage) on different levels is performed. The second step involves the definition of the model using feed-forward neural network architecture with the error back-propagation algorithm for the pertinent machining parameters, to model such a stochastic process predicting the MRR. The output obtained by the application of the neural network is compared with the desired output and testing error has been calculated. Finally, the developed models are validated with experimental data used for model development; at this point, the process parameters are optimized by genetic algorithm (GA). The developed model of the optimum neural network allows giving a good prediction of MRR characterized by an average prediction error of 0.8312% for training (Figure 2.7) and 3.94% for testing (Figure 2.8). So, the process optimization through ANN modelling and GA technique result to be very effective in optimizing the performance of the μEDM process, but no correlation with the production cost was introduced in the algorithm.

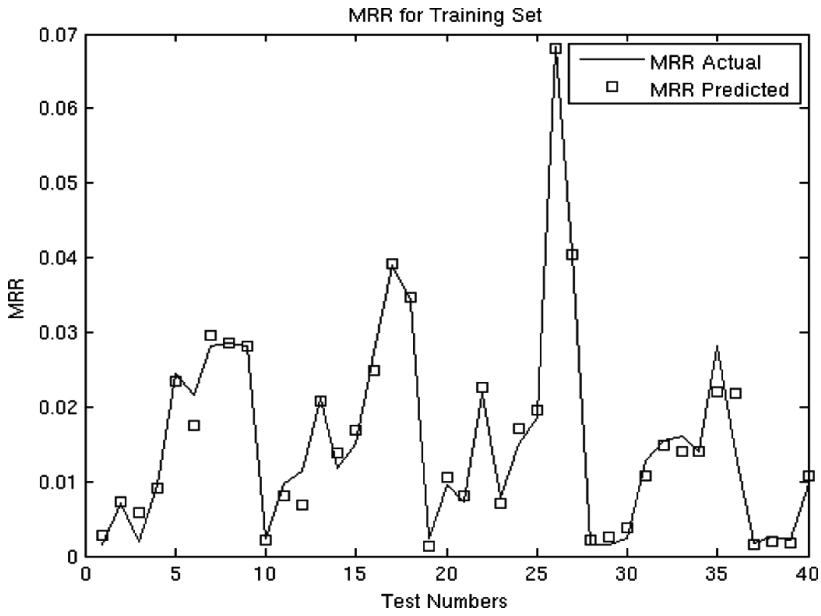

Figure 2.7. Comparison of experimental and ANN output for MRR for training set [70].

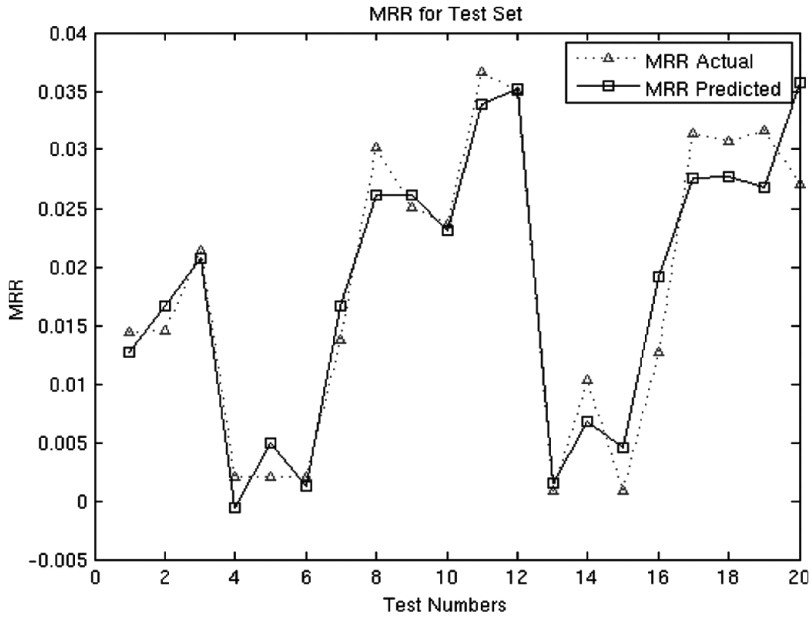

Figure 2.8. Comparison of experimental and ANN output for MRR for test data set [70].

Panda [71] developed a new hybrid approach of neuro-grey modelling (NGM) for parameter design involving multiple attributes characterization and optimization by integrating artificial neural network (ANN) and grey relational analysis (GRA) techniques. A feed-forward back-propagation variant ANN is designed to simulate multiple process attributes of the μEDM process, followed by the use of GRA to carry out process optimization. To train the network, the Levenberg–Marquardt algorithm has been used; this algorithm is based on the second-order derivative of the network error function. For the training of the back-propagation variant of the neural network, the Levenberg–Marquardt algorithm is most preferred and successfully overcomes the limitation of other gradient descent techniques. Based on the Levenberg–Marquardt algorithm, the mean square error is considered to indicate the performance of ANN. A pre-processing of the training and testing data sets is performed to eliminate the outliers. The main process parameters which can be monitored by the set-up of the process are chosen. The training and testing data sets consist of two replicates of experimental results obtained under similar treatment combination of input parameters. The first objective is to develop back propagation variant artificial feedforward neural network of appropriate

architecture and activation function. ANN is trained to provide the values of surface roughness (Ra), depth of heat-affected zone, microhardness value, and MRR as an output matrix with respect to peak current and pulse duration as input matrix. The output matrix represents the decision matrix for using the GRA. The combination of ANN and GRA in NGM technique provides a multi-attributes process modelling and optimization framework to obtain a generalized solution. This technique allows overcoming the limitations of each other's approach: ANN is a recognized modelling tool with the capability to represent the process in a quantitative way; similarly, GRA is capable of aggregating multi attributes of the process irrespective of their dimensions and nature to a unitary grey relational grade and optima corresponds to the highest grey relational grade. The authors demonstrated all these aspects in the context of EDM. Finally, it can be concluded that the quality of the results obtained by NGM is significantly dependent on the quality of the response surface construction by ANN. The reliability of optimization is ensured in grey optimization in spite of the aggregation of different contradicting nature of the process attributes as the process attributes are transformed to dimensionless grey relational coefficients, which in turn is expressed as additive relation to an unobjective function called grey relational grade, needs to be maximized. Thereby it not only has an advantage over multi-objective genetic algorithm but also relatively easier to implement. This methodology integrated some different algorithms to optimize surface roughness and MRR as a function of peak current and width of the pulse. The limitation is the non-consideration of the economic aspects.

Assarzadeh et al. [72] presented a new integrated network-based approach for prediction and optimal selection of machining conditions in EDM process for achieving maximum metal removal subject to appropriate operating constraints on the surface roughness (Ra) and machining variables. Peak current, pulse on time and voltage are selected as the network inputs, while material removal rate and surface roughness are the output parameters of the model. Figure 2.9 reports the configuration of the neural network model developed by the authors.

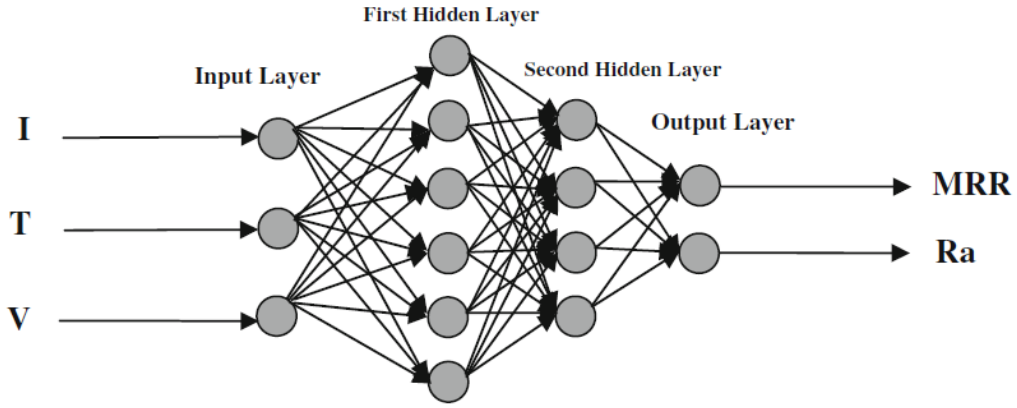

Figure 2.9. Configuration of the back-propagation (BP) neural network mode for the EDM process [72].

Since a single combination of input parameters cannot be optimal for both the material removal rate (MRR) and surface finish (Ra), this led to the notion of separating each level of machining regime based on surface quality. Thus, a general procedure for the modelling and optimization of the EDM process is adopted (Figure 2.10). Firstly, a 3–6–4–2- size back-propagation (BP) neural network model is developed to enable the measures of performance (MRR and Ra) to be predicted as a function of three different process parameters: peak current (I), discharge width (T), and voltage (V). Then, an augmented Lagrange multiplier (ALM) neural network is used for determining the optimum parameter settings in each machining approach.

The integrated BP-ALM neural network system is general and can be used as an instrument for the modelling and optimization of any kind of machining process. The efficiency of this method is clear when there is only experimental data which demonstrate the process behaviour, and no explicit mathematical relationships based on the physics of the process are available to correlate the input and output. Based on the simulation and verification results, BP neural network model for the prediction of the MRR and Ra in the EDM process is validated; in fact, a proper neural network model along with the ALM neural network can successfully summarise the optimal input conditions, in terms of process parameters, for the EDM process. Specifically, the optimal process parameters maximize the MRR,

characterized by necessary process constraints. Furthermore, the main aspect observed in this work is that the process optimization can be implemented by the observation of experimental information, without an analytical process model. Assarzadeh et al. [72] introduced the quality aspects in this evaluation model optimizing the maximum value of the machining speed with the surface quality, but also in this work, no attention was given to the economical part.

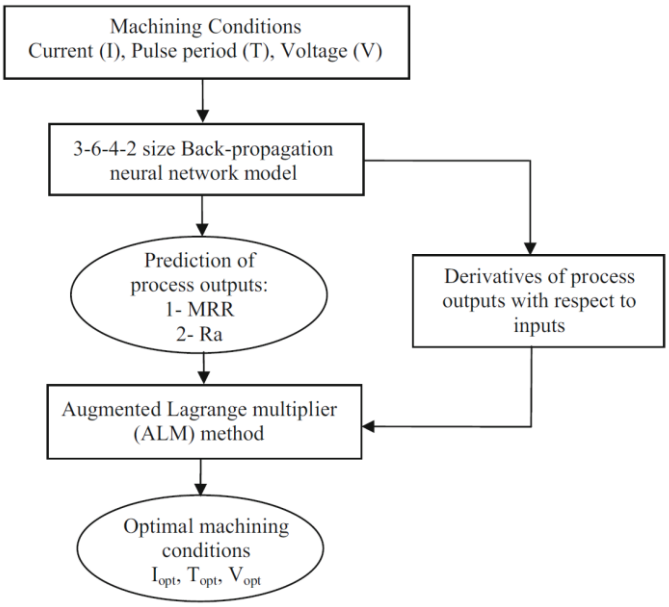

Figure 2.10. General procedure adopted for the modelling and optimization of the EDM [72].

Chiang [73] developed mathematical models for modelling and analysis the influences of discharge current, pulse on time, duty factor and voltage on material removal rate (MRR), tool wear ratio (TWR) and surface roughness (SR) in the EDM process of Al2O3+TiC mixed ceramic. In this work, an experimental plan of a face-centred CCD based on the response surface methodology (RSM) is employed to carry out the experimental study to identify and describe the influences of selected process parameters on the process performances, then the results are analysed based on the developed mathematical model. the analysis showed that the two main significant factors affecting the MRR are the discharge current and duty factor; while for TWR and SR, discharge current and pulse on time have a statistical significance. In general, MRR increase when discharge current and voltage

increase, TWR increases when the pulse on time, voltage and duty factor increase while the increment in discharge current generates a reduction of TWR. The SR is negatively influenced by the increment of discharge current and voltage, while the increment of duty factors performed bets results. The comparison of experimental data and the predicted data shows that the mathematical models of the value of developed for MRR, TWR and SR (Figure 2.11) fairly well fitted with the experimental values with a 95% confidence interval. A very similar investigation approach was presented by Çaydaş et al. [74], who developed a mathematical model to predict the electrode wear (EW) and the recast white layers thickness (WLT) using, also in this case, the surface response methodology (RSM) and the analysis of variance (ANOVA) to check the validity of the models. A central composite rotatable design (CCRD) in RSM consisting of three variables (pulse on time, pulse off time and pulse current) are employed to carry out the experimental study. The analysis finds out that the pulse current affects both EW and WLT, while the pulse off time has no significant effect on both responses. The comparison between the predicted and actual values showed that the predicted values match the experimental values fairly well both for EW and WLT with a high value of R^2 such as reported in Figure 2.12.

Among all the models presented until now, the one presented by Chiang [73] and the one by Çaydaş et al. [74] result to be the more complete because they take into account both process performances and qualitative aspects elaborated by means of many different methodologies and algorithms, but they do not refer to the correlation with the economical sustainability of the processes.

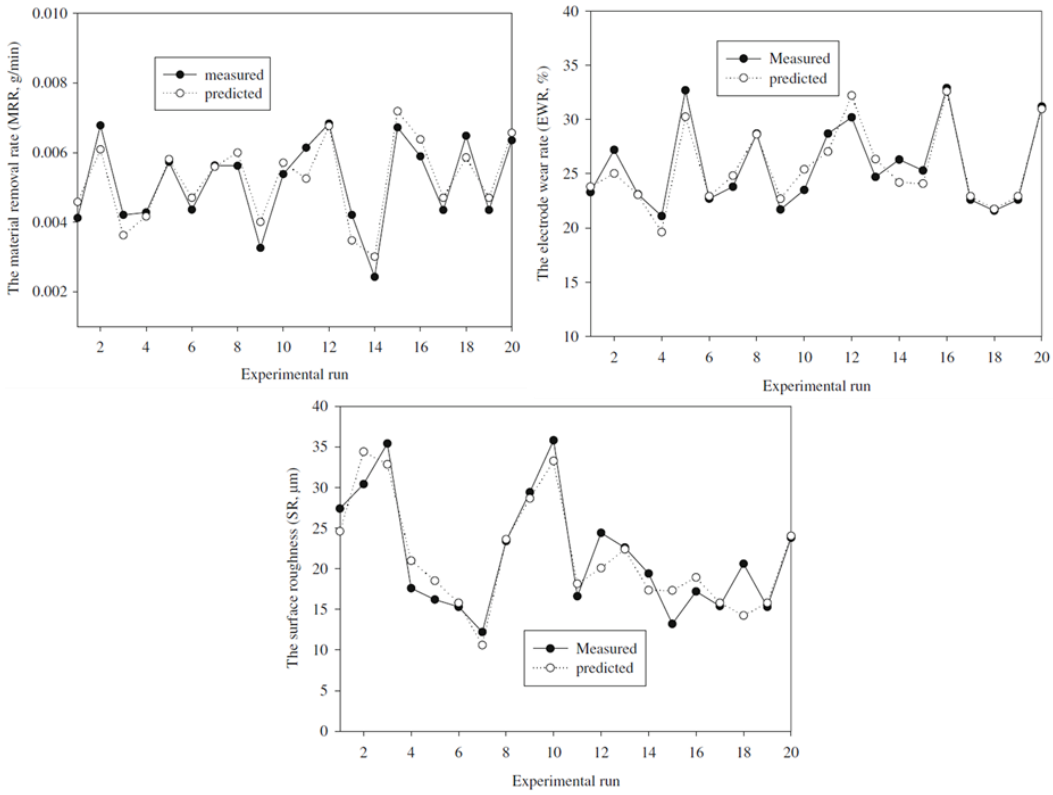

Figure 2.11. Comparison of the measured and predicted value for MRR, TWR and SR [73].

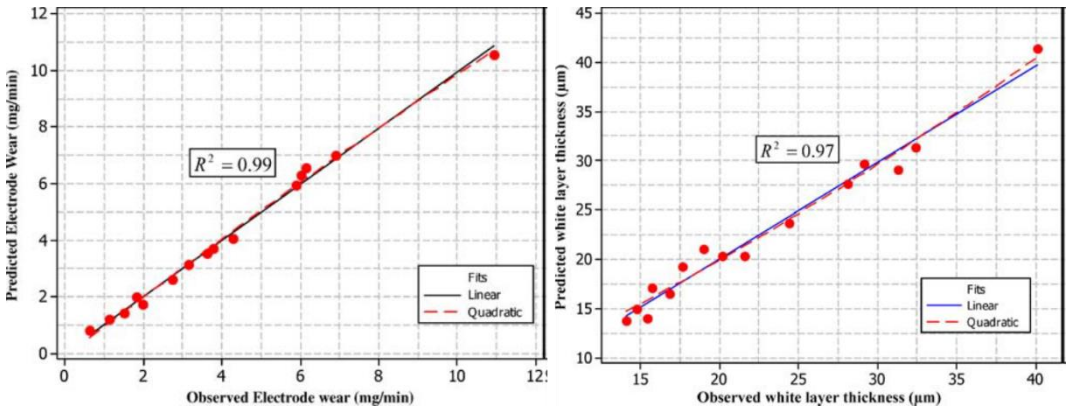

Figure 2.12. Comparison of experimental and predicted values for EW and WLT [74].

Mukherjee et al. [75] applied a Biogeography-Based Optimization (BBO) algorithm to find out the optimal combination of several machining parameters for improved EDM process performances. This algorithm considers the concept of migration of species from one habitat to another. In particular, the selection of one habitat from a set of alternative habitats is influenced by some factors and the

highest suitability habitat is selected during the migration. Optimal process parameters selection in EDM follows the same approach. From an initial set of possible combinations, the optimal solution is selected by the algorithm. They consider the mathematical models of various responses, such as material removal rate, tool wear ratio and surface roughness, seeking the optimal solution. When this algorithm is applied to optimize the responses, it finds out the optimal values of the EDM process parameters that will carry out the best results. Comparative analyses of other optimization algorithms (GA, ACO, ABC) show that the BBO algorithm gives the best results.

Despite the great development of EDM technology, there is a limited research activity concerning the economic aspects of the process. For example, in literature a model for predicting manufacturing cost of μEDM process was developed in [76] and a comparative analysis of different mathematical methods is made in [77], but, in both these works, there is not a correlation between the optimization of the technological aspects, in terms of process parameters and process performances, and the production cost.

Literature shows that there are many studies about the optimization of process performances and parameters through the application of specific algorithms or by the combination of several of them, but there are not investigations or algorithms about how to correlate economic and process optimization.

2.3 Advanced ceramic materials

During last years, the market has required not only miniaturization of the parts, but it has needed also the development of a new kind of material to improve the performances and the characteristics of the parts in several application fields. In particular, great development interested the family of advanced ceramic materials thanks to their continuously ameliorating performances most of all they have two main driving forces in the worldwide context, which can be summarized in two concepts: ecology and energy. The first driving force is referred to the conservation of the natural environment, reducing the emissions to the atmosphere. The second

driving force is related to the economic benefits derived from the saving of energy which, at the same time, is also connected with the preservation of the current fossil fuel stocks.

Ceramics are special materials with many applications in several engineering disciplines, but their importance has often been underestimated. Today's ceramics industry is one of the most rapidly advancing concerns in many parts of the world beginning to expand as a modern industry with the attribution of new techniques and knowledge. Since then it has also been one of the most competitive industries in the market. Ceramic materials typically possess low electrical and thermal conductivity, high melt temperature, and high compressive strengths; moreover, they are generally hard and brittle with very good chemical and thermal stability. Ceramic materials can be labelled as traditional and advanced ceramics.

As its name suggests, traditional ceramics are not supposed to meet rigid specific properties after their production, so low-cost technologies are applied to most of the production processes. Clay, feldspar, silica, dolomite, talc, calcite and nepheline are the common raw materials used for most of the ceramic products; each raw material assigns a certain property such as dry strength, hardness, and shrinkage to the ceramic body. Therefore, desired properties are acquired by the careful selection of materials. Powder preparation is the main step in the ceramic industry. Each characteristic such as surface area, particle size, particles distribution, particle shape and density have their own effect on the production; for this reason, the powder has to be prepared to meet required particle characteristics.

The second category is represented by the advanced ceramics, a special type of ceramics mainly used for electrical, electronic, optical, and magnetic applications. In this sector, ceramic powder preparation is quite important and advanced production techniques are employed to assure that the produced ceramic powders possess sufficient purity. Generally, chemical reactions are used to produce the ceramic powder. Specifically, the term advanced ceramics is applied to a group of materials obtained from inorganic raw materials with a high grade of purity, obtained at high sintering temperatures by means of powder metallurgy

technologies. In this way, high-density materials with good characteristics of hardness, mechanical resistance, wear and corrosion at high temperature, can be obtained. The most important fields of application are the realization of the medical and dental prosthesis, ball bearings, cutting tools and extrusion dies. Some other significant applications are related to high mechanical resistance in critical environments (e.g. gas turbines and heat exchanges), magnetic applications (e.g. lining or insulating material in nuclear reactors) and nanotechnology applications (e.g. micro-electro-mechanical devices and nano-turbines) [78–80]. In general, they are applied to all the sectors which require new materials that can perform in oxidizing or corrosive atmospheres and sometimes over the course of a long working life.

2.3.1 Ultra High Temperature Ceramics

A particular group of advanced ceramics is a class of promising materials used in extreme chemical and thermal environments associated with hypersonic flights, such as sharp leading edges hot structures of the future generation of slender-shaped re-entry vehicles [81]. Ultra-High Temperature Ceramics (UHTCs) are not a new class of materials. Historically, studies about them start between the 1950s and the early 1970s, when Air Force sponsored studies at U.S. laboratories about the thermochemistry, phase equilibria, and oxidation behaviour of transition-metal borides, carbides, and nitrides. This family of ceramics is usually based on group IV-V transition metal borides (ZrB_2, HfB_2), carbide (ZrC, HfC, TaC) and nitrides (HfN, TiN) which are characterized by melting points around 3000 °C (Table 2.1), high hardness, chemical inertness and relatively good resistance to oxidation in several environments [78,82]; furthermore they are ablation resistant and candidates for the design of components of next generation space vehicles, rocket nozzle inserts, and nose cones or leading edges for hypersonic aerospace vehicles. For these reasons, they have to bear high thermo-mechanical loads, which makes strength at a high temperature of great importance. While testing these materials above 2000 °C is necessary to prove their capabilities at anticipated operating temperatures. Two particular examples of UHTCs application in extreme

environments are reported in Figure 2.13 and in Figure 2.14. These images respectively represent the SHARK capsule, which was launched by the European Space Agency (ESA) rocket MAXUS-8 performing an atmospheric re-entry after a parabolic trajectory with an apogee at 700 km of altitude. In particular, this capsule is instrumented with accelerometers, rate pressure sensors, and thermocouples of which three were inserted inside the UHTC Nose Tip [83]. The second image represents a nose-cone manufactured and tested in a plasma torch facility [78].

UHTCs are being studied as candidate materials for the manufacturing of structural thermal protection systems since various decades and recently have been considered as absorber materials in concentrating solar power plants [84]. During the last years, several studies argued that diborides of the group IVb are the most resistant to oxidation and among these compounds, HfB_2 and ZrB_2 are the most performing [78,83,85].

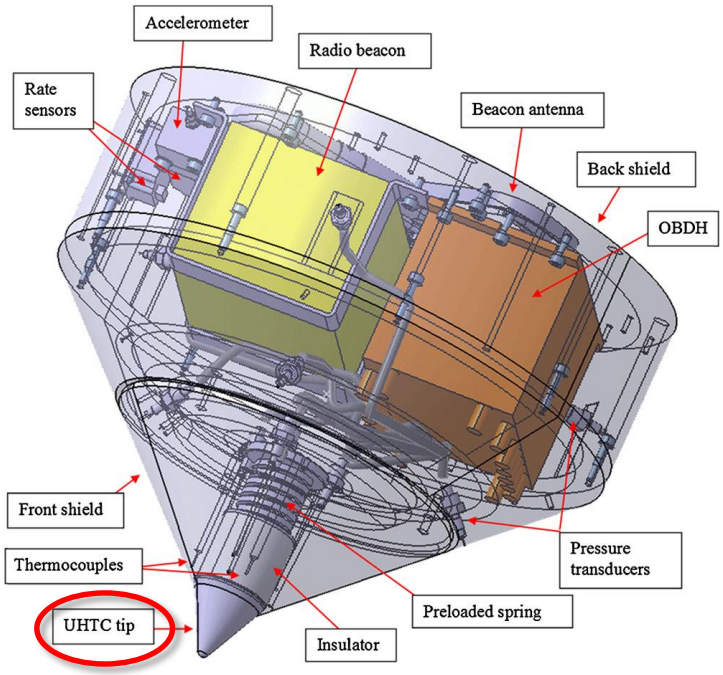

Figure 2.13. An example of UHTCs application: Sounding Hypersonic Atmospheric Re-entering "Kapsule" (SHARK) 3D model [83].

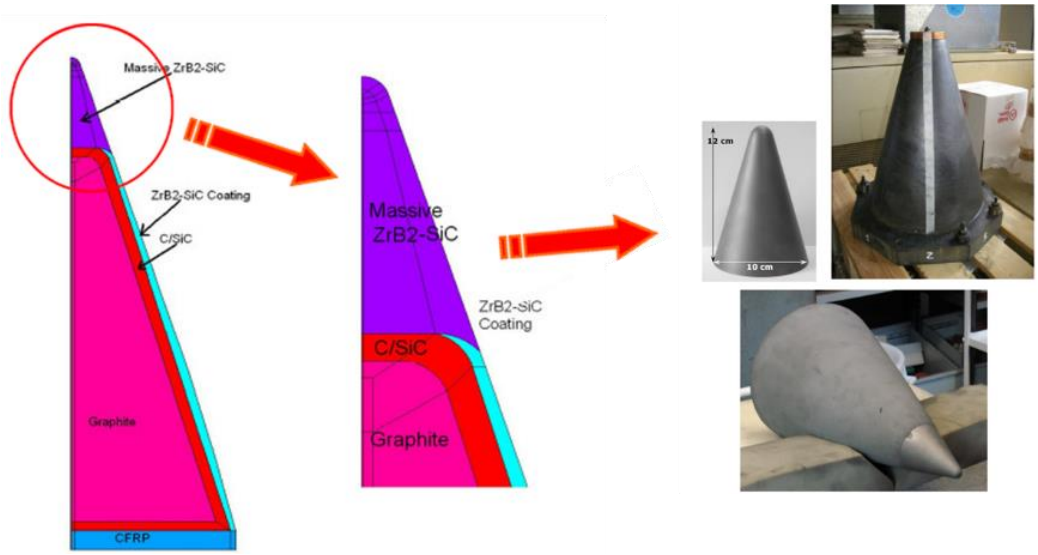

Figure 2.14. An example of UHTCs application: schematic of the nose cone architecture and detail of UHTC conical tip [78].

Table 2.1. Density and melting point of some UHTCs.

Material	Crystal structure	Density (g/cm^3)	Melting Temperature (°C)
HfB_2	Hexagonal	11.2	3380
HfC	Face-cantered cubic	12.76	3900
HfN	Face-cantered cubic	13.	3385
ZrB_2	Hexagonal	6.1	3245
ZrC	Face-cantered cubic	6.56	3400
ZrN	Face-cantered cubic	7.29	2950
TiB_2	Hexagonal	4.52	3225
TiC	Cubic	4.94	3100
TiN	Face-cantered cubic	5.39	2950
TaB_2	Hexagonal	12.54	3040
TaC	Cubic	14.50	3800
TaN	Cubic	14.30	2700

2.3.2 Zirconium diboride-based composite

Melting point over 3000°C, high electrical conductivity, fracture toughness, chemical stability in severe condition, make ZrB_2 a very attractive candidate for application in the ultra-high temperature regime and in critical conditions such as refractories crucible, high-temperature structural application in aerospace, electrical and microelectronics devices, nozzles or armour. Despite these characteristics, the application of pure borides is limited by three major factors:

- The strong covalent bonds hinder its densification, which has previously precluded realization of the true potential of ZrB_2 as a structural material; in fact; these materials are characterized by a highly porous structure and very low apparent density, usually about 85% vol.
- Its oxidation resistance, since ZrB_2 oxidation generates ZrO_2, which is porous and non-protective, and B_2O_3, which readily evaporates.
- It is brittle and susceptible to thermal shock failure.

To mitigate these shortcomings, the addition of secondary phases, composed by a non-reactive additive, is essential. During the design of ZrB_2-based ceramic composites, two main aspects have to be considered: the distribution of the secondary phase, continuous or discontinuous, and the melting point of the second phase or eutectic temperature between ZrB_2 and the second phase that limit the maximum temperature at which these can be used.

In this respect, a large variety of ZrB_2 ceramics containing non-reactive additives such as niobium (Nb), Vanadium (V), Carbon (C), disilicates and silicon carbide (SiC) are evaluated with the aim of bridging the above-mentioned gaps improving the relative density and the mechanical and physical properties. The early studies [80,86–89] aimed to investigate the production of dense materials by mean of pressure assisted sintering and to analyse the influence of various additives in order to improve the oxidation resistance of hafnium and zirconium diborides.

A selected collection of recent data concerning ZrB_2 composites with different percentage and type of additive tested up to ultra-high temperature is reported in

Figure 2.15. The plot shows that the strength of ceramics containing 20–30 vol% SiC is generally retained, or even increased, from room temperature up to 1000 °C. Strengths range between 500 and 700 MPa due to the formation of a continuous silica-based-glass capable of healing surface flaws. However, by 1500 °C, strength decreases to 200–340 MPa, owing to coalescence of micro-voids formed at triple junctions, softening of the grain boundary phases, and grain coarsening. Tungsten additions to ZrB_2 and HfB_2 based ceramics have been examined by several research groups, in view of substantial enhancements in oxidation resistance and bending strength up to 1600 °C. The addition of 5 vol% of WC to a ZrB_2–20 vol% SiC composite resulted in strengths above 600 MPa at 1600 °C when measured in argon. Although several hypotheses have been formulated, the role of W additions has not yet been fully explained [82].

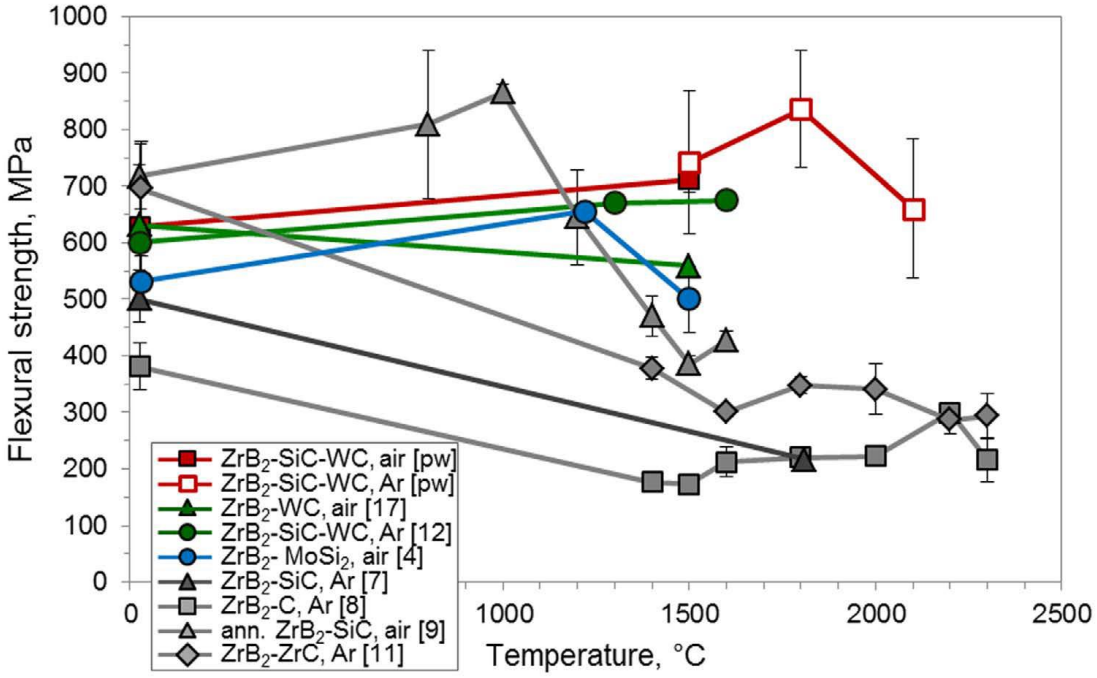

Figure 2.15. Flexural strength as a function of temperature for the highest strength ZrB_2-ceramics or tested at the highest temperatures in air or Argon [82].

Among these additives, SiC is one of the most used and it seems to be the most valuable, firstly to enhance resistance oxidation by the formation of borosilicate

glass, secondly to promote densification by restricting the growth of diboride grains, and lastly to lower their sintering temperature [85,90,91].

Like most ceramics, higher strengths are reported for diborides characterized by finer grain size, and, in general, the strength of diborides based material increases as grain size decreases for ZrB_2 and HfB_2 based ceramics, with and without $MoSi_2$ or SiC. In particular, a strength of ~500 MPa is identified for materials with grain sizes of ~5 μm (Figure 2.16). As reported in the plot's legend, diborides produced by Hot Pressing (HP), reactive Hot Pressing (RHP), Spark Plasma Sintering (SPS) and Pressureless Sintering (PS) are included in the representation.

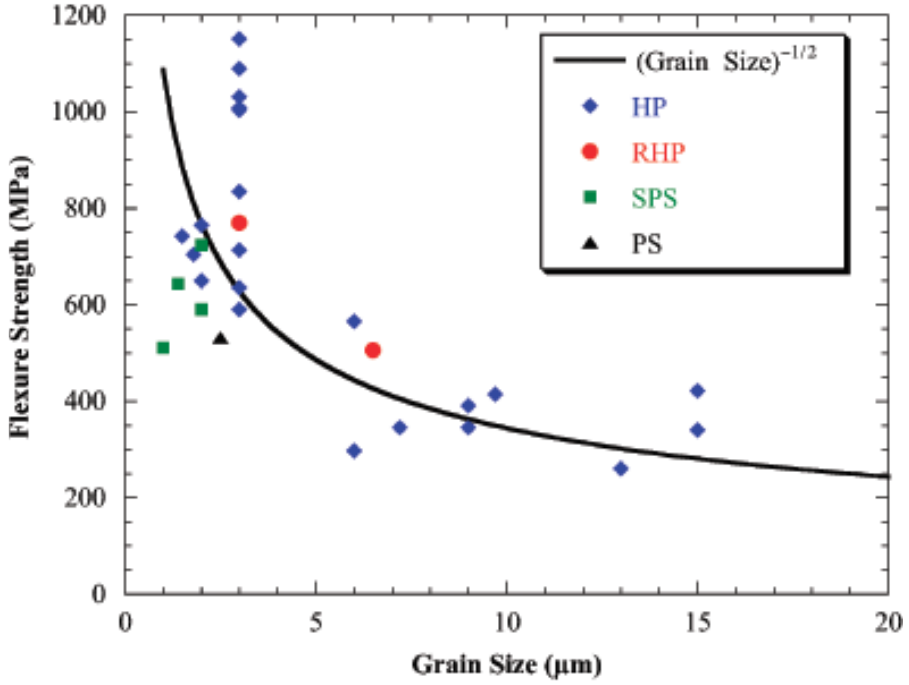

Figure 2.16. Room temperature flexure strength as a function of grain size from the diboride literature [90].

It is important to underline that the plot summarize some data of literature, for this reason, some strengths were measured in four-point bending, but some authors used three-point bending and the specimen size varied, mostly between U.S. and European standards, and this means that the strengths are not directly comparable, but it is useful to have an idea about the trends. However, strengths, in general, show an inverse square root relation with grain size ($GS^{-1/2}$) as would be expected

for ceramics free from other, larger flaws. The addition of second phases such as SiC can increase strength to over 1 GPa by further reducing grain size and promoting favourable residual thermal stresses. Furthermore, SPS is used to produce diboride-based materials that retain their room temperature strength to at least 1500°C. Usually, the addition of an additive is performed by a hot pressed process, which, despite the high pressures required (30-50 MPa), allows to reduce the densification temperature [92,93].

Silvestroni et al. [92], in 2015, try to answer some questions about the behaviour of ZrB_2 with the addition of non-reactive additive:

- How does the fibre oxidize in various oxidation regimes?
- Is SiC in fibre shape really more efficient in imparting oxidation resistance than particles? If yes, is there a range in which one type of morphology is preferred over another one?
- Does the fibre type influence the oxidation behaviour of the composite?

In this work, the oxidation behaviour of ZrB_2 containing SiC short fibres is studied by thermo-gravimetric analyses up to 1500°C for 10 hours, to extract the oxidation kinetics, and in a bottom-loading furnace up to 1650°C for 5–30 min, for investigating the degradation mechanisms at high temperature. $ZrSi_2$ is selected as a sintering additive in order to avoid the introduction of cations and not to modify the chemistry of the already complex system. The results of the analysis show that, after the transition period in the very first oxidation stage, linear kinetics prevails, unlike the parabolic one observed for ZrB_2 or ZrB_2–SiC composites. The apparent activation energy for this composite is calculated to be around 253 kJ/mol, that is higher than the activation energy for ZrB_2 composites with SiC in form of particles. The weight gain after fast-oxidation in bottom-loading furnace matched well with that of other ZrB_2 compounds containing SiC in form of particles or whiskers imparted better oxidation resistance to ZrB_2 than 20 vol% SiC particles or 10 vol% fibre. Although the discontinuous SiC distribution, columnar ZrO_2 and SiC-depleted ZrB_2 formed, only starting from 1650°C, where the fast evolution of

gaseous CO and SiO occurred, due to the oxidation of the fibre into C and SiO_2. The SiC fibres provide higher toughness and behave at least as good as particles in the ZrB_2 matrix during oxidation up to 1650°C. In 2018, a similar study by Silvestroni et al. [93] considered ZrB_2 with the addition of 15% vol. $MoSi_2$ sintered to full density at two temperatures: 1900 and 2150 °C. In this case, the work outlines the importance of an appropriate processing route to obtain ceramic composites suitable for application in a reusable space system, allow to design materials characterized by high oxidation performances at ultra-high temperatures. The results showed that the lower sintering temperature induced the formation of core-shell grains in the diboride matrix, where the core is ZrB_2 and the shell is $(Zr_{0.94}Mo_{0.06})B_2$ solid solution and, of the initial $MoSi_2$ content, 7% vol. of MoB phase is found together with 7% vol. of SiC as a consequence of the silicide dissociation and reaction within reducing atmosphere.

Studies related to the microstructure and the characterization of ZrB_2 sintered with a different fraction of silicon carbide (SiC) was conducted by Chamberlain et al. [94]. ZrB_2 and ZrB2-based ceramics containing 10%, 20%, and 30% in volume of SiC particulates are prepared by hot pressing of commercial powders. The powders are attrition milled with WC media, which led to the incorporation of ~2 vol% WC. Analysis performed by means of the Scanning Electron Microscope (SEM) shows that SiC inclusions are uniformly dispersed in the ZrB_2 base matrix and the average grain size decreased from ~6 μm, for pure ZrB_2, to ~3 μm for samples with SiC addition. Then, four-point bend strength, fracture toughness, elastic modulus, and hardness were measured. The results are shown in Table 2.2. Modulus and hardness did not vary significantly with SiC content; on the contrary, an increment in SiC content generates an increment of strength and toughness: strength increased from 565 MPa for ZrB_2 to 1089 MPa for 30 vol% SiC. The increase in strength was attributed to the reduction of grain size and the presence of WC, which may have reacted with ZrB_2 to form a ternary Zr-B-W phase. In particular, the addition of 10% vol. of SiC, lets to reach 93.2% of density and it is enough to limit the grain growth and maximize the strength.

Table 2.2. Room-temperature mechanical properties of ZrB_2 - SiC ceramics [94].

SiC content [vol.%]	Modulus [GPa]	Hardness [GPa]	Strength [MPa]	Toughness [MPa·m$^{1/2}$]
0	489	23 ± 0.9	565 ± 53	3.5 ± 0.3
10	450	24 ± 0.9	713 ± 48	4.1 ± 0.3
20	466	24 ± 2.8	1003 ± 94	4.4 ± 0.2
30	484	24 ± 0.7	1089 ± 152	5.3 ±0.5

Hwang et al. [95] studied the hot-pressing behaviour of ZrB2/SiC materials as a function of:

- SiC starting-powder size;
- SiC fraction;
- ZrO_2 doping;
- Colloidal dispersion of ZrB_2/SiC powder mixture.

This work also characterized in detail the microstructures of the resulting ZrB_2/SiC materials using electron microscopy, in an attempt to elucidate densification mechanisms, and microstructural effects on the oxidation behaviour and mechanical properties were studied. The selected material specimens and their main characteristics are reported in Table 2.3. The data show that the addition of SiC promotes densification of ZrB_2 at a moderate hot-pressing temperature; the highest density achieved in ZrB_2/SiC materials is 99.9%. A reduction in the SiC starting-powder size, and a colloidal dispersion of the powders, both promote hot-pressing densification of ZrB_2/SiC materials. SiC grain-size reduction results in improved oxidation- resistance in ZrB2/SiC materials. The results reported in Table 2.3 and Figure 2.17 shows that the addition of SiC particles promotes densification of ZrB_2-based ceramics at a moderate hot-pressing temperature of 1650 °C. The explanation for the beneficial effect of SiC on densification may lie in the fact that most SiC powder particles are known to have an oxidized surface layer. That layer may promote the formation of liquid phases during hot-pressing, assisting in

densification at lower temperatures. Improvement in densification with increasing SiC content (Figure 2.17), and hence increasing oxide content, supports this hypothesis. The increment in the density of ZrB_2/22.4 vol% SiC materials with decreasing SiC starting-powder size (Figure 2.18) further supports the hypothesis that the higher surface oxide content in smaller SiC particles (high specific surface area) is expected to promote densification.

Table 2.3. Processing details and microstructural parameters of ZrB_2/SiC materials hot-pressed at 1650°C under 60MPa pressure for 2 h investigated [95].

Name	SiC content [vol.%]	SiC powder size	Relative Density [%]	ZrB_2 grain size [μm]	SiC grain size	Remarks
Z1	0	-	71.6	3.4	-	Ball-milled
ZS1	5.7	1.7 μm	81.7	3.6	1.8 μm	Ball-milled
ZS2	11.4	1.7 μm	91.5	3.6	1.9 μm	Ball-milled
ZS3	22.4	1.7 μm	97.9	3.9	1.8 μm	Ball-milled
ZS4	22.4	0.6 μm	98.6	3.7	0.8 μm	Ball-milled
ZS5	22.4	40 nm	99.6	.3.4	80 nm	Ball-milled
ZS6	22.4	40 nm	99.9	3.4	80 nm	Colloidal + ball-milled
ZS7	22.4	1.7 μm	90.9	3.4	1.8 μm	Not ball-milled
ZS8	22.4	1.7 μm	96.4	3.6	1.9 μm	ZrO_2 + not ball-milled

The ZS7 material made from non-ball-milled powders has a lower density (90.9%) compared to the material ZS3 made from ball-milled powders (97.9%). It may be argued that ball- milling results in better mixing and particle-size reduction, which in turn results in better densification. This work outlines clear evidence that decreasing the SiC grain size in ZrB_2/SiC materials results in an increase in the oxidation- resistance. A qualitative explanation for this beneficial effect of SiC grain reduction lies in the consideration of the beneficial effect of any SiC additions to ZrB_2. It is generally accepted that the oxidation of pure ZrB_2 proceeds with the formation of ZrO_2 and boria at the exposed surface. Boria is highly volatile, and it does not provide adequate protection against further oxidation of ZrB_2. In the case

of ZrB_2/SiC materials, the oxidation of SiC grains provides a steady supply of silica glass. The silica glass combines with the boria formed on the neighbouring ZrB_2 grains, to result in a more refractory borosilicate glass. With the further evaporative loss of boron, the borosilicate glass eventually becomes silica-rich glass, which essentially glazes the surface and provides oxidation protection. Now consider a decrease in the size of the SiC grains from 1.8 to 0.8 μm, while maintaining the SiC content of 22.4 vol%.

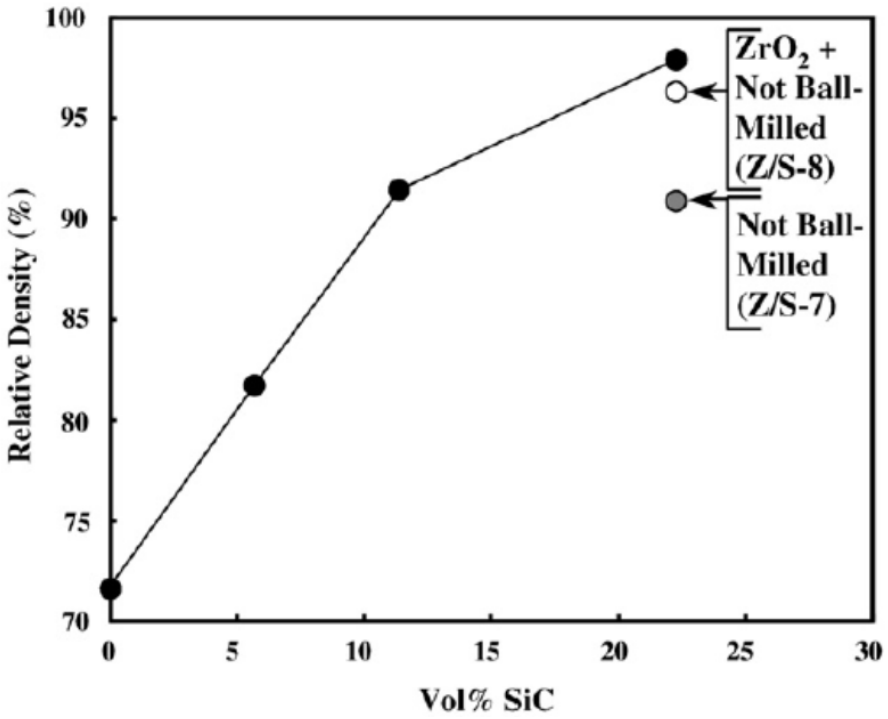

Figure 2.17. Plots of relative density (%) of ZrB_2/SiC materials hot processed under identical conditions as a function of vol% SiC. Relative densities of material ZS7 made from non-ball-milled powder mixture and material ZS8 made from non-ball-milled powder mixture but with ZrO_2 additions are also shown [95].

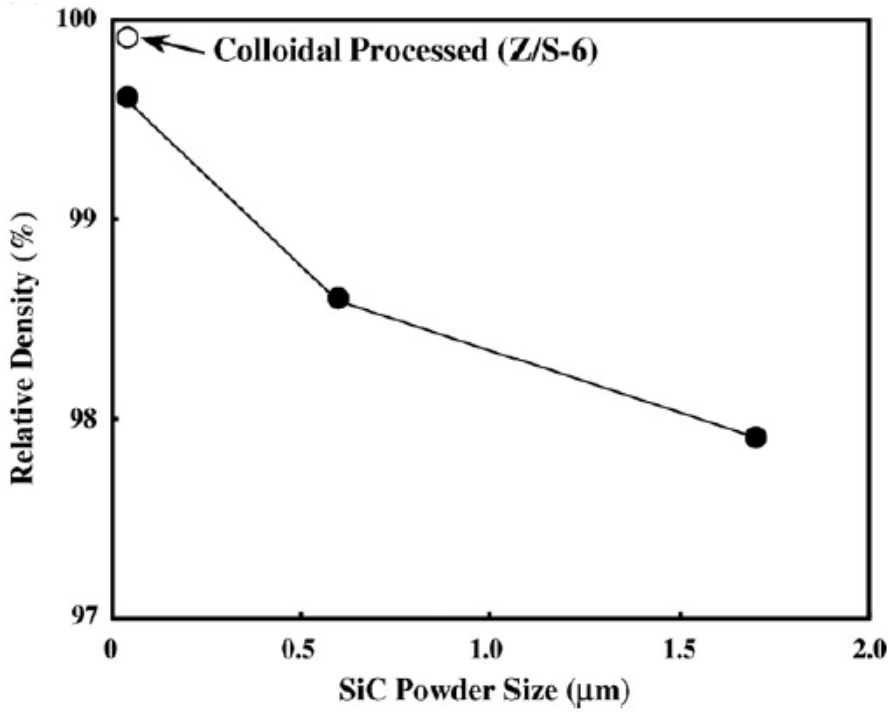

Figure 2.18. Plots of relative density (%) of ZrB_2/SiC materials hot processed under identical conditions as a function of SiC starting powder size. % relative density of material ZS6 made from colloidally dispersed, ball-milled powder mixture is shown [95].

Assuming spherical SiC grains and uniform distribution, this results in an increase in the ZrB_2/SiC interface-length per unit area of exposed-surface and a decrease in the spacing between SiC grains. This is expected to make SiC more effective in providing the silica-rich glass, leading to the formation of the protective silica-rich layer on the material early on during oxidation. Using this argument expected to result in a dramatic improvement in the oxidation, a further decrease in the SiC grain size to ~80nm is resistance in materials ZS5 and ZS6. However, only marginal improvements in the oxidation-resistance in materials ZS5 and ZS6 have been observed (Table 2.4). The hardness of the dense ZrB_2/SiC materials reported increases with decreasing SiC grain size. This can be attributed to dispersion hardening of ZrB_2 with the harder SiC phase that is finer and better dispersed. The higher toughness of the dense ZrB_2/SiC materials with coarser SiC grains can be attributed to crack-bridging toughening by SiC grains.

Table 2.4. Hardness, toughness and oxidation properties of dense ZrB_2/22.4%vol SiC materials [95].

Name	SiC grain size	Hardness, H [GPa]	Toughness, K_{IC} [MPa $m^{0.5}$]	Average silica layer thickness [μm]
ZS3	1.8 μm	15.2	3.8	13
ZS4	0.8 μm	16.7	3.8	4
ZS5	80 nm	19.9	3.1	3
ZS6	80 nm	21.3	2.4	2

Zhang et al [98] investigated the oxidation behaviour of ZrB_2–SiC composites with different percentage of SiC addition at 1273 and 1473 K in air for 12. The SiC addition contents ranged from 0 to 30 wt%. When ZrB_2–SiC composites were oxidized at 1273 K in the air, a two-oxide layer-structure is formed: a continuous glassy layer and a ZrO_2 layer contained unoxidized SiC. When SiC content is 5 and 10 wt%, the glassy layer is mainly composed by B_2O_3. When SiC content is 20 and 30 wt%, a borosilicate glass could be formed on the top layer, which could improve the oxidation resistance of ZrB_2. When ZrB_2–SiC composites were oxidized at 1473 K in the air, the oxide layer was composed of ZrO_2 and SiO_2 and unreacted SiC. Additionally, when SiC addition content was higher than 10 wt%, a continuous borosilicate glass layer could be formed on the top of the oxide layer at 1473 K. With the increase of SiC content in ZrB_2, the oxide layer thickness decreased at both 1273 and 1473 K.

Taking into account all these aspects derived from the literature and previous investigation, the addition of 20% of SiC generates the best combination of oxidation resistance and mechanical behaviour [95–98].

2.3.3 Materials preparation

The composition selected for the investigation carried out for the present study is characterized by the ZrB_2 base matrix. Materials were supplied by CNR-ISTEC of Faenza that produce these materials using commercial powders. Hexagonal ZrB_2 was characterized by:

- Specific surface area: 1.0 m^2/g;
- Max impurity content: C: 0.25 wt%, O: 2 wt%, N: 0.25 wt%, Fe: 0.1 wt%, Hf: 0.2 wt%;
- Particle size range 0.1–8 μm.

SiC can be added to the base matrix under fibres configuration, characterized by:

- diameter: 14μm;
- length: 1mm,
- 1–5wt% vinyl alcohol polymer with vinyl acetate wt% Si:C:O=62:37:0.5.

The starting fibres utilized for the composites are shown in Figure 2.19.

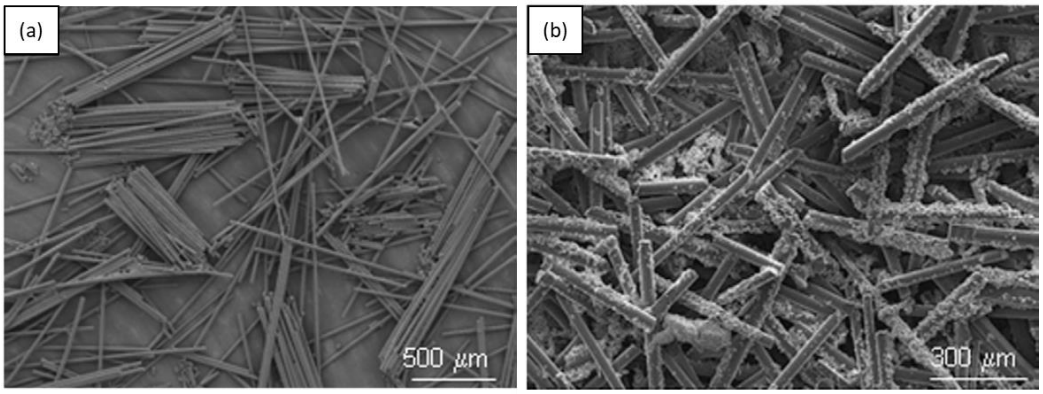

Figure 2.19. Reinforcing phases added to the ZrB_2 matrix (a) and the powder mixtures before sintering.

The powder mixtures were ball milled for 24 h in pure ethanol using silicon carbide media. Subsequently, the slurries were dried in a rotary evaporator. Hot-pressing cycles were conducted in low vacuum (~100Pa) using induction-heated graphite die. The maximum sintering temperature was set on the basis of the shrinkage curve. Free cooling followed.

From the mechanical characteristics, the analysis conducted on ZrB_2 base materials are characterised by high stability if the additive used is characterized by

fibres. The core of the fibres was constituted by SiC, then a Si–C–O interlayer containing ZrC nanoparticles acted as a grab for the outermost jagged layer composed by SiC1−x and Si–C–N phases. This graded structure of the fibres formed a very strong interface with the matrix and hindered any fibre pull-out.

Despite these extraordinary properties are significant from an application point of view, in the past the use of these materials has been very limited. On the contrary, today, these excellent mechanical properties lead to very high demands with regard to suitable manufacturing processes.

2.3.4 Materials machining

In general, all materials characterised by good mechanical properties tend to be really difficult to be processed; for this reason, for the processing of advanced ceramics, both advanced and traditional processes have been developed and studied. The traditional processes are only applicable to a limited extent by requiring specific and expensive tools.

One possible solution could be the near-net-shape fabrication of ceramics parts, but these materials are characterized by a high shrinkage during the sintering process, so it is hard to achieve functional dimensions. Because of this, postprocessing often is unavoidable for the fabrication of precision parts.

One of the main requirements of ceramic materials machining is the generation of fine shapes without micro-cracks, which is very difficult to be addressed by traditional mechanical machining technologies, owing to the intrinsic brittleness of this class of ceramics. Considering this requirement, in most cases, the solution can be found in advanced processes. This kind of machining can suitably overcome the disadvantages offered by the traditional machining methods due to the difference in material removal mechanisms. Mechanisms such as thermal material removal (electrical discharge machining (EDM)), mechanical material removal (abrasive jet, abrasive water jet, ultra- sonic machining), chemical (chemical machining), ionic dissolution (electro-chemical machining), etc. can be used individually or in hybrid form to shape hard to cut brittle materials) [99]. Due to their material removal mechanism, these processes are independent of the mechanical properties such as

the hardness, brittleness, and strength. Among all of these processes, electrical discharge machining (EDM) can prove to be very effective and advantageous when it comes to machine complex 3D shapes [99,100]. Over the past years, the advances in this technology allow the application of this process to the manufacture of conductive ceramic materials; in fact, despite the higher characteristics of UHTCs materials, the energy developed during the discharges event allows to reach a very high temperature in the machining area. In this way, the heat transferred to the surface during this process produce heat that melts and vaporises the workpiece material, thus the melt parts and debris are removed from the surface by the dielectric flow. A particular characteristic of the process is the surface texture generates on the machined surface; in fact, the dielectric medium is unable to remove every single debris or recasted particles, so the machined area is typically characterized by craters which represented the sign of the discharges. This is a general consideration about the μEDM process, referring to the machining on ceramics the considerations are a little bit different. The machined ceramic surfaces reported some imperfection such as micro-cracks and pores usually related to a wrong optimization of the process parameters set up. The presence of these imperfections can cause a loss of efficiency of the part reducing its performances, resistance and the life cycle. To avoid these contingencies and losses, in terms of quality but also economical, the analysis of the machinability of these particular materials is fundamental to improve the use of UHTCs and to develope system for machining them.

CHAPTER 3

FIRST RESEARCH PAPER

A model to predict manufacturing cost for micro-EDM drilling

This chapter is derived from the article "D'Urso, G.; Quarto, M.; Ravasio, C. (2017). A model to predict manufacturing cost for micro-EDM drilling. International Journal of Advanced Manufacturing Technology, 91(5-8), p.2843-2853". DOI: 10.1007/s00170-016-9950-0.

I am immensely grateful to the support received from my co-authors. I am responsible for all the changes in this chapter with respect to the published version.

3.1 Introduction

As reported in the previous chapters, the progressive reduction of devices and components dimension and the simultaneous integration of functions is a core subject of product development in many different fields of application. This miniaturization process can be considered as a strategic need in the industry and, at the same time, this trend has intensified the development of manufacturing techniques able to achieve these miniaturization purposes [101].

In Paragraph 2.1 the literature review shows that the cost estimation of general mechanical processes covers issues from manufacturing cost estimation of standard mechanical components to cost analysis of complex products [59], but just few research works are about a specific method to overhead costing for the μEDM process.

In this chapter, the first activity of this research project is described. In particular, a model to estimate μEDM machining costs was developed. A correct model for the estimation of manufacturing costs is an important success factor for

some companies because it helps to evaluate if the benefits of the project outweigh the cost and it allows to know how to distribute resources over multiple projects. The model developed in this work was applied to two case studies to demonstrate its capability. The first case study considers a drilling application on stainless-steel using two different types of electrodes. The second one regards an EDM application on tungsten carbide plates.

3.2 Assessment modelling methodology

The aim of the model cost developed in this part of the project is to estimate the overall manufacturing costs, considering the manufacturing process, tool, and workpiece information.

A process-based cost calculation method is used to build the cost model. The total cost is divided into two different categories and the costs related to each category are calculated based on the associated process steps. As illustrated in Figure 3.1, one category is represented by the fixed costs, which include ownership and routine maintenance, that is the costs incurred regardless of the production level. The second category is identified by the variable costs, which include labour, extraordinary maintenance, utilities and all the costs influenced by the productivity level.

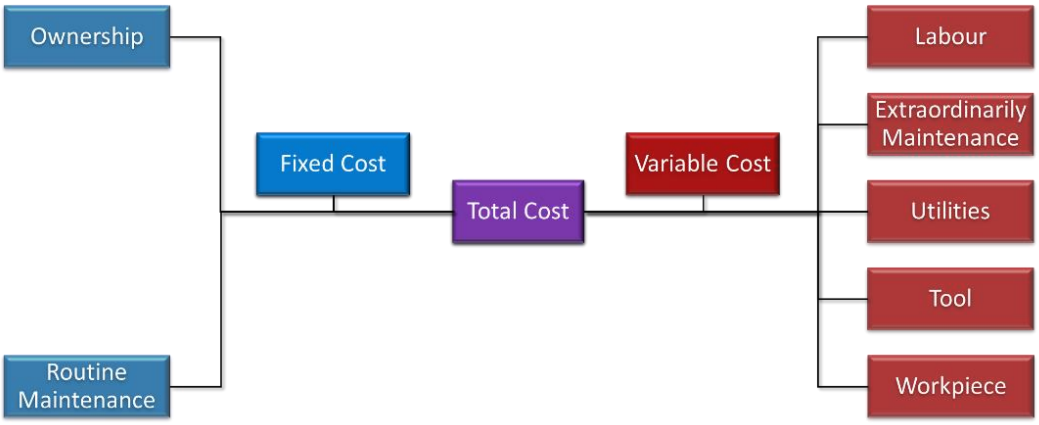

Figure 3.1. Contributors to product manufacturing costs.

3.2.1 Fixed costs

Fixed costs are those expenses that are more or less independent of the level of activity of the machine and the output. These remain constant throughout the relevant range and are usually considered sunk for the relevant range (not relevant to output decisions). The most common fixed costs are presented below.

Ownership cost is the most significant fixed cost, as they exist whether the machine runs or not. Most machines are financed with a fixed monthly payment and often it is not referred to cost management, in order to fully recover the cash flows for the monthly payments. In some cases, it might be useful to estimate the economic life of the machine and divide its cost to this value, but most EDM machines have limited residual value at the end of their economic life, so this factor can often be omitted [102]. The most affecting aspects to calculate the cost of ownership are accrued interest and the amortization, taking into account the coefficient of depreciation of tangible assets. The annual amortization is calculated and it is added to passive interests.

Routine maintenance includes all the maintenance actions performed regularly to prevent disruption of the system or the component. This is slightly affected by the level of activity of the machine for most installations.

3.2.2 Variable costs

Variable costs are those that vary depending on a company production volume, they rise as production increases and fall as production decreases. Variable costs differ from fixed costs, which tend to remain the same regardless of production output. These costs, described below, include wages, utilities, materials, etc. Labour costs (Eq. 3.1) can be direct or indirect. Direct costs include wages for the employees physically making a product, like workers on an assembly line. Indirect costs are associated with support labour, such as employees that maintain factory equipment but do not operate the machines themselves. In this case, labour costs include the operator wage rate and overhead. The operator's overhead includes training costs, contributions, medical and other fringe benefits. This is estimated at

60% of the wage rate [77]. The labour costs depend on the amount of operator attention. In general, it could be written as (Eq. 3.1):

$$C_L = (wg + 60\%wg) \cdot n_p \cdot t \quad \text{Eq. 3.1}$$

where:

- C_L is the total labour cost [€];
- wg is the wage rate of manufacturing personnel [€/h];
- n_p is the number of manufacturing personnel;
- t is the total time needed for machining. It encloses 33% of machining time, setup time and design time [h].

Extraordinary maintenance (Eq. 3.2) is performed on a part of the system to increase its useful life by over a year. It includes problem detection and failure correction. The total cost of extraordinary machining is calculated considering the cost of damage of experts necessary to the failure correction.

$$C_M = C_r + n_{exp} \cdot C_{h\,exp} \cdot t_r \quad \text{Eq. 3.2}$$

where:

- C_M is the total cost of extraordinary maintenance [€];
- C_r is the cost of replacement [€];
- n_{exp} is the number of experts necessary to solve the problem;
- $C_{h\,exp}$ is the expert hourly cost [€/h];

- t_r is the time needed for the failure correction [h].

Utility cost (Eq. 3.3) includes the costs of all the utilities needed to work the machine. It includes the cost of water, electricity and dielectric fluid. All these costs are calculated considering the quantity of utility used during the machining and their unit costs.

$$C_U = n_w \cdot C_w + n_e \cdot C_e + n_d \cdot C_d \quad \text{Eq. 3.3}$$

where:

- C_U is the total utilities cost [€];
- n_w is the quantity of water used [m^3];
- C_w is the unit cost of water [€/m^3];
- n_e is the quantity of electricity used [kWh];
- C_e is the unit cost of electricity [€/kWh];
- n_d is the quantity of dielectric fluid used [L];
- C_d is the unit cost of the dielectric fluid [€/L].

Tool cost includes the purchase of tools for the machining. μEDM presents two types of tool: electrode and wire. The cost of each electrode depends on the material (brass, tungsten carbide, copper, etc.), geometry (tube, coreless, hole star shape, etc.) and diameter. From the user point of view, the electrode cost is directly influenced by the tool wear while the wire cost is calculated considering the feed rate (to establish the amount of wire used during the machining). In some cases, the two tools (electrode and wire) can coexist at the same time, for example, when the electrode is dressed to reduce the diameter. Specifically, the tool cost is calculated as follow (Eq. 3.4):

$$C_{tool} = tw \cdot C_{el} + n_{wire} \cdot C_{wire} \quad \text{Eq. 3.4}$$

where:

- C_{tool} is the total tool cost [€];
- tw is the quantity of electrode used, in particular, it corresponds to the tool wear [mm];
- C_{el} is the unit cost of the electrode [€/mm];
- n_{wire} is the quantity of the wire used [mm];
- C_e is the unit cost of wire tool [€/mm].

3.3 Case studies

In order to validate the developed model, two case studies were used to demonstrate its capability. The first one takes into account micro holes on stainless-steel (AISI 304), while the second one takes into account micro holes machined on tungsten carbide plate varying the process parameters and the electrode material.

The choice of evaluating the validity of the model using drilling case studies is related to the greater simplicity of evaluation of the variables. This does not exclude that the model can also be applied to the milling process.

Both machining operations were executed by means of tubular electrodes made of two different materials (tungsten carbide and brass) having an external diameter equal to 0.3 mm and an internal diameter equal to 0.12 mm. Hydrocarbon oil was used as a dielectric. The experimental campaign was carried out by varying several process parameters such as peak current (I), voltage (V) and frequency (F), in order to study the relation between the process parameters and the machining performances, such as Material Removal Rate (MRR) and Tool Wear Ratio (TWR).

For each electrode material, the combination of the process parameters and the experimental sequence were defined based on a Design of Experiment (DOE) with three levels for each factor and five repetitions. Table 3.1 shows the fixed process parameters while Table 3.2 and Table 3.3 the variable ones for stainless-steel and tungsten carbide workpieces respectively.

Table 3.1. Fixed process parameters.

Workpiece	Electrode	Polarity	Width [µs]	Gap [%]	Energy
SS	**WC**	- (neg)	4.7	70	365
	Brass	-(neg)	4	50	365
WC	**WC**	- (neg)	5	20	365
	Brass	- (neg)	3.8	5	365

Table 3.2. Combination of Technologies created by DOE for stainless-steel workpiece.

Electrode	Tungsten Carbide (WC)			Brass (BR)		
	I [index]	V [V]	F [kHz]	I [index]	V [V]	F [kHz]
Tech.1	40	110	110	65	110	130
Tech.2	40	93	110	65	135	113
Tech.3	40	127	110	65	135	130
Tech.4	40	110	127	65	135	147
Tech.5	40	110	93	65	160	130
Tech.6	50	120	100	40	135	130
Tech.7	50	100	120	50	120	140
Tech.8	50	120	120	50	120	120
Tech.9	50	100	100	50	150	140
Tech.10	30	100	100	80	120	140
Tech.11	30	120	120	80	150	140
Tech.12	30	100	120	80	150	120
Tech.13	30	120	100	90	135	130
Tech.14	57	110	110	80	120	120
Tech.15	23	110	110	50	150	120

Table 3.3. Combination of Technologies created by DOE for tungsten carbide workpiece.

Electrode	Tungsten Carbide (WC)			Brass (BR)		
	I [index]	V [V]	F [kHz]	I [index]	V [V]	F [kHz]
Tech.1	40	110	83	26	120	130
Tech.2	30	100	90	40	100	110
Tech.3	50	100	90	40	140	110
Tech.4	30	120	90	40	100	150
Tech.5	50	120	90	40	140	150
Tech.6	40	93	100	60	120	96
Tech.7	23	110	100	60	86	130
Tech.8	40	110	100	60	120	130
Tech.9	57	110	100	60	154	130
Tech.10	40	127	100	60	120	160
Tech.11	30	100	110	80	100	110
Tech.12	50	100	110	80	140	110
Tech.13	30	120	110	80	100	150
Tech.14	50	120	110	80	140	150
Tech.15	40	110	117	94	120	130

Moreover, to study the progress in the drilling process, each hole was carried out in several sub-steps having the same drilling tool displacement. For each combination workpiece/electrode material, progressive MRR and TWR technology windows were elaborated to predict the performance as a function of the drilling depth. From these data, it was possible to elaborate progressive machining time and tool wear technology windows. The plots related to the machining time and the tool wear shows the trendlines (regression equations) of the data collected during the experimental campaigns. It is important to remark how the electrical input parameters have a strong influence on these machining performance parameters. These equations are used to estimate the cost drivers' equations, in fact, in Eq. 3.1-Eq. 3.3 machining time and tool wear are replaced by trendlines of machining time and/or tool wear.

3.3.1 Stainless-steel plates

The execution of 100 holes was considered for cost estimation. The following hypothesis were assumed:

- Machining setup was equal to 1.5 h (start-up, cantering, preparation of electrode and workpiece, setup process parameters);
- Operator's wage was equal to 25€/h;
- The operator monitored the machine only partially during the processing (e.g. 33%).

Figure 3.2 and Figure 3.3 show the trend of machining time and tool wear respectively for the execution of a single micro hole on a stainless-steel plate, varying the process parameters as a function of the hole depth for two electrode materials. In particular, Figure 3.2 shows the comparison of the progressive machining time technology window for the tungsten carbide and the brass electrode. The limits of each region were defined by the process conditions, giving rise to the minimum and maximum. In Figure 3.2, the limits of each area permit to define the minimum and maximum of tool wear. The trend of the interpolating equations for each condition is linear with a correlation index higher than 99%.

The machining time function was inserted into the equation used to calculate the labour cost (Eq. 1) and the utility cost (Eq. 3). After the estimation of these costs, the sum of labour and utility costs was calculated. Figure 3.4 shows the area in which the cost changes as a function of both hole depth and electrode material. The cost is higher for the machining conducted with tungsten carbide electrode. This difference is due to the duration of machining; in fact, the machining performed with the brass electrode is faster than the others regardless of the technologies used. The plot shows that the tungsten carbide machining has a greater window in which the cost varies.

To estimate the tool electrode costs, the unit cost of the electrode was calculated considering the price lists equal to 0.03 €/mm for tubular brass electrode and 0.12 €/mm for tubular tungsten carbide electrode. To calculate the tool wear cost, the

slope of the curve reported in Figure 3.2 was multiplied for the unit cost of the electrode and for the number of holes performed during the experimental campaign. Figure 3.5 shows the tool cost estimation for the execution of 100 holes on a stainless-steel plate using two types of the electrode as a function of the drilling depth. The tungsten carbide area is always higher than the brass one because the first electrode is more expensive than the second one even though the tool wear of brass is higher than the tungsten carbide. It is evident how both labour+utilities cost and tool cost, calculated for the machining performed by the brass electrode, are always smaller than the cost estimated for the tungsten carbide electrode; moreover, the windows described by the brass electrode machining is narrow than the other one.

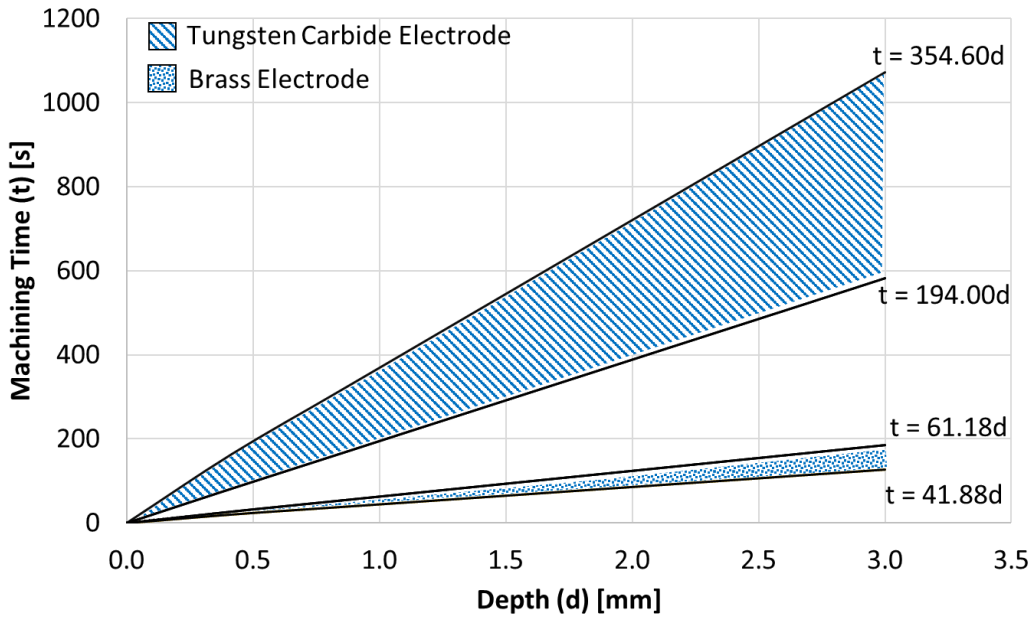

Figure 3.2. Machining time for a single hole on stainless-steel plates, as a function of the hole depth for two electrode materials, varying the process parameters.

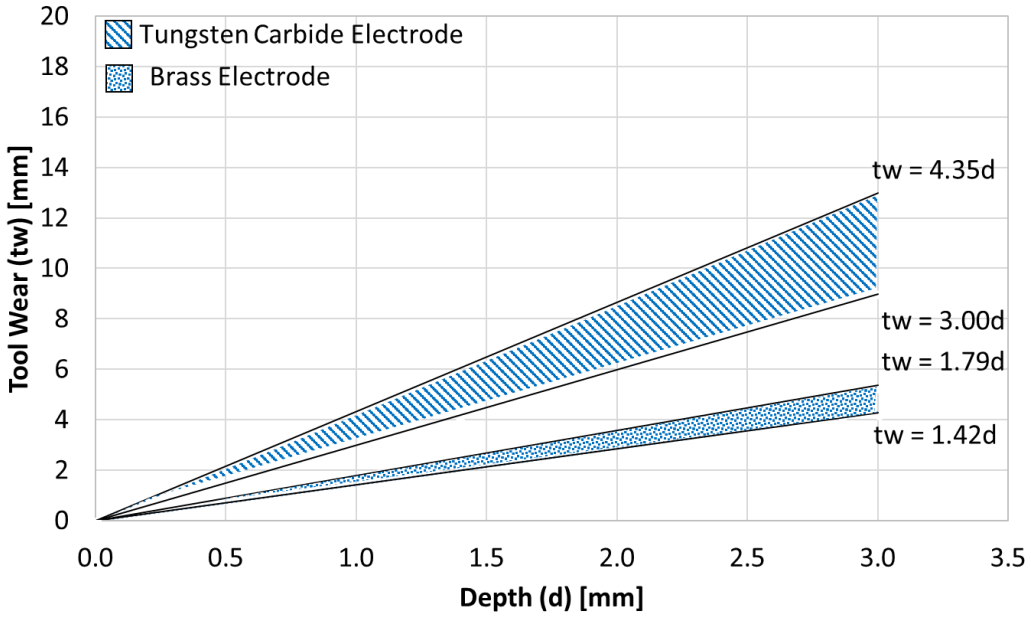

Figure 3.3. Tool wear for a single hole on stainless-steel plates, as a function of the hole depth for two electrode materials [13], varying the process parameters.

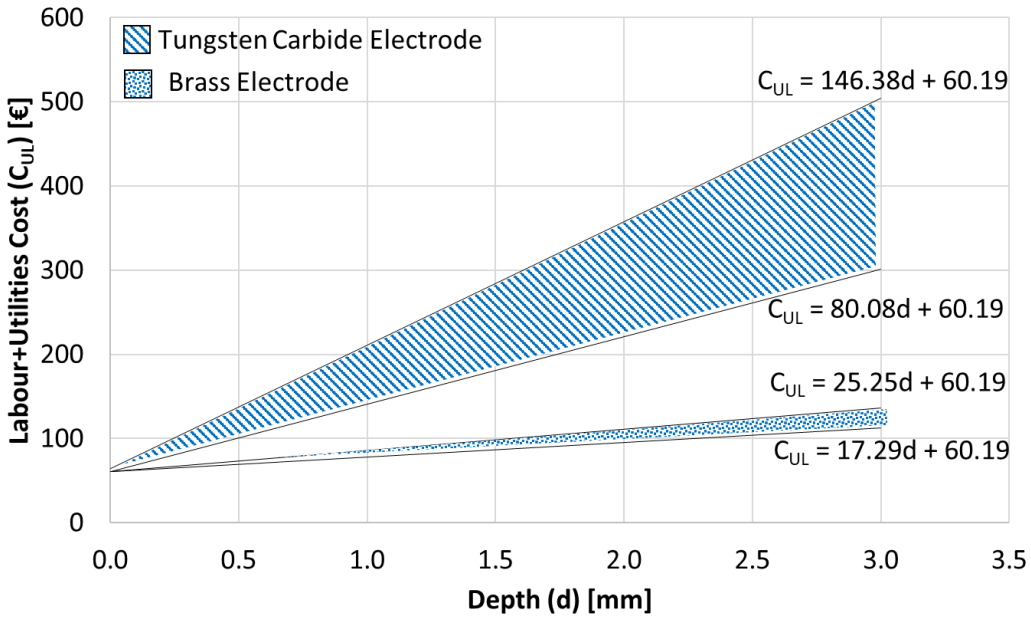

Figure 3.4. Labour cost + utilities cost as a function of the drilling depth varying the electrode materials for 100 holes performed on a stainless-steel plate.

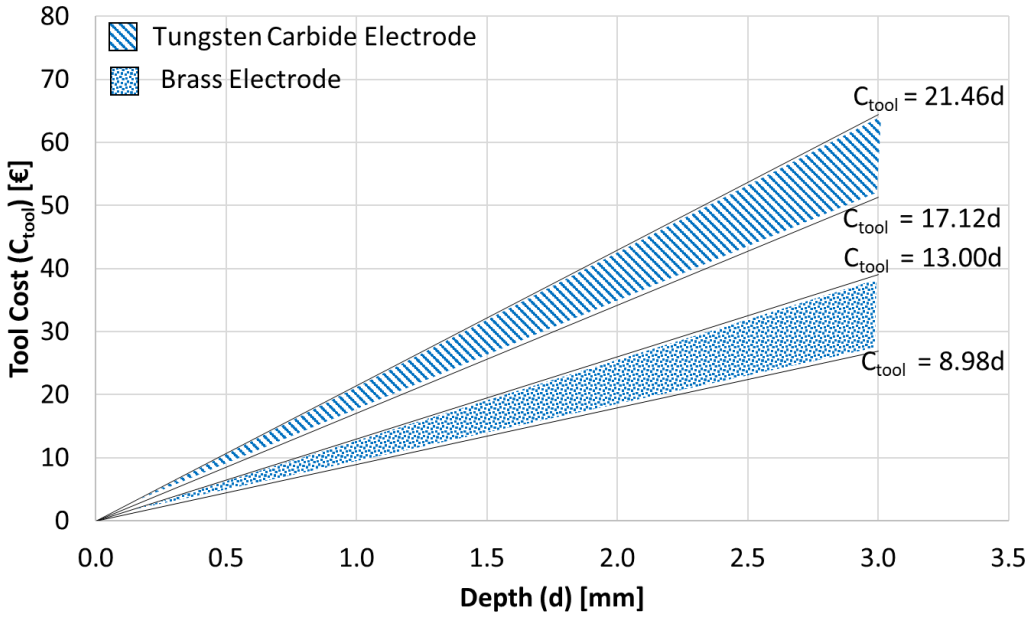

Figure 3.5. Tool cost as a function of the drilling depth varying the electrode materials for 100 holes performed on stainless-steel.

Brass has higher tool wear than tungsten carbide but it permits to have higher MRR. Despite brass has a high level of tool wear, its low price and its high MRR make it competitive with respect to tungsten carbide. It is important to remark that where the accuracy is required, the tungsten carbide electrode is the best solution. Figure 3.6 shows that when the hole depth increases, the total cost is characterized by constant growth, directly proportional to the depth. In particular, the subtended area of tungsten carbide electrode for stainless-steel plate grows more quickly than the brass electrode ones. Within the limits of the tested conditions, a general scheme for the prediction of the variable cost was obtained.

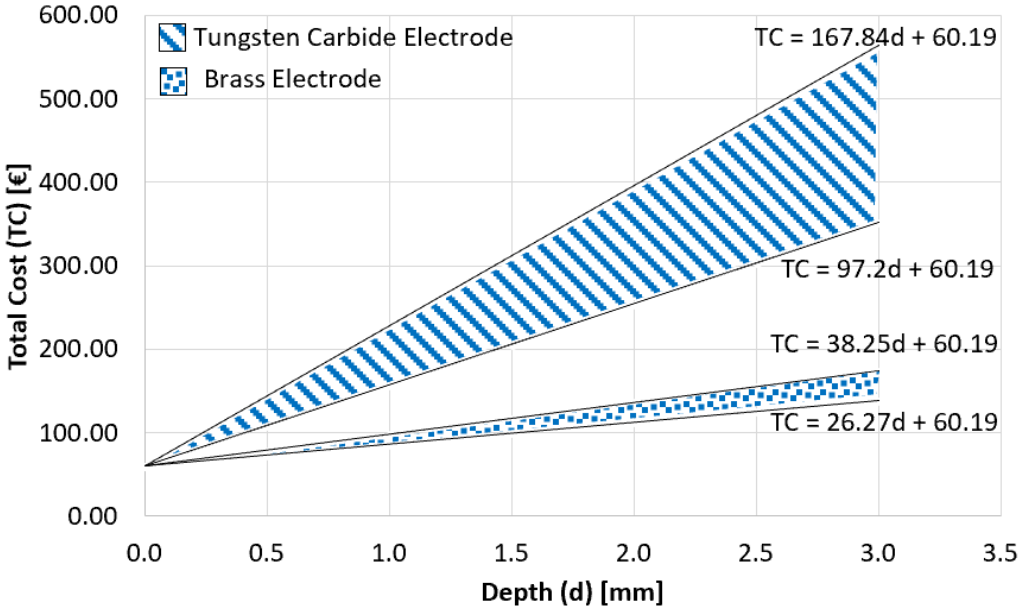

Figure 3.6. Total variable cost as a function of the hole depth for the execution of 100 holes, performed on a stainless-steel plate, varying the electrode material.

3.3.2 Tungsten Carbide

In this section, the experimental campaign performed on tungsten carbide plates was considered. The same hypothesis of the case study conducted on stainless-steel were assumed:

- Machining setup was equal to 1.5 h (start-up, cantering, preparation of electrode and workpiece, setup process parameters);
- Operator's wage was equal to 25€/h;
- The operator monitored the machine only partially during the processing (e.g. 33%).

The progressive machining time (Figure 3.7) and the tool wear (Figure 3.8) technology window were elaborated from the data obtained in a dedicated experimental campaign. The limits of each region were defined by the process conditions, giving rise to the minimum and maximum machining time and tool wear. The behaviours of tungsten carbide and brass electrodes were interpolated by linear curves ($R^2 > 98\%$). Regarding the machining time, since brass electrode has

a higher electrical conductivity and commonly requires higher power discharge, it allows obtaining micro-holes quickly. For the tool wear, tungsten carbide electrode, having a higher melting temperature than brass, was subjected to minor wear; the wide technology window of brass electrode corroborates its sensitivity to the hole depth. Figure 3.9 shows the trend of the labour+utilities cost as a function of the hole depth, obtained considering two electrode materials. For the cost estimation, the execution of 100 holes was considered. Using tungsten carbide electrode, the costs are higher than the ones obtained using the brass electrode, due to the high tool wear.

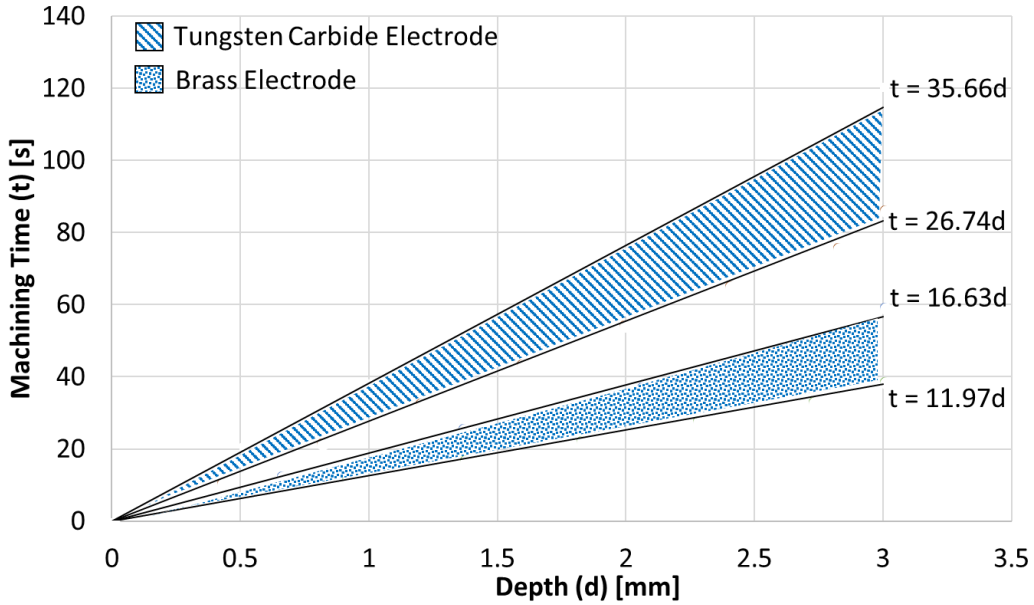

Figure 3.7. Machining time as a function of the hole depth, varying the process parameters, for a single hole on a tungsten carbide plate, for two electrode materials.

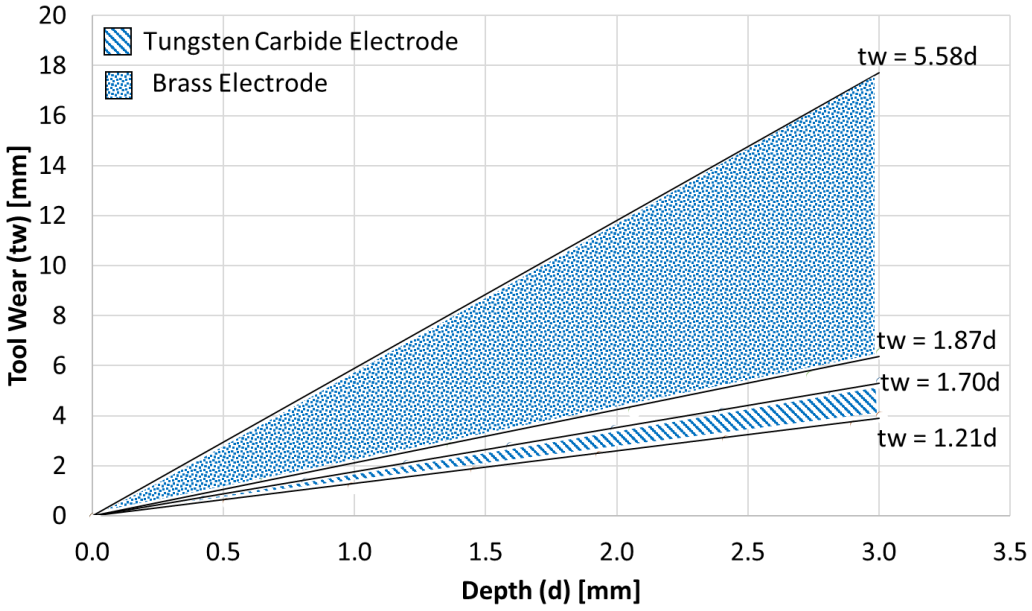

Figure 3.8. Tool wear as a function of the hole depth, varying the process parameters, for a single hole on a tungsten carbide plate, for two electrode materials.

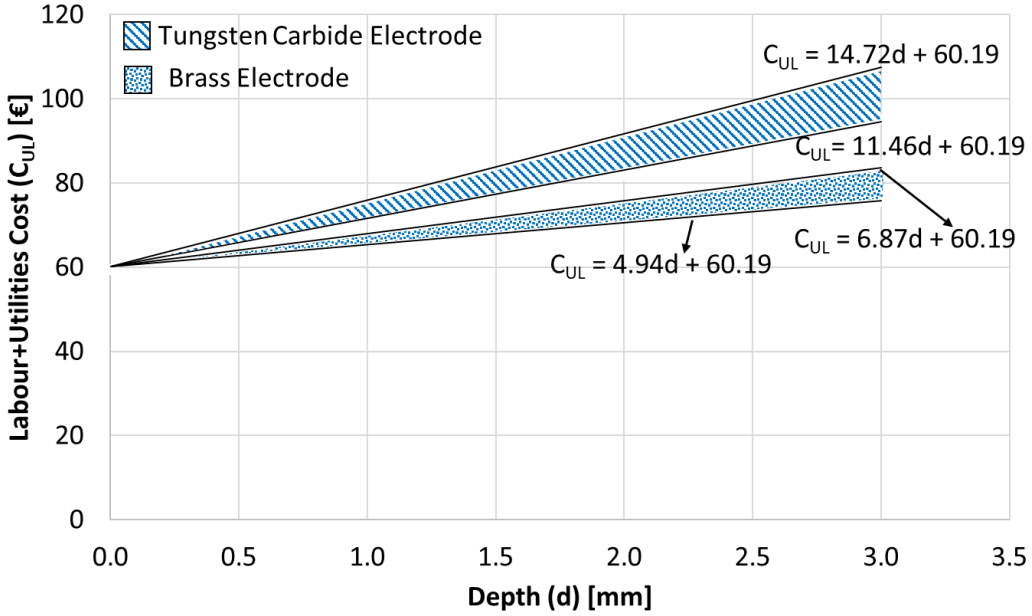

Figure 3.9. Labour cost + utilities cost for 100 holes as a function of the drilling depth, on a tungsten carbide plate, varying the electrode materials.

Figure 3.10 shows the tool cost trend. In general, tool cost using tungsten carbide electrode is higher than the one obtained using a brass electrode. Moreover,

in this case, the two areas are partially overlapped. It means that for a few technologies, from the tool cost point of view only, there are no differences using the two electrode materials.

For the machining of the tungsten carbide plate (Figure 3.11), the total cost has a smaller slope than the other machining and, in general, the total cost for the machining on stainless-steel plate is higher than the total cost for the machining on tungsten carbide plate.

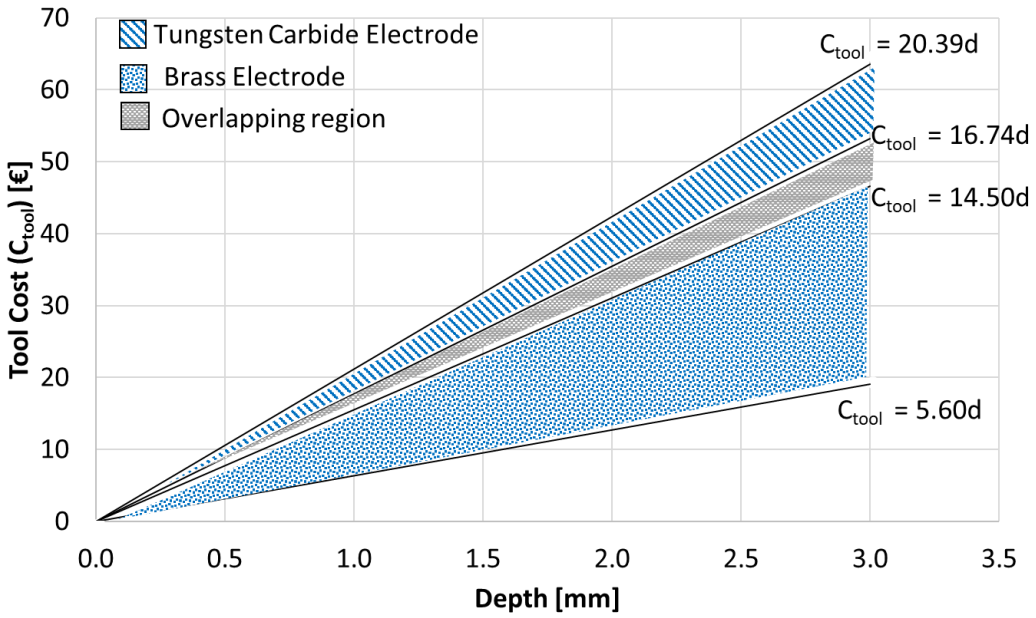

Figure 3.10. Tool cost for 100 holes as a function of the drilling depth, performed on a tungsten carbide plate, varying the electrode materials.

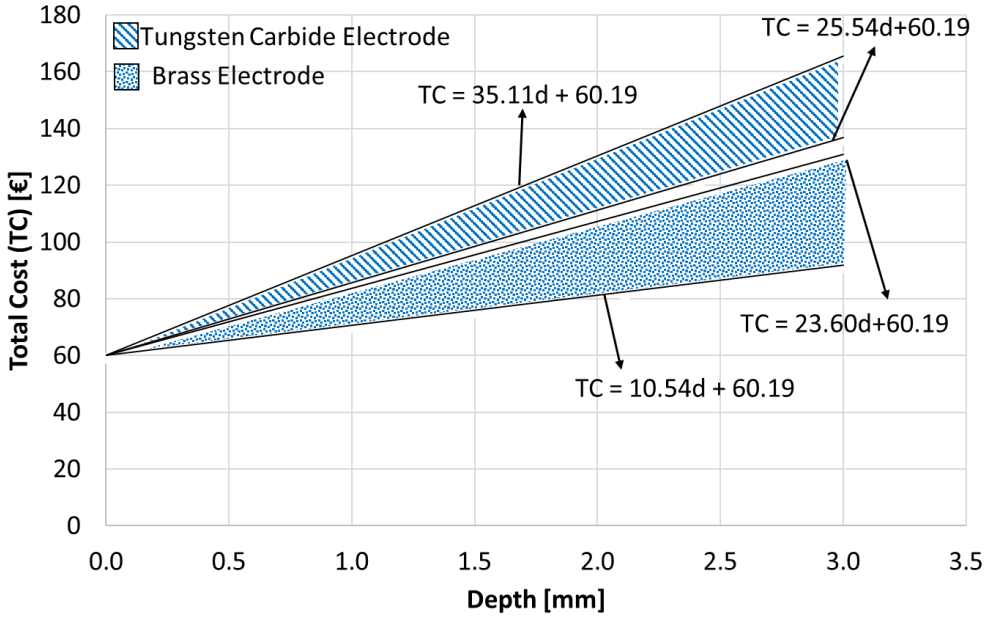

Figure 3.11. Total variable cost for the execution of 100 holes as a function of the hole depth, performed on tungsten carbide plate, varying the electrode material.

3.3.3 Comparison

New comparison plots were finally built. These new plots (Figure 3.12 and Figure 3.13) represent the windows in which machining time and tool wear vary during the machining for some sampling depth when the machining technology changes. In this specific case, a depth equal to 1-2-3-mm is considered.

The plots show how the variability changes when the hole depth increases. A different variability is present in the cost estimation. In particular, in all cases, the wide of the window changes but it always increases when hole depth grows.

Considering the machining time, it is possible to observe that the variability of machining performed on tungsten carbide plates by tungsten carbide electrode is smaller than the machining performed on stainless-steel plates. The tungsten carbide electrode wear has the same variability in both machining conditions. On the contrary, the situation of the brass electrode wear is very different: if the machining is performed on a tungsten carbide plate, the window will be wider than the previous machining. The tool wear is almost five times higher than the previous one.

Figure 3.14 shows a total cost comparison as a function of machining depth for all the combinations of workpiece and electrode materials. The use of tungsten carbide electrode for machining the stainless-steel plates is the most expensive condition with high variability for each depth. The other combinations (workpiece-electrode material) have a similar width and the window covers an analogue range of cost.

As a general remark, it is possible to state that the electrical process parameters have a remarkable influence on the performance indexes (tool wear and machining time) and consequently on the machining cost. The same consideration can be done for the combination of workpiece and tool materials. Anyway, when the problem is limited to a specific workpiece material, the selection of the tool material represents a very important factor for the minimization of machining time, wear, and costs. Based on these considerations, Brass electrodes results to be much more performing than tungsten carbide electrodes, at least in terms of machining time and cost. On the contrary, it is possible to demonstrate that, in general, other hard metal electrodes (e.g. tungsten carbide) give much better results in terms of geometry accuracy and surface finishing [39,103,104]. Furthermore, for some micro manufacturing or ultra-precise applications, hard metal electrodes represent the best solution, because of their mechanical properties (e.g. hardness and rigidity). Then, the electrode material and process conditions can be properly selected only once a precise objective function is defined.

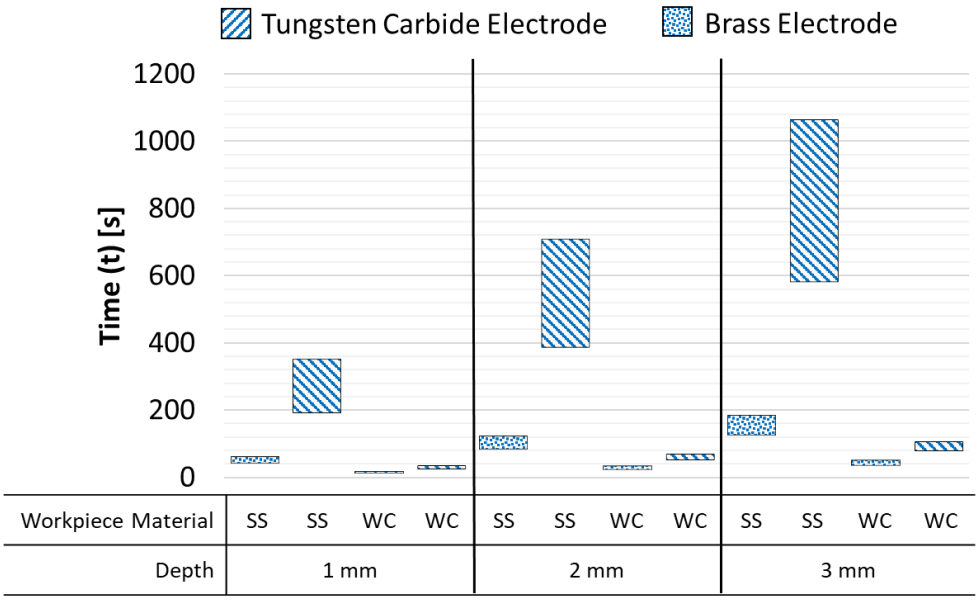

Figure 3.12. Machining time comparison as a function of the machining depth for all the combination workpiece-electrode.

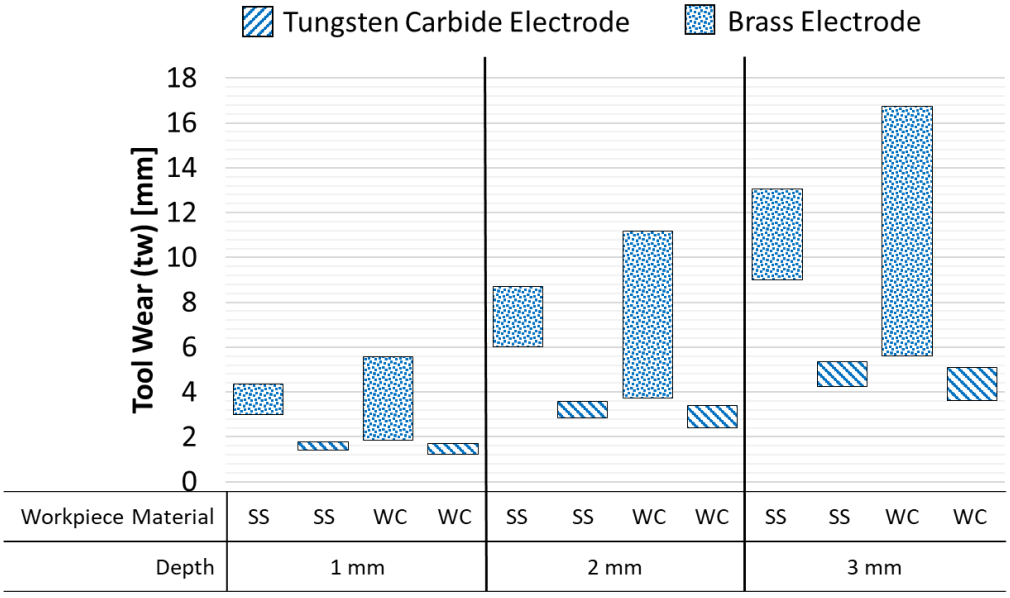

Figure 3.13. Tool wear comparison as a function of the machining depth for all the combination workpiece-electrode.

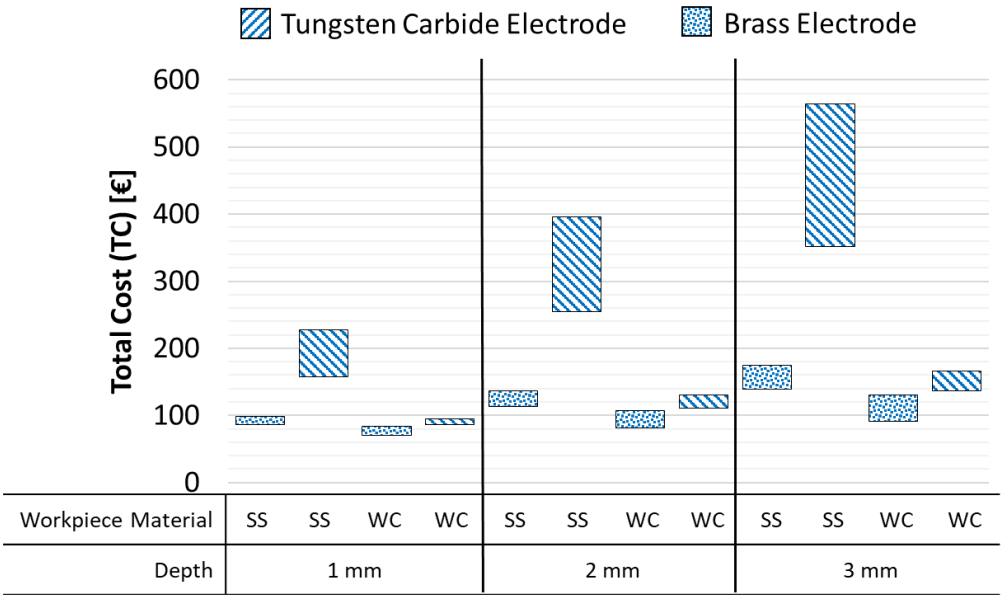

Figure 3.14. Tool wear comparison as a function of the machining depth for all the combination workpiece-electrode.

3.4 Conclusions

A model for the cost estimation of μEDM drilling, considering both fixed and variable costs, was presented. To demonstrate the capability of the model, two case studies were considered, taking into account only variable costs. In particular, micro holes on stainless-steel and on tungsten carbide plates, using two types of electrode materials, varying the electrical process parameters, were performed. The effect of the hole depth on the costs was investigated and it was observed that the total cost has a linear trend as a function of the hole depth with a different slope for the two workpiece materials. The total variable costs obtained using tungsten carbide electrode resulted to be always higher than that obtained using a brass electrode. Moreover, when stainless-steel workpiece is considered, increasing the hole depth, the cost increases more quickly using tungsten carbide electrode with respect to the brass electrode; for the tungsten carbide workpiece, the difference between the two electrodes is lower. Despite brass electrode has a high level of tool wear, its low price and its high MRR makes it competitive with respect to tungsten carbide one. Brass electrodes resulted to be more performing than tungsten carbide in terms of machining time and cost. Anyway, tungsten carbide electrode, or other hard metal

materials, represent the best choice for some ultra-precise or micro manufacturing applications, as it is possible to observe in Figure 3.15 where the differences in diameters can be easily identified. Plots show the higher dimensions obtained by the machining performed by the brass electrode in comparison to the diameters obtained for holes machined by tungsten carbide tool.

This model can be applied to other combinations of workpiece-electrode materials and can be useful to determine the cost of operation in an industrial field. A change in workpiece/electrode combination and process parameters (with respect to the conditions used for the validation) can give rise to a change in machining time and tool wear windows but do not alter the model validity for the estimation of μEDM machining costs.

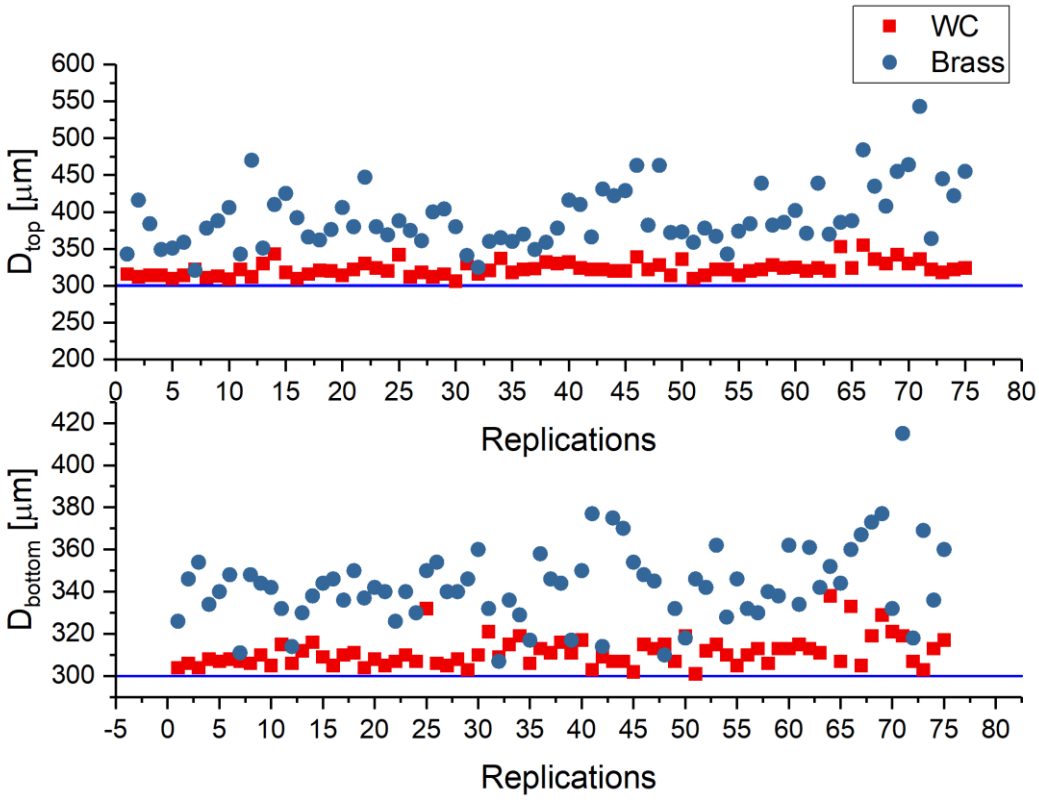

Figure 3.15. Comparison between Top and Bottom diameters for both electrode materials.

CHAPTER 4

SECOND RESEARCH PAPER

Cost index model for the process performance optimization of micro-EDM drilling on tungsten carbide

This chapter is derived from the article "D'Urso, G.; Giardini, C.; Quarto, M.; Maccarini, G. (2017). Cost index model for the process performance optimization of micro-EDM drilling on tungsten carbide. Micromachines, 8(8), p.251-262"
DOI: 10.3390/mi8080251.

I am immensely grateful to the support received from my co-authors. I am responsible for all the changes in this chapter with respect to the published version.

4.1 Introduction

Despite the great development of EDM technology, there is a limited research activity concerning the economic aspects of the process. For example, in literature, a model for predicting the manufacturing cost of the μEDM process was developed in [76] and a comparative analysis of different mathematical methods is made in [77], but, in both these works, there is not a correlation between the optimization of the process performances and the production cost.

The present chapter aims to evaluate the influence of variable process parameters on process performance for the production of micro-holes on tungsten carbide plates. Peak current, open circuit voltage and discharges frequency are varied to achieve low and high limits to identify the technology window suitable for the specific combination between workpiece and electrode materials. Moreover, a cost index model was proposed for the optimization of the process performance. In this way it is possible to correlate the economic and technological aspect of the

μEDM technology and optimize them at the same time, finding the optimal solution for both aspects without making one worse. In this case, only the performances, in terms of quantitative aspects, were considered to develop an objective general index easily applicable by the companies. In this way, the introduction of a penalty term due to the tolerances required by the companies or typical of each machined feature can be avoided without complicating the index estimation.

4.2 Experimental procedure

Experimental tests based on the execution of through micro-holes were carried out using a μEDM machine Sarix SX-200. Tungsten carbide plates having a thickness equal to 3 mm were used as workpiece material. The experimental campaign was carried out by varying several process parameters, namely peak current (I), voltage (V) and frequency (F). Tubular electrodes made of tungsten carbide and brass, having an external diameter equal to 0.3 mm and an internal diameter equal to 0.12 mm, were used. Hydrocarbon oil was used as a dielectric fluid and an internal electrode washing pressure equal to 30 bar was set for all the experiments. For each tool material type, the combination of the process parameters and the experimental sequence were defined based on a Central Composite Design-CCD (Factors: 3, Base runs: 20, Base blocks: 1, Replicates: 5, Total runs: 100, Total blocks: 1). Based on this approach, 15 combinations of process parameters were defined (Table 4.1). Preliminary experimental tests were performed for the identification of a suitable technology window, in terms of minimum and maximum values of peak current, voltage, and frequency, for each combination workpiece–electrode materials. The ranges were defined based on the stability of the electrical discharges, evaluated in a qualitative way from the frequency of short circuit occurred during the tests. The fixed parameters and the ranges of the variable ones differ for the two electrode materials; this solution was used for testing suitable technology windows (in other words, ranges of suitable process parameters) for both materials. The execution order of the experiments was randomized to avoid possible systematic errors. The fixed process parameters used for the tests are

reported in Table 4.2. At the end of each hole drilling operation, the electrode tip was cut using the wire EDM unit, to restore a standard initial condition.

Table 4.1. Combination of Technologies based on CCD for tungsten carbide workpiece.

Electrode	**Tungsten Carbide (WC)**			**Brass (BR)**		
	I [index]	**V [V]**	**F [kHz]**	**I [index]**	**V [V]**	**F [kHz]**
Tech.1	40	110	83	26	120	130
Tech.2	30	100	90	40	100	110
Tech.3	50	100	90	40	140	110
Tech.4	30	120	90	40	100	150
Tech.5	50	120	90	40	140	150
Tech.6	40	93	100	60	120	96
Tech.7	23	110	100	60	86	130
Tech.8	40	110	100	60	120	130
Tech.9	57	110	100	60	154	130
Tech.10	40	127	100	60	120	160
Tech.11	30	100	110	80	100	110
Tech.12	50	100	110	80	140	110
Tech.13	30	120	110	80	100	150
Tech.14	50	120	110	80	140	150
Tech.15	40	110	117	94	120	130

Table 4.2. Fixed process parameters.

Electrode	**Polarity**	**Width [µs]**	**Gap [%]**	**Energy [index]**
Tungsten Carbide	- (neg)	5	20	365
Brass	- (neg)	3.8	5	365

It is important to remark that in Sarix EDM machine, some process parameters are expressed as indexes. In particular, the instantaneous values cannot be set, because the machine presents an autoregulating system. In particular, the peak current is an index defining the maximum current that the pulse can reach. This

index must be set up for respecting the required roughness for the part to be machined and to avoid the burns and coarse melting that would be inevitable with pulses of uncontrolled current. The peak current parameter regulates the maximum amplitude of the long pulses and of the high-power pulses. A similar consideration can be done for the gap: in this case, the value is proportional to the distance between the electrode and the workpiece. The higher the gap index, the higher the actual distance between the two elements. Furthermore, the regulation index represents a certain regulation management algorithm for the setting of the electrode movement. Finally, the energy level is an index that establishes the shape of the pulse identifying a range in which the parameters characterizing the discharges can vary.

4.3 Evaluation of process performances

4.3.1 Performance criteria

In μEDM, the performances criteria usually evaluated consider both process performances and the quality of the machined products. For the quality evaluation, surface roughness and geometry tolerances are the main aspects, usually evaluated by 3D reconstruction of by CMM. Surface roughness is strictly related to the process parameter, in particular to the discharge duration which influences the amount of energy transferred to the workpiece and consequently the dimensions of the crater, a key element for the calculation of roughness. In fact, the main difference between μEDM machining approaches (roughing, finishing, fine-finishing) is the duration of the discharges, long pulses generate poor surface quality while very-short pulses allow obtaining high-quality surfaces. From the process performances point of view, MRR and TWR were selected as performance criteria for the micro-holes drilling. Due to the debris movement and secondary discharges occurring between the hole wall and the electrode side, the machined hole is not perfectly cylindrical; therefore, the diameter was measured at both the top (D_{top}) and the bottom (D_{bottom}) of each hole through an optical measuring microscope with a magnification of 100x.

MRR [mm^3/s] was calculated as the rate of material removed from the workpiece (MRW [mm^3], estimated as the frustum volume as showed in Figure 4.1 (a) with respect to the machining time t [s] recorded by the EDM system Eq. 4.1.

$$MRR = \frac{MRW}{t} = \frac{\pi h\left(D_{top}^2 + D_{top} \cdot D_{bottom} + D_{bottom}^2\right)}{12t} \quad \text{Eq. 4.1}$$

where h is the thickness of the plate.

TWR (Eq. 4.2) was calculated as the ratio between the material removed from the electrode (MRT - Eq. 4.3) and the material removed from the workpiece. The material removed from the electrode tool is measured through a touching procedure executed in a reference position: the length of the electrode is taken before and after the single drilling operation (Figure 4.1 (b)).

$$TWR = \frac{MRT}{MRW} \quad \text{Eq. 4.2}$$

$$MRT = \frac{\pi TW(D_{ext}^2 - D_{int}^2)}{4} \quad \text{Eq. 4.3}$$

where D_{ext} is the external diameter and D_{int} is the internal electrode diameter of the tubular electrode; TW is equal to the length of the electrode worn for each hole.

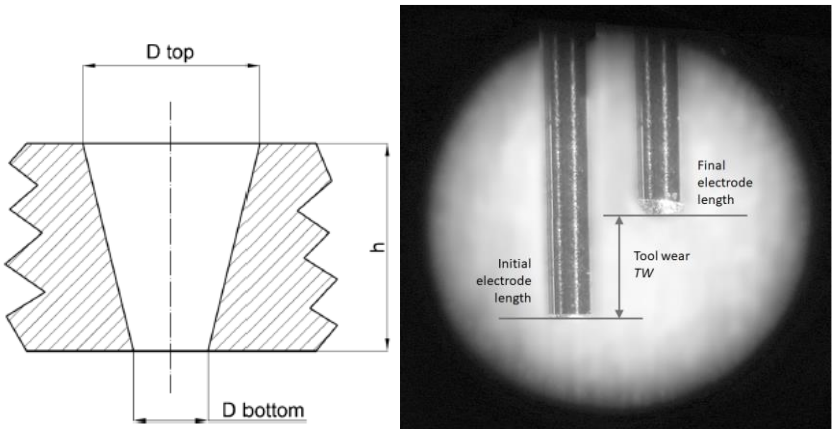

Figure 4.1. Hole geometry scheme (a) and electrode tool wear (TW) definition (b).

4.3.2 Cost Index

In this specific case, the authors choose to develop an index to define the optimal solution for a specific machining approach. In other words, the index can be applied individually to each machining approach. In this way, the surface roughness can be excluded from the index definition, in fact, for each machining approach the surface roughness is defined in a very small range.

In general, the optimal machining performances are expected to be characterized by high MRR and low TWR. Since these two indicators have opposite behavior, they are combined in a single index starting from the machining cost C [€] (Eq. 4.4):

$$C = C_0 \cdot t + C_t \cdot MRT \qquad \text{Eq. 4.4}$$

Where C_0 [€/s] is the cost per time unit of the machining operation, t [s] is the machining duration, C_t [€/mm^3] is the tool cost related to the material removed from the electrode (i.e. the MRT [mm^3]). This index can be expressed as a function of MRR and TWR using Eq. 4.1 and Eq. 4.2 as reported below in Eq. 4.5 and Eq. 4.6:

$$t = \frac{MRW}{MRR} \qquad \text{Eq. 4.5}$$

$$MRT = MRW \cdot TWR \qquad \text{Eq. 4.6}$$

Then, the Cost Index per unitary volume of removed material (CI) can be obtained by replacing Eq. 4.5 and Eq. 4.6 in Eq. 4.4:

$$CI = \frac{C}{MRW \cdot C_0} = \frac{1}{MRR} + \frac{C_t}{C_0} \cdot TWR \qquad \text{Eq. 4.7}$$

Eq. 4.7 represents the objective function to be minimized. To describe MRR and TWR data coming from the experiments, the regression equations, as a function of variable process parameters (I, V and F), were used. It is important to remark that these regression equations are different for each combination of workpiece-electrode materials. The minimization of CI, that must be carried out under the physical constraints of I, V and F values, can be expressed as follows:

$$Min\ CI\left(\begin{matrix}Under\\ constraints\end{matrix}\right)\begin{cases} MRR(I,V,F) \\ TWR(I,V,F) \\ I_{min} \le I \le I_{max} \\ V_{min} \le V \le V_{max} \\ F_{min} \le F \le F_{max} \end{cases}$$

To minimize the Cost Index (CI) it is necessary to identify the critical points of the function. In particular, the first partial derivatives $\left(\frac{\partial CI}{\partial I};\frac{\partial CI}{\partial V};\frac{\partial CI}{\partial F}\right)$ were calculated and the critical points were obtained by simultaneously satisfying the equations:

$$Min(CI) = \begin{cases} \frac{\partial CI}{\partial I}(I,V,F) = 0 \\ \frac{\partial CI}{\partial V}(I,V,F) = 0 \\ \frac{\partial CI}{\partial F}(I,V,F) = 0 \end{cases}$$

Since the critical points could be either minimum, maximum or saddle point, the second order partial derivatives $(\frac{\partial^2 CI}{\partial I^2};\frac{\partial^2 CI}{\partial V^2};\frac{\partial^2 CI}{\partial F^2};\frac{\partial^2 CI}{\partial I \partial V};\frac{\partial^2 CI}{\partial I \partial F};\frac{\partial^2 CI}{\partial V \partial I};\frac{\partial^2 CI}{\partial V \partial F};\frac{\partial^2 CI}{\partial F \partial I};\frac{\partial^2 CI}{\partial F \partial V})$ were calculated and the 3x3 Hessian matrix, representing the local curvature of the function in several variables, was built. Hessian matrix is a square matrix of second-order partial derivatives of a scalar-valued function. It describes the local curvature of a function of several variables.

$$H(I,V,F) = \begin{bmatrix} \frac{\partial^2 CI}{\partial I^2} & \frac{\partial^2 CI}{\partial I \partial V} & \frac{\partial^2 CI}{\partial I \partial F} \\ \frac{\partial^2 CI}{\partial V \partial I} & \frac{\partial^2 CI}{\partial V^2} & \frac{\partial^2 CI}{\partial V \partial F} \\ \frac{\partial^2 CI}{\partial F \partial I} & \frac{\partial^2 CI}{\partial F \partial V} & \frac{\partial^2 CI}{\partial F^2} \end{bmatrix}$$

The nature of critical points was defined by calculating the matrix determinant for these points; if the Hessian is positive definite and $\frac{\partial^2 CI}{\partial I^2} > 0$ at a critical point, the function will attain an isolated minimum. In this case, the critical point represents the combination of process parameters I, V and F, minimizing the cost index CI, that is the

most performant material removal rate (MRR) and tool wear ratio (TWR) combination.

4.4 Analysis of the results

The response surface analysis was applied to the experimental results. Figure 4.2 and Figure 4.4 report the P-values derived from ANOVA for tungsten carbide and brass electrode respectively, calculated using Minitab software. The parameters are considered to influence the process when the P-value is less than 2.5% since a confidence interval of 97.5% was used.

As a general remark, all the performance indexes resulted to be influenced by peak current and voltage. In some cases, also the second order parameters and some interactions showed a no negligible effect. The residuals, in all cases, demonstrated to be normally distributed and randomly scattered with an average value near to zero. Figure 4.2 and Figure 4.4 show the residual plots of the data collected about the material removal rate and tool wear ratio, for machining performed by tungsten carbide electrode, while Figure 4.4 and Figure 4.5 for machining performed by a brass electrode.

Figure 4.6 and Figure 4.7 show the main effects plots for MRR and TWR of machining performed by tungsten carbide electrode and brass electrode respectively, as a function of the process parameters; in some cases, a relative maximum can be observed within the defined domain, in other cases, the curves show a progressive monotonous trend in the defined domain. The plot shows that the brass electrode always allows obtaining quickly machining with respect to the tungsten carbide one due to the higher electrical characteristics and the discharge energy transferred during the machining. From the point of view of the TWR brass electrode suffers from higher wear and its variability range is wider with respect to the tungsten carbide one. These aspects are probably correlated to the high electrical conductivity and a low melting point of the brass electrode.

The interaction plots reported in Figure 4.8 show that the TWR obtained by using tungsten carbide electrode is influenced by the interaction between peak current (I) and the voltage (V) and this is confirmed by the P-values (Table 4.4).

The other interaction plots show, according to the P-values reported in Table 4.3-Table 4.6 , the non-influence of the interactions among the parameters on MRR and TWR.

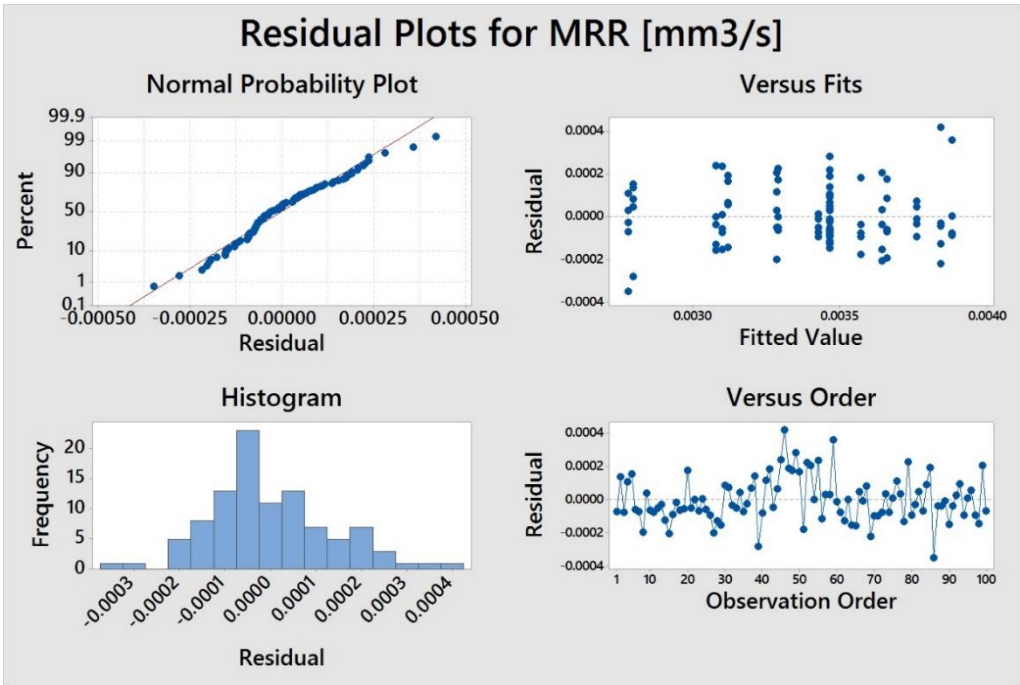

Figure 4.2. Residual plots for MRR obtained using tungsten carbide electrode

Table 4.3. Results of ANOVA for MRR obtained using tungsten carbide electrode.

Tool type	***Tungsten Carbide***		
Performance	**MRR**		
Factors	**MS**	**F-value**	**P-value**
I	0.000007	331.02	**0.000**
V	0.000001	62.28	**0.000**
F	0.000001	37.66	**0.000**
I*I	0.000000	9.50	**0.003**
V*V	0.000000	6.56	**0.012**
F*F	0.000000	0.00	0.981
I*V	0.000000	0.03	0.869
I*F	0.000000	0.52	0.472
V*F	0.000000	1.57	0.213
Error	0.000000		

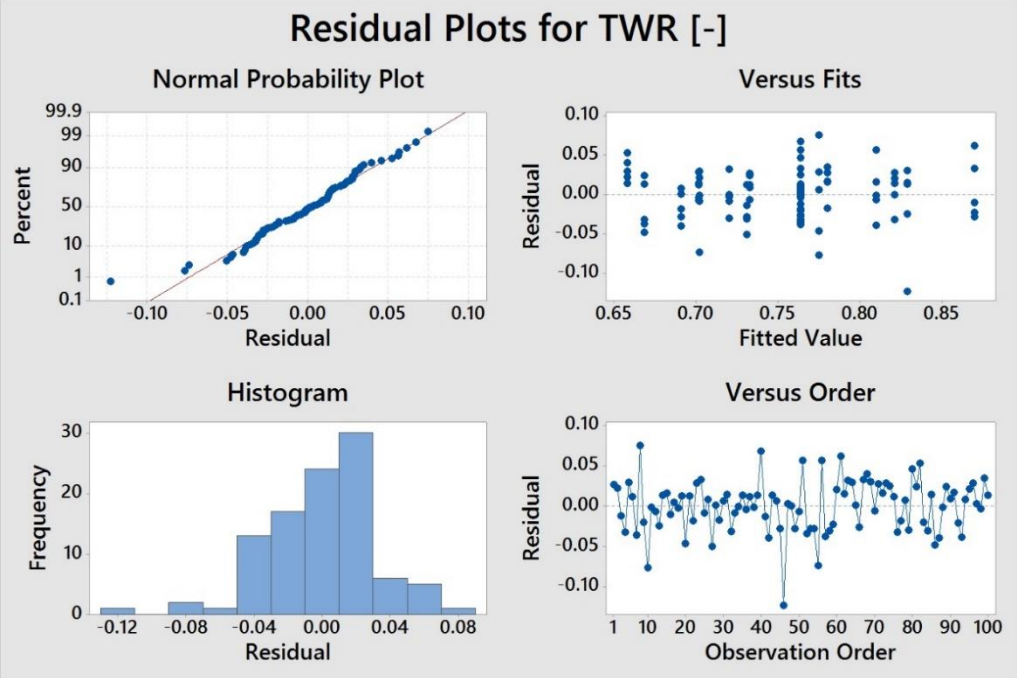

Figure 4.3. Residual plots for TWR obtained using tungsten carbide electrode

Table 4.4. Results of ANOVA for TWR obtained using tungsten carbide electrode.

Tool type	***Tungsten Carbide***		
Performance	**TWR**		
Factors	**MS**	**F-value**	**P-value**
I	0.176793	159.19	**0.000**
V	0.070834	63.78	**0.000**
F	0.021695	19.54	**0.000**
I*I	0.003660	3.30	0.073
V*V	0.000559	0.50	0.480
F*F	0.001649	1.48	0.226
I*V	0.007501	6.75	**0.011**
I*F	0.000976	0.88	0.351
V*F	0.000108	0.10	0.756
Error	0.001111		

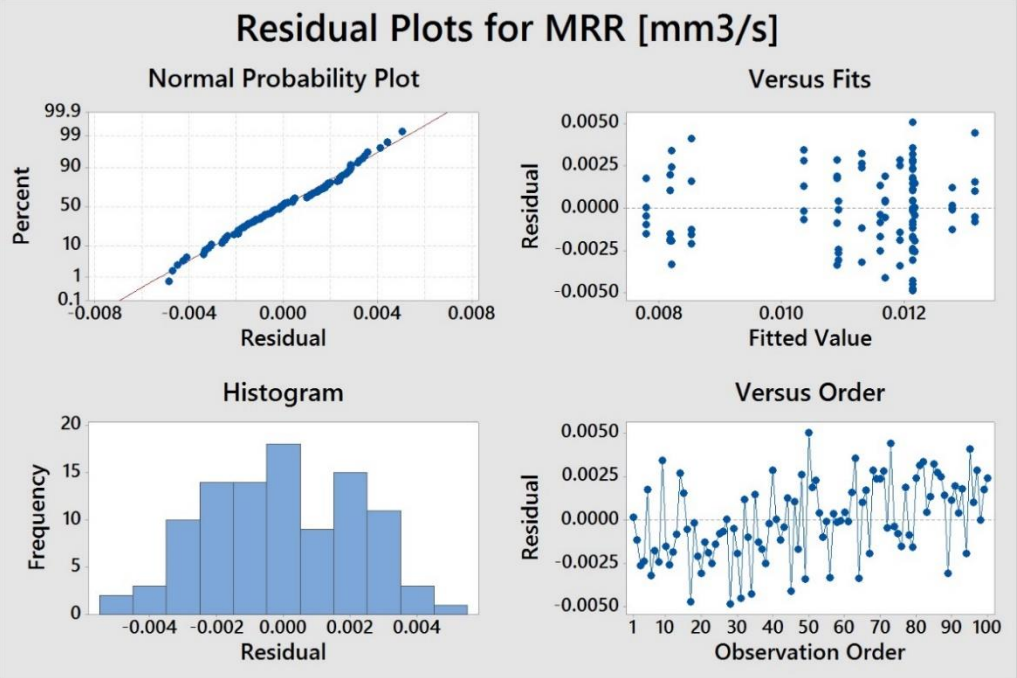

Figure 4.4. Residual plots for MRR obtained using brass electrode.

Table 4.5. Results of ANOVA for MRR obtained using brass electrode.

Tool type	***Brass***		
Performance	**MRR**		
Factors	**MS**	**F-value**	**P-value**
I	0.000060	10.66	**0.002**
V	0.000084	15.08	**0.000**
F	0.000014	2.59	0.111
I*I	0.000052	9.28	**0.003**
V*V	0.000039	6.96	**0.010**
F*F	0.000001	0.10	0.757
I*V	0.000008	1.43	0.234
I*F	0.000001	0.23	0.629
V*F	0.000003	0.52	0.471
Error	0.000006		

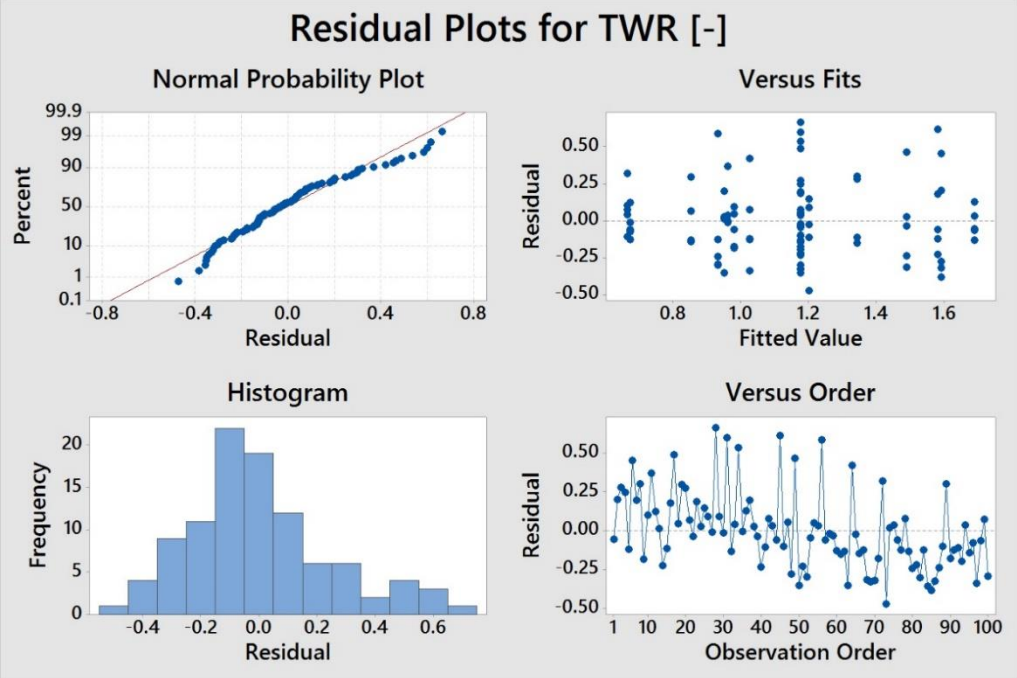

Figure 4.5. Residual plots for TWR obtained using brass electrode.

Table 4.6. Results of ANOVA for TWR obtained using brass electrode.

Tool type	***Brass***		
Performance	**TWR**		
	MS	**F-value**	**P-value**
I	5.07752	75.62	**0.000**
V	1.86666	27.80	**0.000**
F	0.37869	5.64	**0.020**
I*I	0.01835	0.61	0.602
V*V	0.01030	0.27	0.696
F*F	0.09167	0.15	0.246
I*V	0.14186	2.11	0.150
I*F	0.04143	0.62	0.434
V*F	0.10797	1.61	0.208
Error	0.06715		

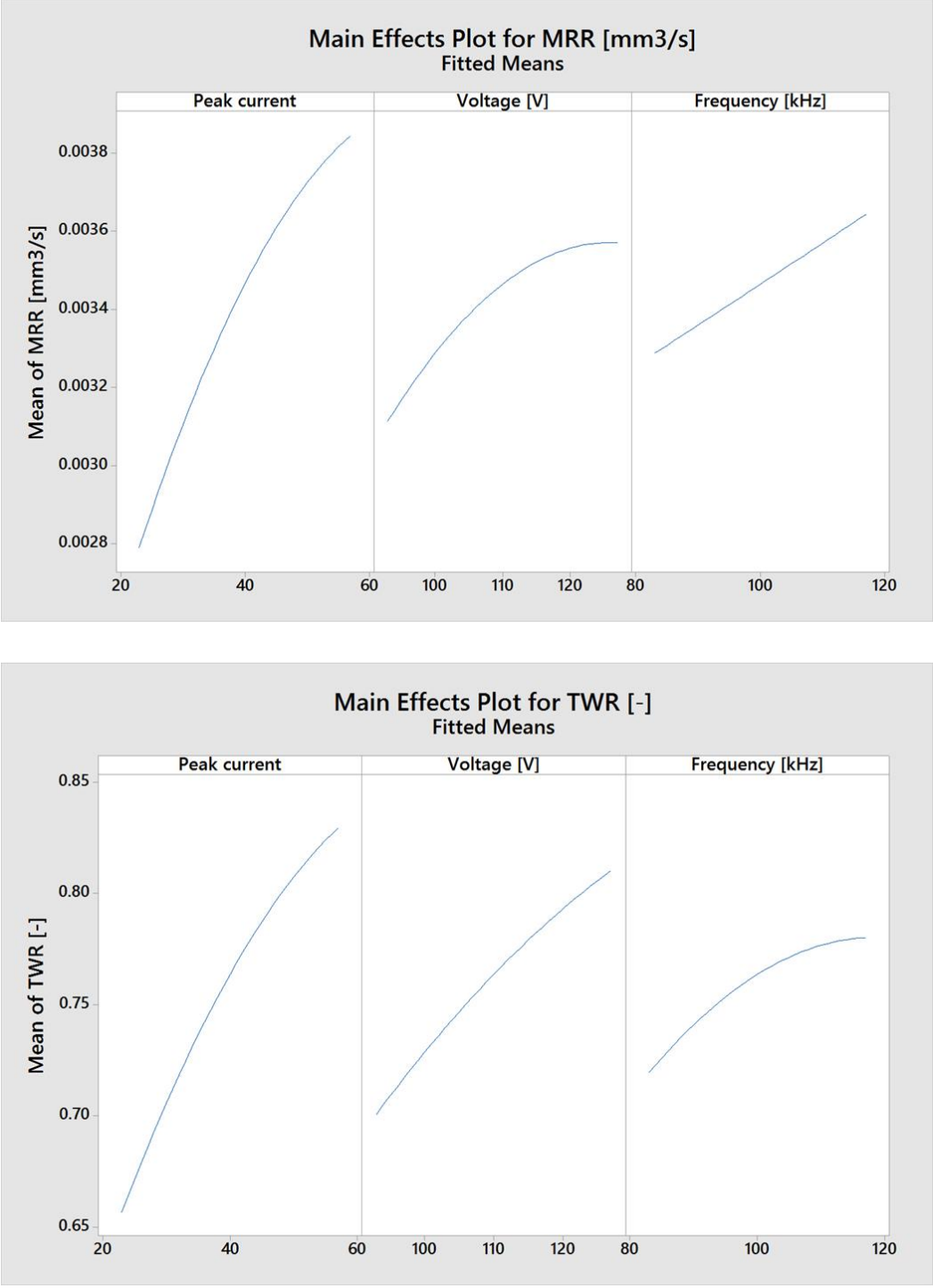

Figure 4.6. Main effects plots for MRR and TWR for tungsten carbide electrodes.

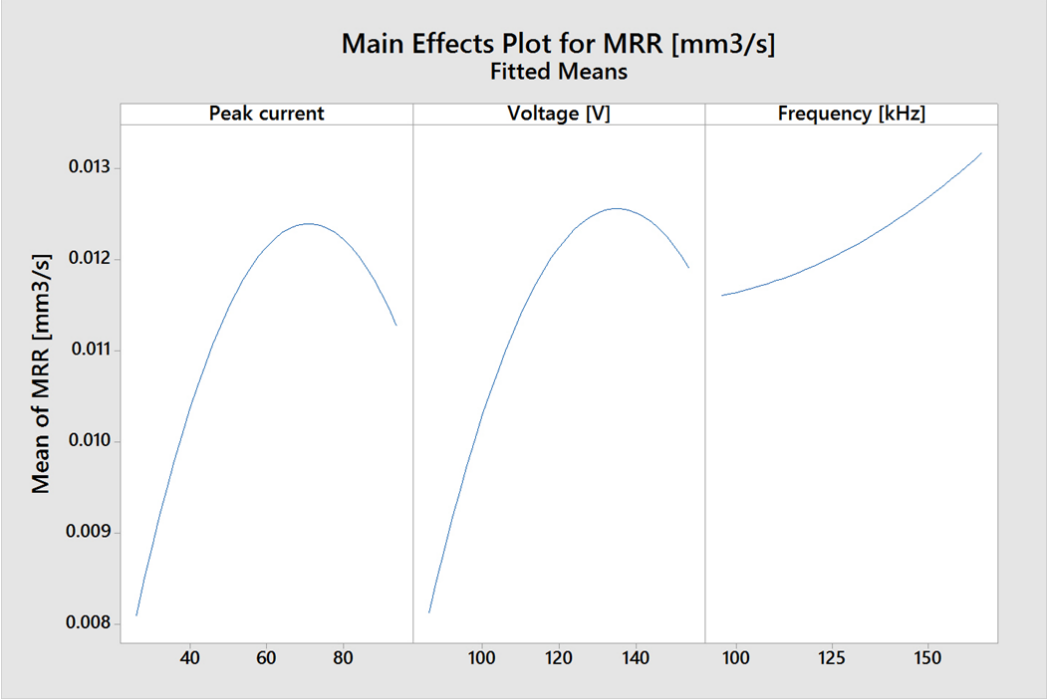

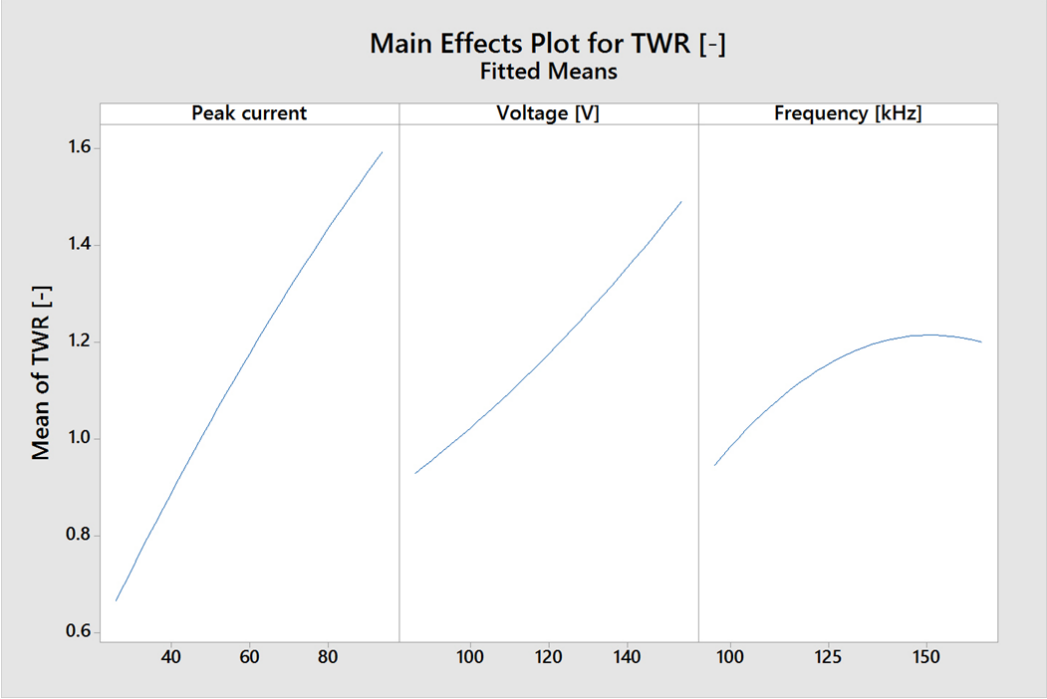

Figure 4.7. Main effects plots for MRR and TWR for brass electrodes.

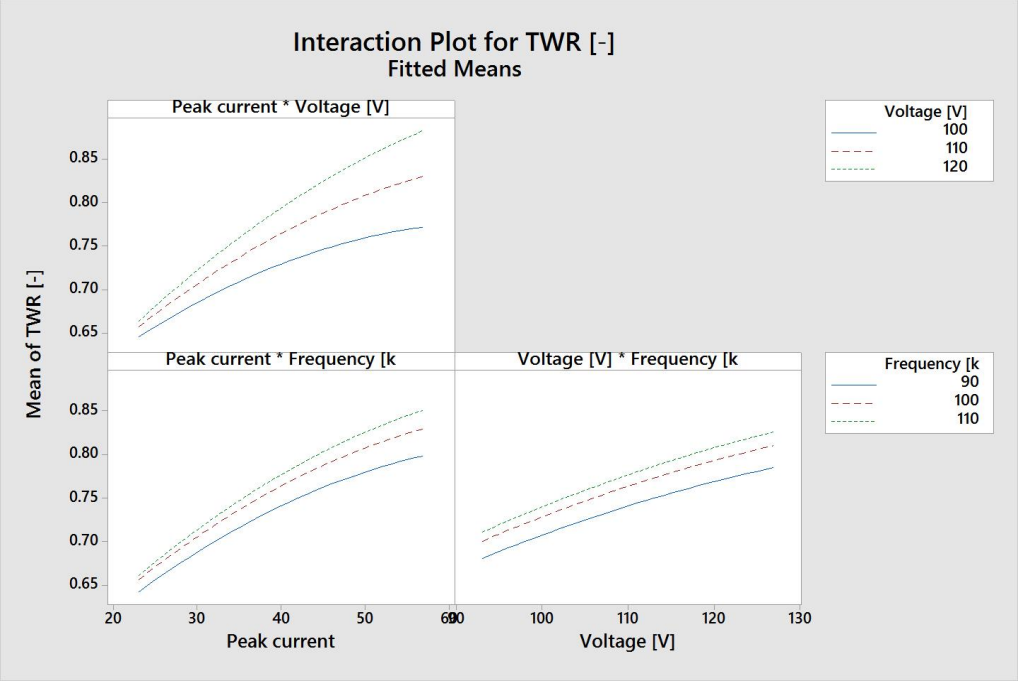

Figure 4.8. Interaction plots for TWR obtained by tungsten carbide electrode.

4.5 Estimation of CI

4.5.1. Tungsten carbide electrode

As already said, the cost index function to be minimized is (as reported in Eq. 4.7):

$$CI = \frac{1}{MRR} + \frac{C_t}{C_0} \cdot TWR \qquad \text{Eq. 4.7}$$

The response surface analysis returned, as a result, the regression equation in coded units of MRR (Eq. 4.8) and TWR (Eq. 4.9) as a function of the process parameters in which the influencing factors and interactions are considered:

$$MRR = 0.003466 + 0.000310I + 0.000134V + 0.000105F - 0.000051I^2 - 0.000042V^2 \qquad \text{Eq. 4.8}$$

$$TWR = 0.76367 + 0.05088I + 0.03221V + 0.01782F + 0.01369VI \quad \text{Eq. 4.9}$$

In this specific case, the estimated tool cost is about 1.90 €/mm^3, while it was assumed that the cost per hour of the machine is equal to 70 €/h, corresponding to C_0 equal to 0.019 €/s. C_0 is the average cost to which some surveyed companies sell their EDM work time.

Moreover, the CI equation must be minimized according to the following constraints:

$23 \leq I \leq 57$

$93V \leq V \leq 127V$

$83kHz \leq F \leq 117kHz$

The critical points are identified solving the system of equations given by the first order partial derivatives of CI equal to zero. The critical points nature is defined by the estimation of Hessian matrix determinant.

By carrying out all the calculus, it is possible to find the point in coded units (I = 1.7; V = 0.496; F = 1.7) is an absolute minimum for the CI function. This means that the cost index is minimized for the process parameters equal to:

$$I = 57; V = 115\ V; F = 117\ kHz.$$

Figure 4.9 shows the surface generated corresponding to CI as a function of I and V while considering the optimal value for F = 117 kHz. It is possible to observe that the optimal conditions are obtained in correspondence with the limits of the technological window (maximum values of process parameters suitable for this applications). The figure could suggest that the process parameters range is not large enough to find the optimum, but the constraints of the process parameters

were defined based on preliminary test for identifying the best range in which the machining do not generate short circuits and the trend of discharges and voltage is constant. Thus, the optimal solution is on the surface bound and this could make think that the parameters range was not larger enough. If a larger process parameters rage was taken into account, perhaps, the optimal solution generates lower cost and higher process performances, but at the same time, the machining quality was lower in terms of efficiency and short circuits.

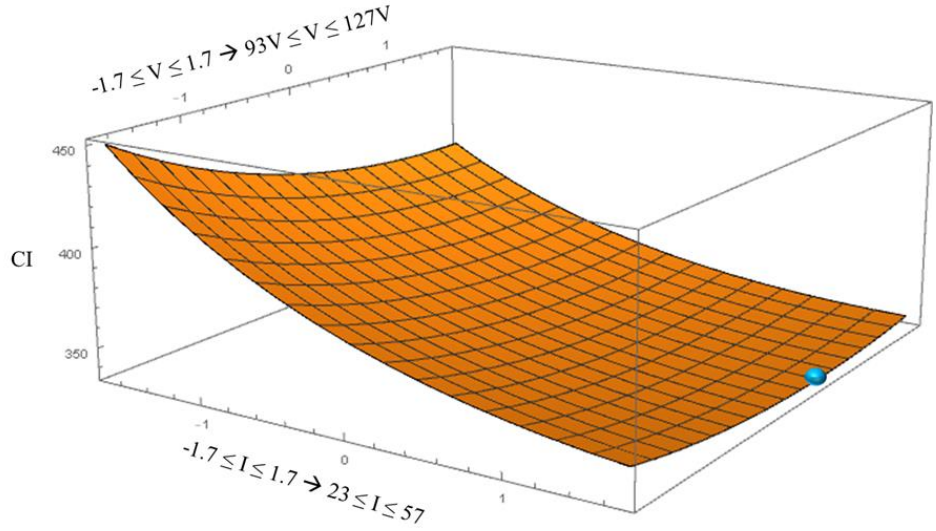

Figure 4.9. Surface plot of CI for machining performed by tungsten carbide electrode.

4.5.2 Brass electrode

For the machining performed by brass electrode the regression equations in coded units are, obviously, different with respect to the tungsten carbide ones, and in particular:

$$MRR = 0.12144 + 0.000934I + 0.001111V - 0.000849I^2 - 0.0007352V^2 \quad \text{Eq. 4.10}$$

$$TWR = 1.1774 + 0.2727I + 0.1653V + 0.0745F \quad \text{Eq. 4.11}$$

In this case, the estimated tool cost is about 0.41 €/mm^3 while C_0 remains equal to 0.019 €/s and the constraints are expressed as follows:

$$26 \leq I \leq 94$$

$$86V \leq V \leq 154V$$

$$96kHz \leq F \leq 160kHz$$

For the brass electrode, the system of first partial derivatives and the estimation of Hessian matrix determinant resulted in a minimum in the following point: I = 0.011; V = 0.378; F = -1.7 in coded units. This means that the cost index is minimized for the process parameters equal to:

$$I = 60; V = 128\,V; F = 96\,kHz.$$

Figure 4.10 represents CI behaviour as a function of I and V while considering the optimal value of F = 96 kHz.

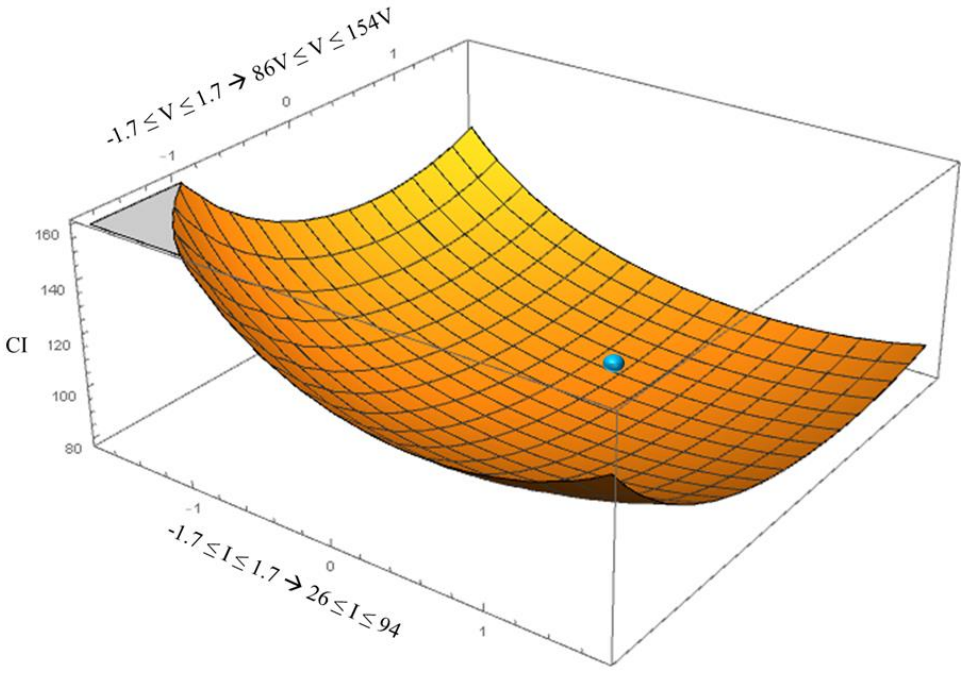

Figure 4.10. Surface plot of CI for machining performed by the brass electrode.

4.6 Conclusions

In this chapter, the influence of I, V, F and of their interactions on the process performance in μEDM drilling, was analysed and presented in terms of MRR and TWR. The experiments have been designed according to the CCD method. Since the optimal machining configuration is expected to be characterized by high MRR and low TWR, a cost index (CI), able to combine these two opposite effects, has been defined. This index is based on both the tool cost and the cost per time unit of the machining operation where MRR and TWR have been expressed by means of the regression equations identified with the Response Surface Method. The minimization of the cost index allowed to identify the optimal working conditions.

The experiments showed that the ranges of the process parameters and their effects greatly depend on the materials combination. For this reason, also the cost index equation significantly differs and must be written for the specific workpiece-electrode materials couple.

The algorithm developed in this part of the project takes into account two important aspects of the productivity chain. Specifically, the economic aspects were correlated to the technological characteristics of the μEDM process. This index allows minimizing the productivity cost optimizing the process performances as a function of the main process parameters. As previously reported, it was applied to two different case studies to validate it, but it was developed with the possibility to be applied to any configuration of the EDM process. In fact, adjusting the evaluation way of the technology window, the algorithm could be used to optimize not only the drilling process (such as demonstrated in the case studies) but also the sinking and wire EDM.

CHAPTER 5

THIRD RESEARCH PAPER

Study on Zirconium Boride reinforced with silicon carbide fibres machined by micro Electrical Discharge Machining

This chapter is derived from the working paper "Quarto, M.; Bissacco, G.; D'Urso, G. (2018). Study on Zirconium Boride reinforced with silicon carbide fibres machined by micro Electrical Discharge Machining"

I am immensely grateful to the support received from my co-authors, in particular to prof. G. Bissacco for the opportunity to increase my knowledge and expertise at the Technical University of Denmark, where this part of the research was performed.

5.1 Introduction

Melting point over 3000°C, low theoretical density, high electrical conductivity, fracture toughness, chemical stability in severe condition, make ZrB2 a very attractive candidate for application in critical conditions such as refractories crucible, high-temperature structural application in aerospace, electrical and microelectronics devices, nozzles or armour. In addition, thanks to the high wear resistance, Zirconium Boride is a good option for sinking EDM electrodes production. The structural, physical and thermodynamic properties are summarized in Table 5.1.

The apparent density of this material is very low, usually about 85% vol., because of the high level of porosity of the structure. For this reason, the use of single-phase materials is not sufficient for high-temperature structural applications. Thus, many non-reactive additives such as niobium (Nb), Vanadium (V), Carbon (C), disilicates and silicon carbide (SiC) are evaluated to improve the relative

density and the mechanical and physical properties. Among these additives, SiC is one of the most used and it seems to be the most valuable, firstly to enhance resistance oxidation by the formation of borosilicate glass, secondly to promote densification by restricting the growth of diboride grains, and lastly to lower their sintering temperature [85,90,91]. Usually, the addition of an additive is performed by a hot pressed process, which, despite the high pressures required (30-50 MPa), allows to reduce the densification temperature [92,93].

Table 5.1. ZrB_2 characteristics [90,94,105].

Property	**ZrB_2**	
Crystal system space group	Hexagonal	
Density	6.119	g/cm^3
Melting temperature	3245	°C
Young's modulus	489	GPa
Hardness	23	GPa
Coefficient of thermal expansion	$5.9 \cdot 10^{-6}$	K^{-1}
Heat capacity at 25°C	48.2	J/(mol·K)
Electrical conductivity	$1.0 \cdot 10^{7}$	S/m
Thermal conductivity	60	W/(m·K)

Studies related to the microstructure and the characterization of ZrB2 sintered with a different compound fraction of silicon carbide (SiC) demonstrated that a high additive percentage reduces the grain size down to 2-3 μm and allows to increase the flexural strength to 700-1000 MPa [94]. In particular, the addition of 10% vol. of SiC, lets to reach 93.2% of density and it is enough to limit the grain growth and maximize the strength. Specifically, previous works affirmed that the addition of 20% of SiC generates the best combination of oxidation resistance and mechanical behaviour [95–98].

In general, materials characterized by good mechanical properties tend to be really difficult to be processed and ceramic materials are not an exception. Two

main categories of machining are effective for processing of this kind of materials: the abrasive particle processes (such as grinding, ultrasonic machining, and abrasive water-jet) and the thermal processes (such as laser technology and electrical discharge machining-EDM) [99].

In this study, μEDM technology is applied because of the promising results of earlier researches in the field [99,106]. Since many research works demonstrated the impressive characteristics of ZrB_2, it was chosen such as a base matrix for this study, and SiC was selected as the additive material. In the third part of the Ph.D program, the machinability of ZrB_2 reinforced by SiC fibres was studied. In particular, different fractions of additive were taken into account to evaluate the stability and repeatability of the μEDM process from both performance and geometrical point of view. Aim of this part is to define if the application of μEDM technology can be a good option for machining particular UHTCs, taking into account ZrB_2-based composites doped with different additive fractions and to identify if the presence of the second phase affects the process performances. The economic aspects in terms of productivity costs were considered in the last part of this chapter.

5.2 Materials

The materials investigated in the present work were prepared by hot-pressed ZrB_2 with different percentage of non-reactive additive to reduce the porosity level and to improve their characteristics. Commercial powders were used to prepare the ceramic composites: ZrB2 Grade B (H.C. Starck, Goslar, Germany), SiC HI Nicalon-chopped fibres, Si:C:O = 62:37:0.5, characterized by 15 μm diameter and 300 μm length. The powder mixtures were ball milled for 24 h in pure ethanol using silicon carbide media. Subsequently, the slurries were dried in a rotary evaporator. Hot-pressing cycles were conducted in low vacuum (∼100 Pa) using induction-heated graphite die with the uniaxial pressure of 30 MPa during the heating and increased up to 50 MPa at 1700 °C. The maximum sintering temperature was set

on the basis of the shrinkage curve and a free cooling followed [107]. Table 5.2 shows the relative density of the samples taken into account.

Table 5.2. The relative density of the raw materials considered.

Materials	Density	Sample Name
ZrB_2	~83%	ZrB
ZrB_2 + 5% SiC	~92%	ZrB5
ZrB_2 + 20% SiC	~97%	ZrB20
ZrB_2 + 30% SiC	~91%	ZrB30
ZrB_2 + 50% SiC	~94%	ZrB50

The raw materials were analysed by a Scanning Electron Microscope (SEM). The analysis showed a very clear separation between the base matrix and the non-reactive additive for all additive fractions. The fibres were generally well dispersed into the matrix, still recognizable as an elongated dark structure in backscattered SEM images. Figure 5.1 reports an example of the typical appearance of ZrB5 and ZrB50; it is possible to notice the different aspect related to the additive fraction. The fibres were distributed in a randomized way and the dispersion into all matrices was homogeneous since no agglomeration was observed. As reported in the literature [108,109], the fibres showed a tendency to align their long axis perpendicular to the direction of the applied pressure. The length of the fibres was further reduced from the starting mixture, due to the applied pressure reached during the sintering. In fact, after the preparation, the SiC fibres have dimensions of about 10 μm for diameters and 200 μm in length (Figure 5.3). Characterization of the as-sintered microstructure by Scanning Electron Microscopy coupled with Energy Dispersive X-Ray Analysis (SEM-EDX) was performed. As illustrated in Figure 5.4, there is a clear separation between the base matrix and the additive, evidence that during the sintering process the base matrix and the additive do not undergo chemical reactions.

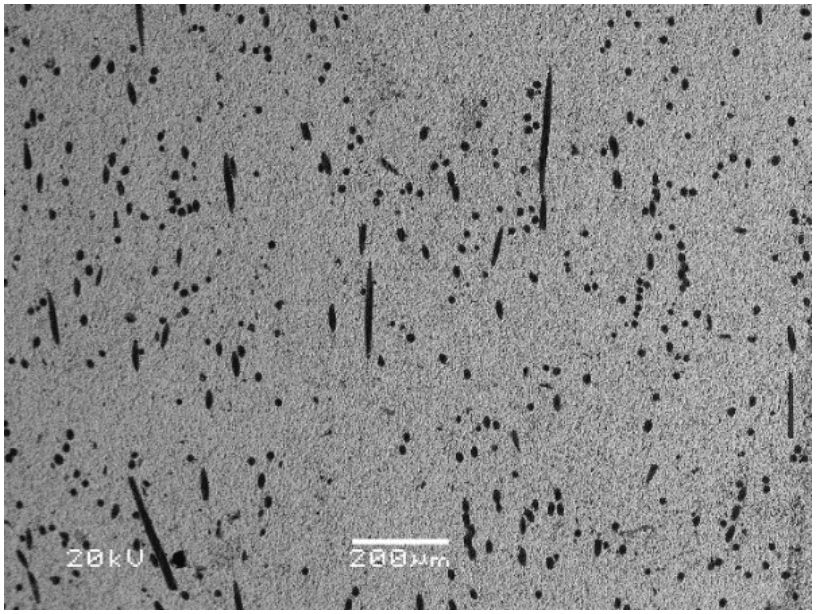

Figure 5.1. SEM backscatter images of typical appearance of ZrB5. Magnification 75x.

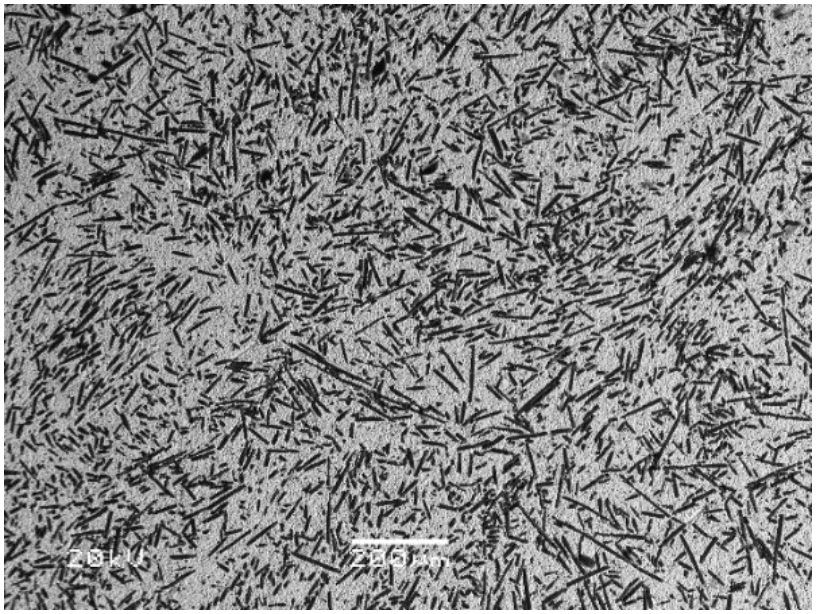

Figure 5.2. SEM backscatter images of typical appearance of ZrB50. Magnification 75x.

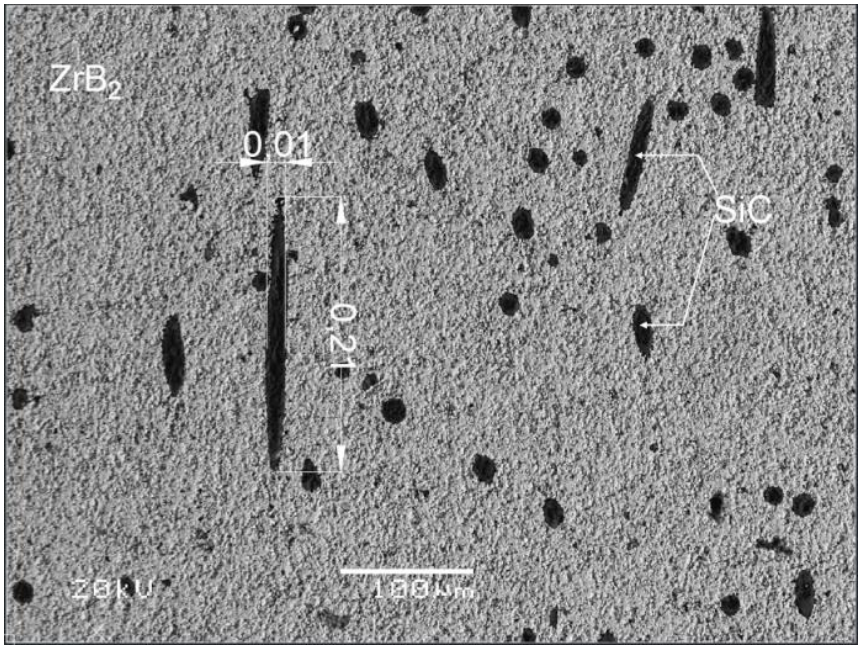

Figure 5.3. SEM backscatter image of fibre dimension, magnification 150x.

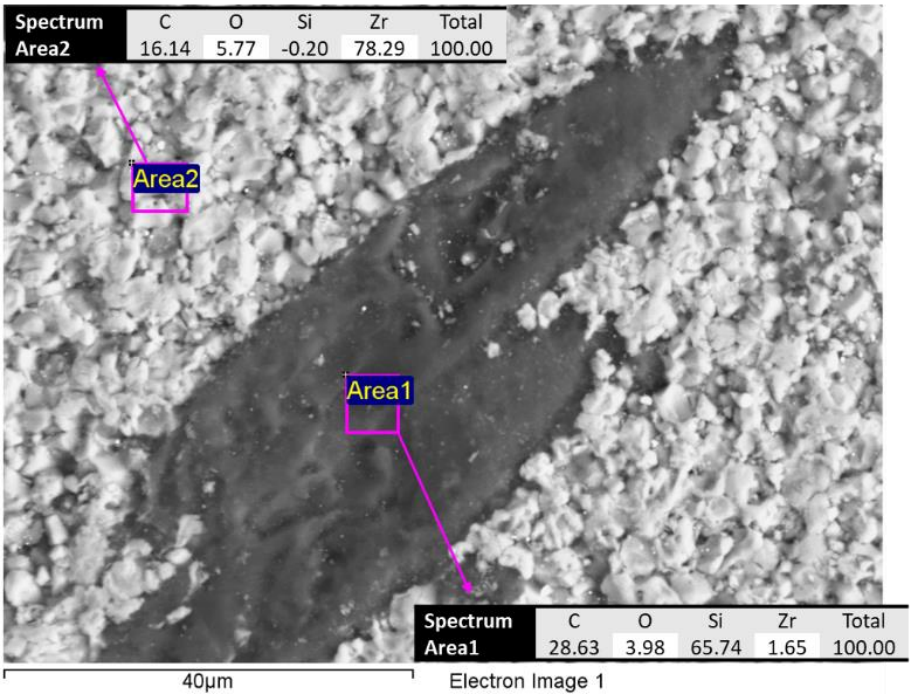

Figure 5.4. Example of an EDS analysis of the base material ZrB5, magnification 1500x.

5.3 Experimental procedure

The test feature selected for the machining experiments was a circular pocket having a diameter equal to 1 mm and a depth of about 200 μm. These micro-features were processed by μEDM milling using a SARIX® SX-200 machine. Solid tungsten carbide electrodes with a diameter equal to 300 μm were used as a tool; while the dielectric fluid was hydrocarbon oil.

The experiments were performed using three different process parameters settings, corresponding to different pulse shapes. It is important to remark that in the Sarix EDM machine, some process parameters such as the peak current and width are expressed as indexes. In particular, the instantaneous values cannot be set, because the machine has an autoregulating system. For this reason, another aspect considered for the evaluation of the stability and repeatability of the process was the distribution of the discharges occurred in the gap between tool and workpiece during the machining. This task was performed using a current probe and a voltage probe to measure and assess the electric current and voltage during machining. A current monitor with a bandwidth of 200 MHz was used to measure and to further characterize the population of the current signals. A Rohde & Schwarz RTO1014 oscilloscope was used to acquire the current waveforms. Furthermore, a Hameg HM8123 programmable counter was connected to counting the discharges occurred during the process. A schematic diagram of the experimental set up is shown in Figure 5.5.

Preliminary tests were performed to define the optimal process parameters for each combination of material and pulse type. The experimental campaign was based on a general full factorial design, featured by two factors: the additive fraction, defined by five levels, and the pulse type, defined by three levels. Different levels of pulse types identify the different duration of the discharges, in particular, level A is referred to long pulses while level C identify the short pulses. Four repetitions were performed for each run.

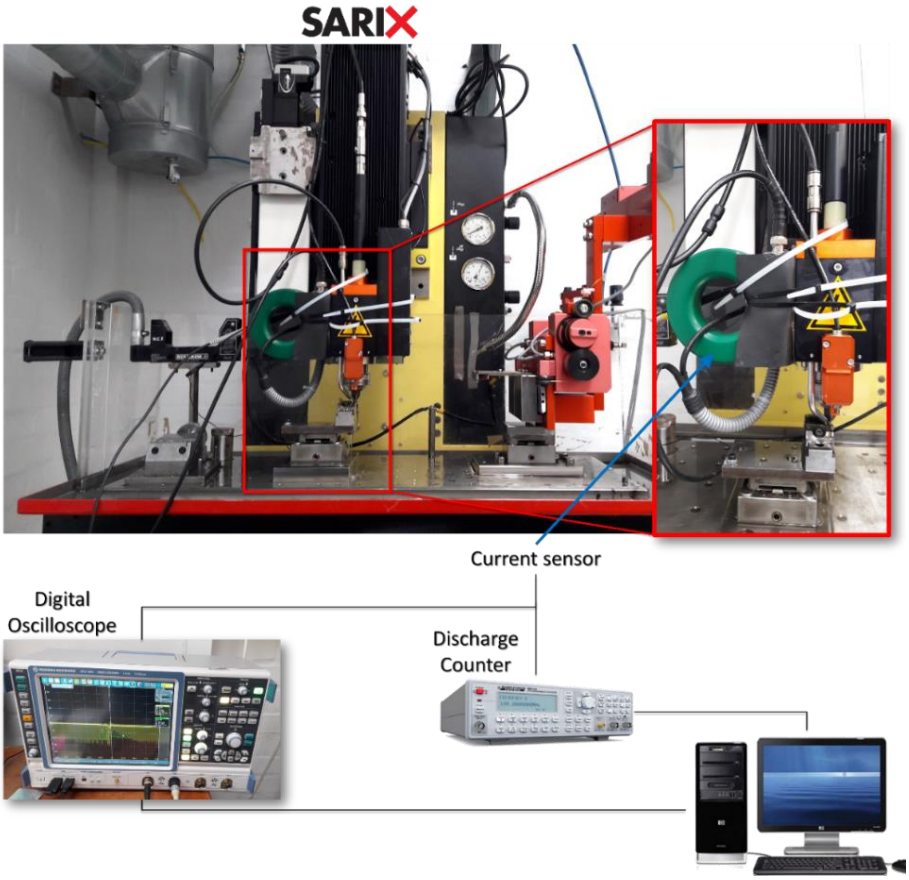

Figure 5.5. A schematic diagram of the experimental procedure.

5.3.1 Discharge population characterization

In this work, the discharge population was characterized in order to determine the trigger level for counting discharges and then to estimate the process performances. For the selected pulse types, combined with each material, discharge populations were characterized by repeated waveform samples of current and voltage signals. The current and voltage probes were connected to the digital oscilloscope having a real-time sample rate of 40 MSa/s. The trigger level on the current signal was set to a low value in order to acquire all discharges. The acquired waveform samples were stored in the oscilloscope buffer and then transferred to a computer. The waveform samples were then processed to extract peak current, voltage, and width. The frequency distribution histogram for the discharges was plotted for each waveform sample. Figure 5.6-Figure 5.10 shows the results obtained about the discharges distribution for all the pulse types combined with all levels of the additive fraction.

As it is possible to observe from the histograms, the discharge samples are well represented by a normal distribution. This means that the discharges are characterized by good reproducibility. Thanks to the discharge characterization it was possible to define the real value of the process parameters. The pulse characteristics of the parameter settings used in the experiments are reported in Table 5.3-Table 5.7.

Table 5.3. Details of pulse type for ZrB.

Material	Pulse Type	Peak Current [A]	Voltage [V]	Width [µs]	Energy per Discharge [µJ]
ZrB	A	29.56	72	0.72	792.16
	B	10.78	94	0.28	101.84
	C	4.81	101	0.06	14.64

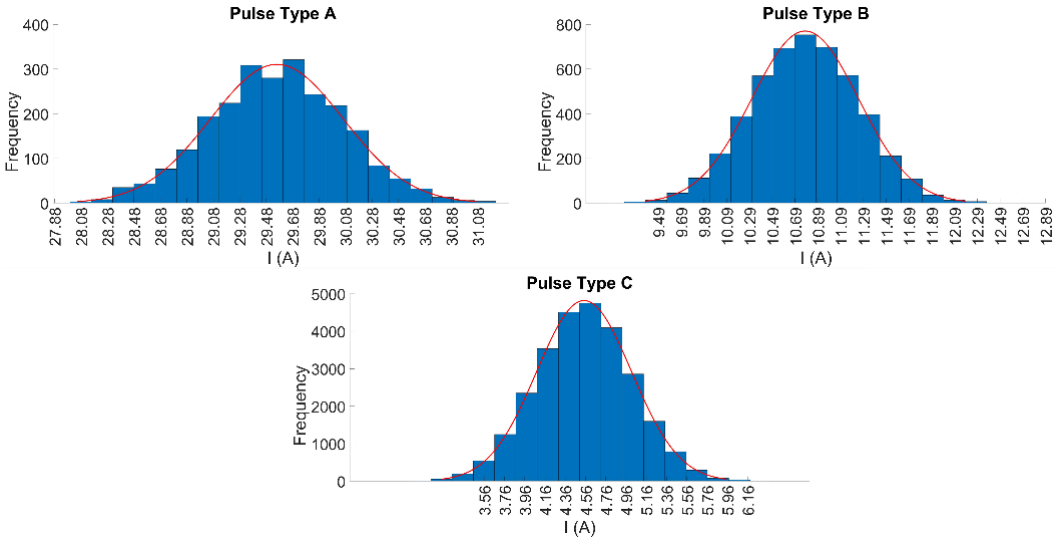

Figure 5.6. Frequency distribution histograms for pulses occurred during ZrB machining.

Table 5.4. Details of pulse type for ZrB5.

Material	Pulse Type	Peak Current [A]	Voltage [V]	Width [µs]	Energy per Discharge [µJ]
ZrB5	A	28.61	73	0.69	844.39
	B	10.84	93	0.32	152.42
	C	4.57	100	0.06	17.60

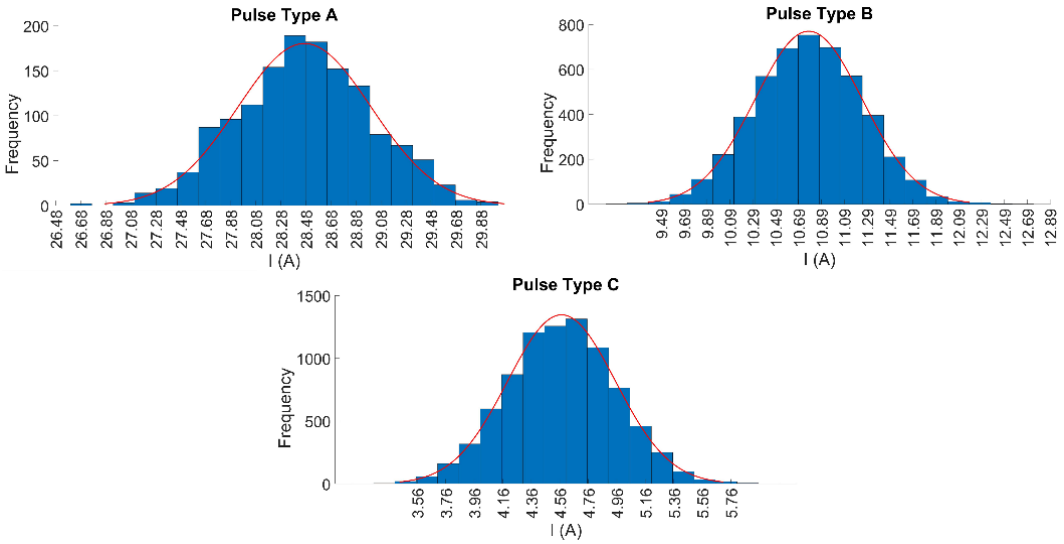

Figure 5.7. Frequency distribution histograms for pulses occurred during ZrB5 machining.

Table 5.5. Details of pulse type for ZrB20.

Material	Pulse Type	Peak Current [A]	Voltage [V]	Width [µs]	Energy per Discharge [µJ]
ZrB20	A	29.44	70	0.70	779.36
	B	10.93	93	0.33	150.30
	C	4.61	101	0.06	14.73

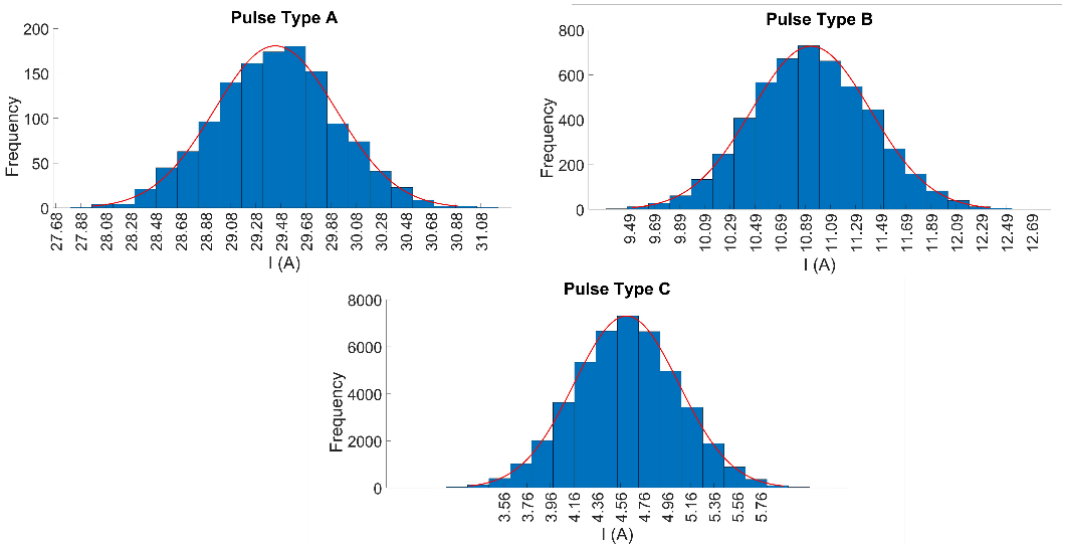

Figure 5.8. Frequency distribution histograms for pulses occurred during ZrB20 machining.

Table 5.6. Details of pulse type for ZrB30.

Material	Pulse Type	Peak Current [A]	Voltage [V]	Width [µs]	Energy per Discharge [µJ]
ZrB30	A	29.09	73	0.67	784.99
	B	10.56	98	0.32	161.00
	C	4.45	101	0.06	21.41

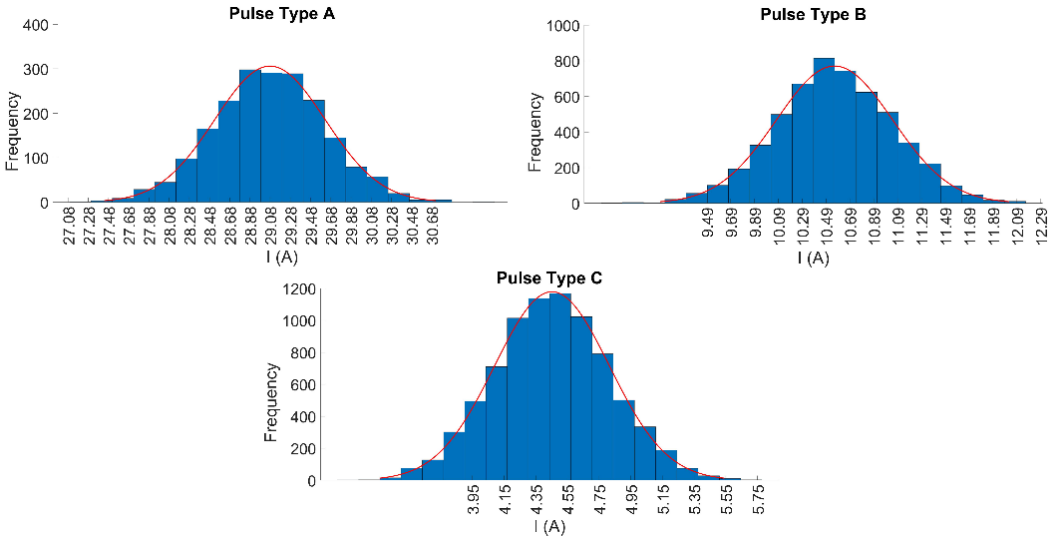

Figure 5.9. Frequency distribution histograms for pulses occurred during ZrB30 machining.

Table 5.7. Details of pulse type for ZrB50.

Material	Pulse Type	Peak Current [A]	Voltage [V]	Width [µs]	Energy per Discharge [µJ]
ZrB50	A	29.15	74	0.69	714.13
	B	10.82	91	0.33	147.64
	C	4.49	101	0.06	12.15

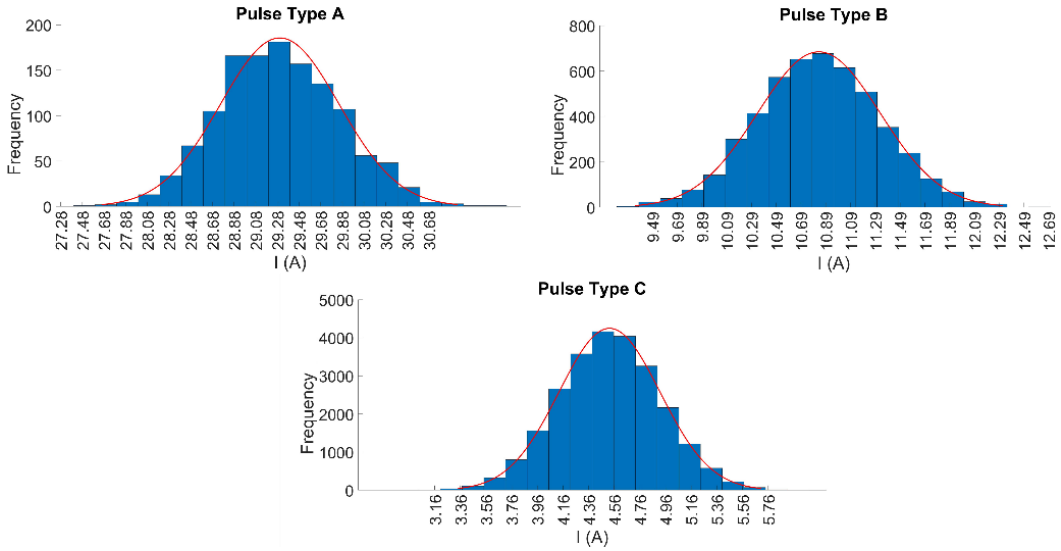

Figure 5.10. Frequency distribution histograms for pulses occurred during ZrB50 machining.

5.3.2 Methods

A 3D reconstruction of the micro-slots was performed by a confocal laser scanning microscope (Olympus LEXT) with a magnification of 20x. This system recognizes the peaks of the reflected light intensities of multiple layers and setting each layer as the focal point, allows to analyse multiple layers and to measure the thickness of each layer. After the data acquisition by the laser microscope, the images were analysed with a scanning probe image processor software. A plane correction was performed on all the images to level the surfaces and to remove primary profiles. In this way, it was possible to estimate the geometrical elements necessary for the following evaluation, such as micro-slots depth, volume and surface roughness (Sa).

The depth of the micro-slot was estimated based on the height distribution of the z(x;y) plot. On the histogram two normal distribution could be identified: one describes the machined surface, while the other one describes the top surface of the workpiece, not affected by the machining.

The volume of the micro-slots was evaluated in an automatic way by the software to reduce possible systematic errors related to the operator. The surface roughness (Sa) of the machined surfaces was evaluated by the software, based on

the international standard UNI EN ISO 25178:2017. Figure 5.11 shows an example of the surface texture of a machined surface portion.

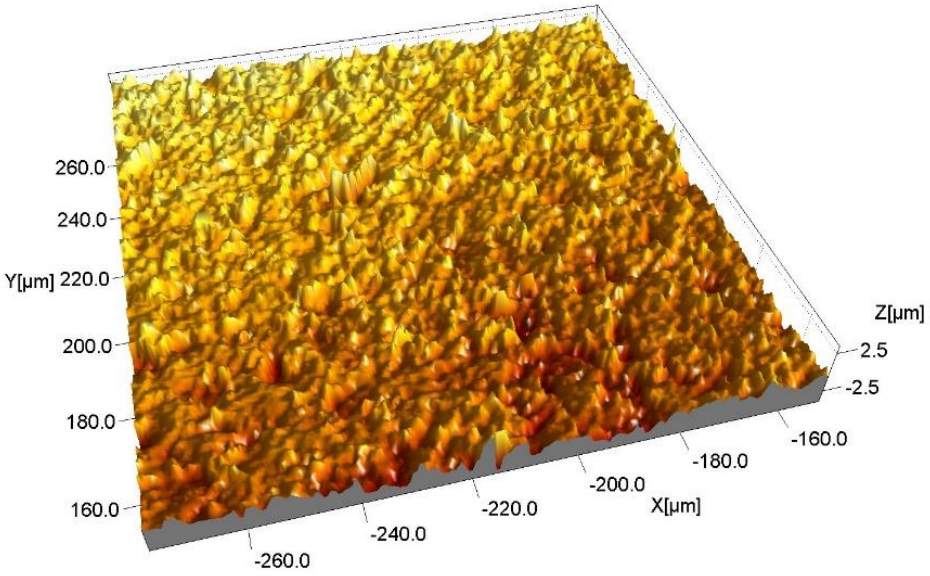

Figure 5.11. Example of the machined surface.

Tool Wear per Discharge (TWD), Material Removal per Discharge (MRD) and Tool Wear Ratio (TWR) were selected as performance criteria for the process evaluation. TWD (Eq. 5.1) was calculated as the ratio between the material removed from the electrode (MRT [mm^3] and the number of discharges (N) recorded. The length of tool wear is measured through a touching procedure executed in a reference position: the length of the electrode is measured before and after the single milling operation. The electrode wear volume is estimated starting from the length of the tool wear, considering the electrode as a cylindrical part.

$$TWD = \frac{MRT}{N} \qquad \text{Eq. 5.1}$$

MRD (Eq. 5.2) was calculated as the ratio between the material removed from the workpiece (MRW [mm^3]), estimated by the scanning probe image processor

software as the volume of micro-slots, and the number of discharges (N), recorded by the programmable counter.

$$MRD = \frac{MRW}{N} \qquad \text{Eq. 5.2}$$

TWR (Eq. 5.3) was calculated as the ratio between the previous performance indicators.

$$TWR = \frac{TWD}{MRD} = \frac{MRT}{MRW} \qquad \text{Eq. 5.3}$$

Finally, the machined surfaces were observed by Scanning Electron Microscope (SEM). These qualitative observations allowed to analyse the microscopic aspects and to identify the possible presence of imperfection related to the process.

5.4 Results and discussion

Figure 5.12 shows the tool wear per discharge (TWD) as a function of the additive fraction and the pulse type applied during the process. A magnification of the pulse type C is added to clarify its trend. The indicator is characterized by a great variability as a function of the additive fraction, in particular when the pulse duration increase. The best results in terms of tool wear and low variability were obtained for the pulse type C, which is the shorter pulse. The trends generated by the pulse type A and B are similar, while the pulse type C is characterized by a more stable value as a function of the additive fraction. The performance indicators show a high level of stability and repeatability for the pulse type C, both in terms of variability of results of the performed runs and for the different level of additive fraction selected.

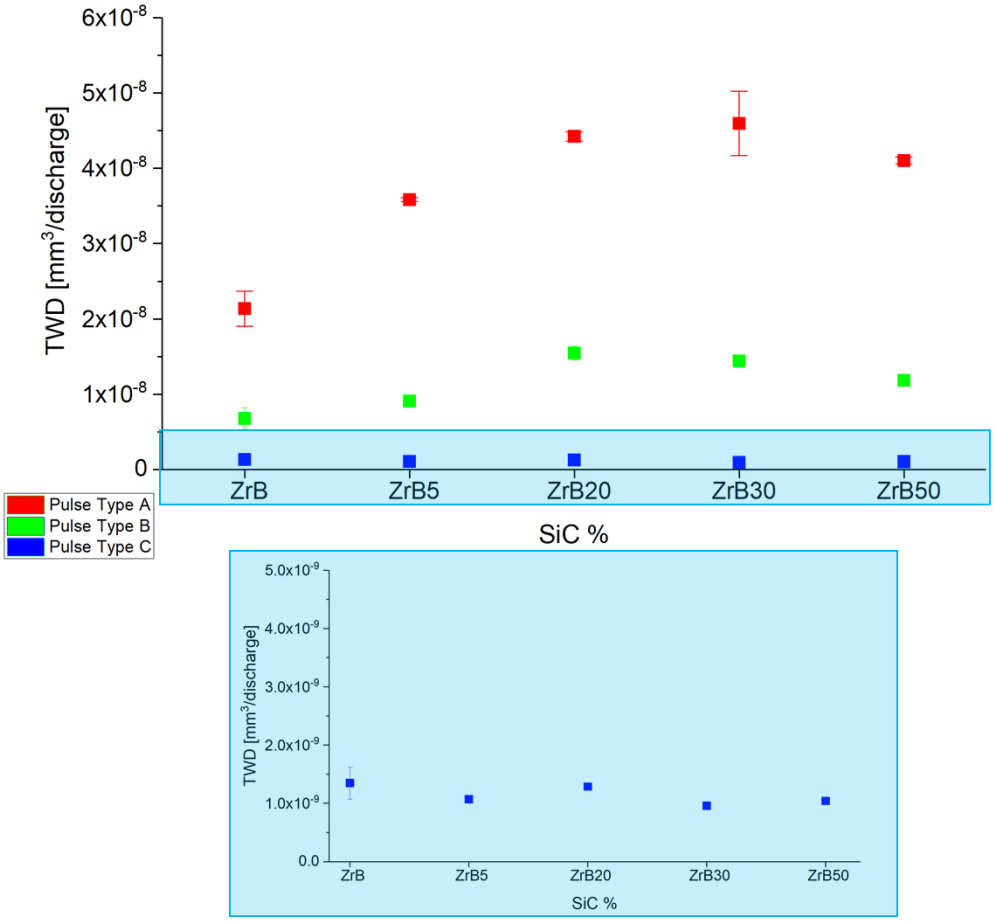

Figure 5.12. Average TWD as a function of the additive fraction and pulse type.

Figure 5.13 shows a significant difference in the machining speed as a function of the pulse type. Longer pulses generate faster machining. In particular, pulse type A is about six times faster than pulse type C. It is not possible to identify a direct effect of the additive fraction on the MRD trends. Considering the ratio between the TWD and MRD (Figure 5.14), the data are characterized by high variability as a function of both the additive fraction and the pulse type.

In general, it is possible to observe a maximum of the tool wear ratio in correspondence of an additive fraction equal to 20% vol. For ZrB20 the process is characterized by high electrode wear and low MRD compared to other samples taken into account. Nevertheless, to have a better comprehension of this aspect it is important to consider the volume removed from the workpiece (Figure 5.15).

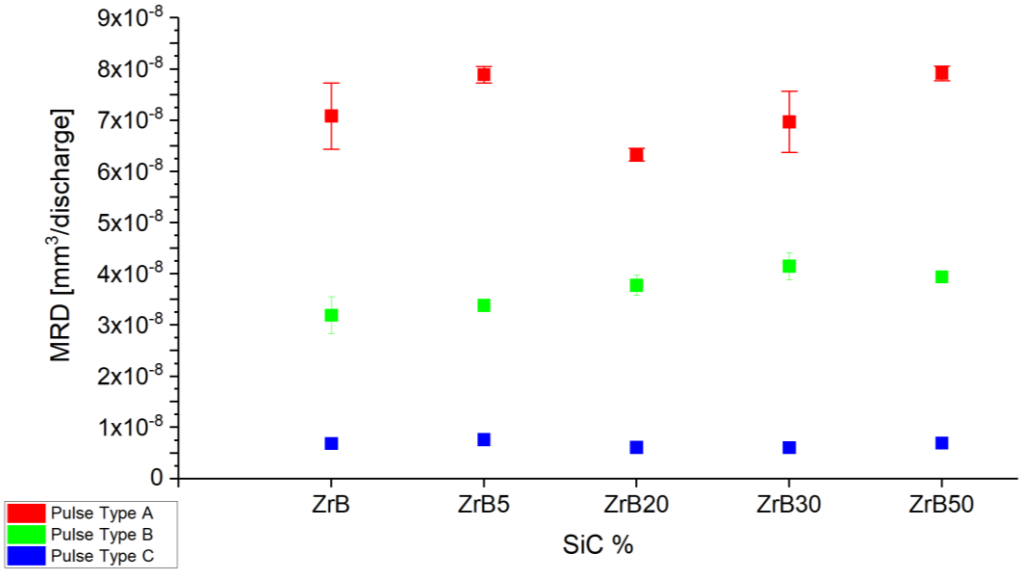

Figure 5.13. Average MRD as a function of the additive fraction and pulse type.

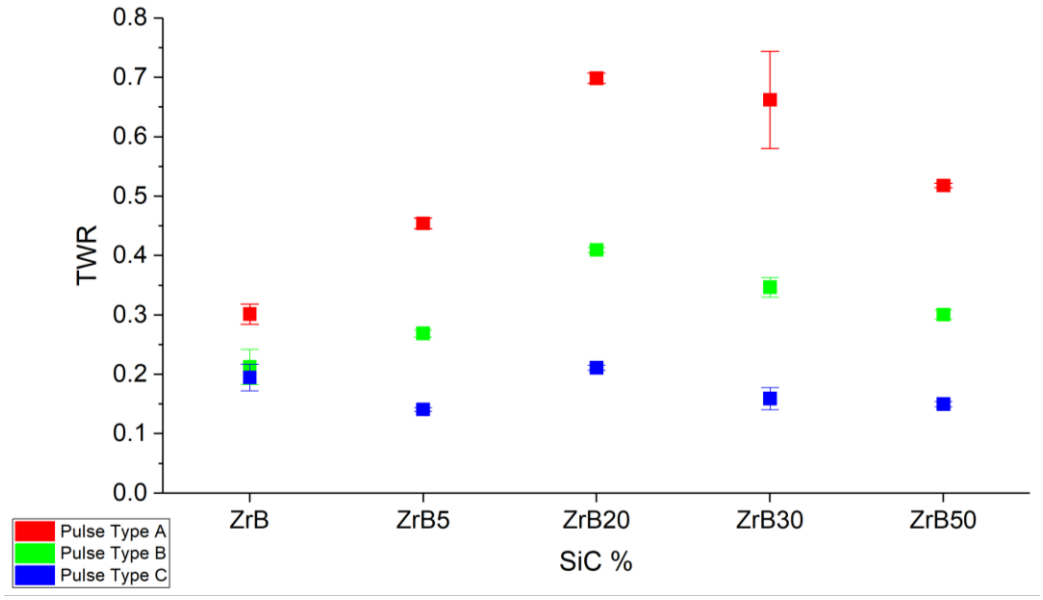

Figure 5.14. Average TWR as a function of the additive fraction and pulse type.

It is possible to observe that the process in many cases is not able to remove the entire amount of material needed to obtain the nominal micro-slot. In fact, the values of the removed material result to be closer to the nominal value and with a low variability for ZrB5 and ZrB20 only. This aspect underlines a possible relation between the relative density of the sample and the amount of removed material. A

higher value of relative density allows obtaining a more stable and repeatable process with a low deviation from the nominal value of the volume ($\sim 0.157\ mm^3$).

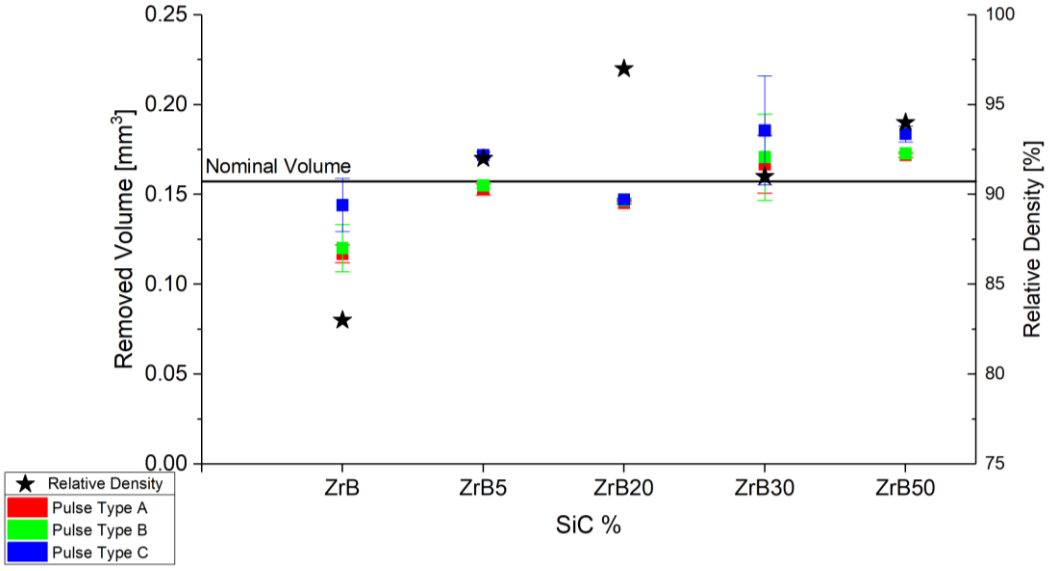

Figure 5.15. Average values and standard deviation of the volume of micro-slots machined.

The analysis of the surface roughness (Sa) identifies a strong correlation between the pulse type and the surface finishing. Longer pulses generate low-quality surfaces. As for the removed volume, also in this case, the results are influenced by the relative density; in fact, the high value of relative density generates surfaces with lower Sa for all the pulse types on all the samples.

Considering the surface roughness (Sa) and its standard deviation (Figure 5.16), the variability obtained for pulse type "A" is higher with respect to the other pulse types. In general, surface quality tends to improve, for all pulse types, when the relative density of the materials increases and then when the porosity level is lower. In effect, the machined surfaces characterized by better surface finishing are obtained on the ZrB20.

A particular aspect can be observed in the reconstruction of a limited area which includes the SiC fibres after ED-machining. As reported in Figure 5.17, the area corresponding to the fibre is characterized by higher values of z(x; y) with respect to the ZrB2 matrix. This suggests that the SiC fibres are not directly affected by the

typical EDM removal mechanism, probably because of their electrical insulation property.

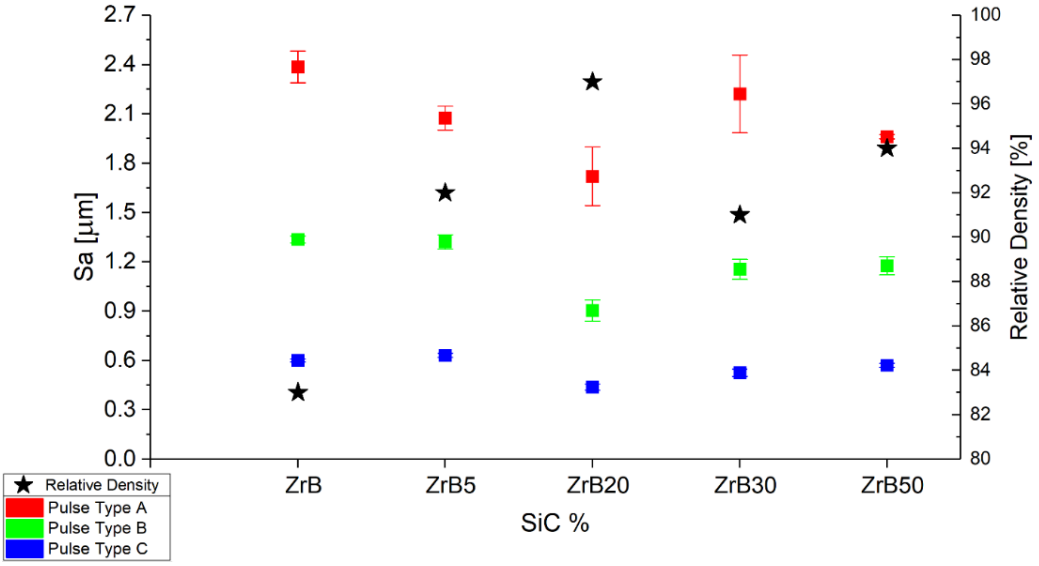

Figure 5.16. Average values and standard deviation of surface roughness (Sa).

The backscatter SEM images show the presence of some microcracks on the machined surfaces, especially when long pulses are used. Another aspect identified through these images is the layer of recasted material. This layer is not characterized by uniform aspect such as for the metal workpieces; in particular, some "pores", probably related to the formation of gas bubbles and their "explosion" during the removal process, can be observed. (Figure 5.18).

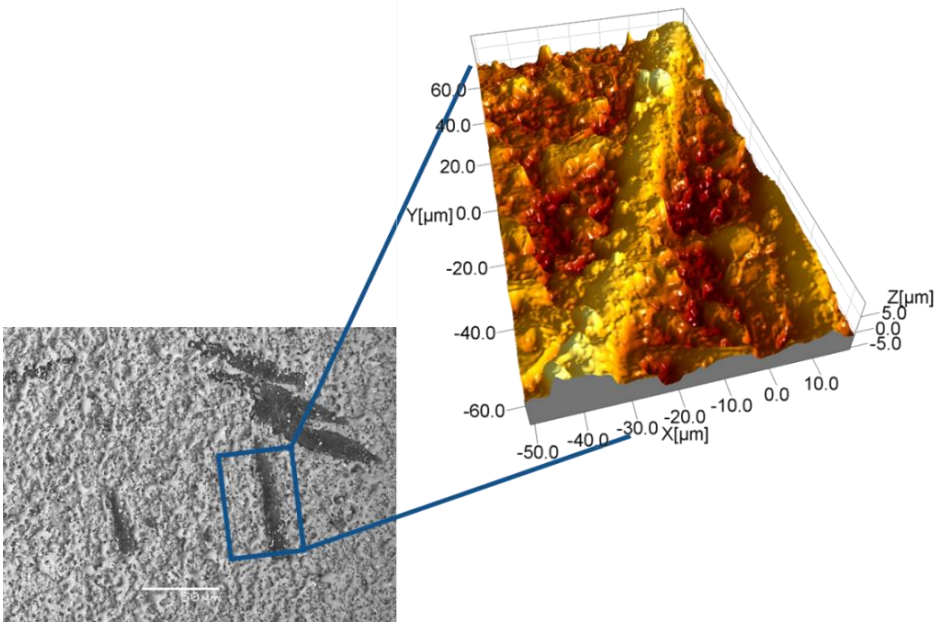

Figure 5.17. Details of SiC fibre (backscattering magnification 500x – 3D reconstruction magnification 100x).

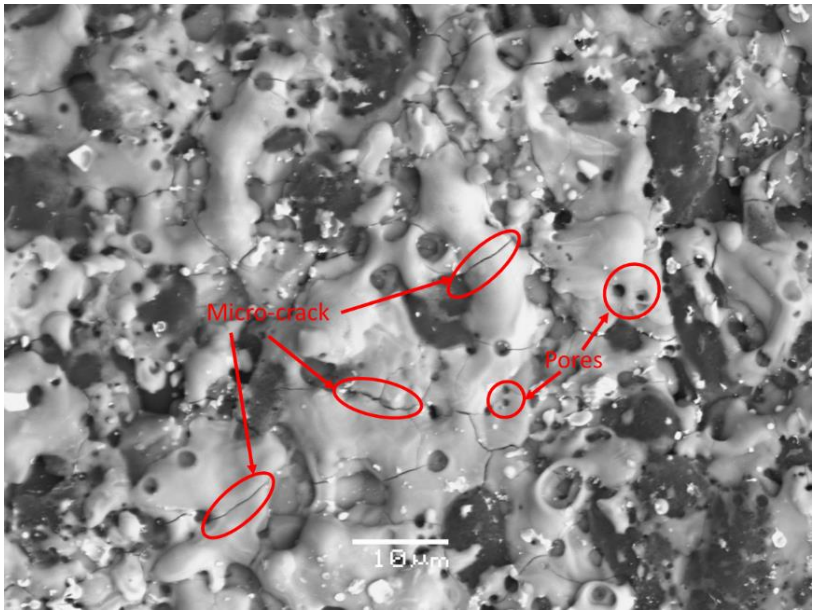

Figure 5.18. SEM backscatter image of the machined surface. An example of micro-cracks and "pores" generated during the process.

5.5 Evaluation Cost

Since the materials taken into account in this study are relatively new for the electrical discharge application, a cost evaluation through the application of the

model costs previously developed was performed. The cost evaluation model developed in CHAPTER 3 is specific for μEDM and its capability was investigated by the application to two drilling case studies. This aspect did not exclude the opportunity to apply it to other machining configuration.

As reported in the previous chapter, the cost estimation was performed taking into account the variable costs, which are the main representative for an economical evaluation of technology since this class of costs were strictly related to the productivity level. An important difference to be underlined is that for drilling configuration the combination electrode-workpiece is characterized by a range of main process parameters suitable for the success of the process. For this reason, the plots and the results presented a range in which the production costs can vary. In the milling configuration, the behaviour is a little bit different because the process parameters were optimized before the production through the definition of the depth of each layer and the compensation of the tool wear.

The cost evaluation was performed by applying the equation Eq. 3.1 -Eq. 3.4 to each pocket performed during the experimental campaign. The following hypothesis were assumed:

- Machining setup was equal to 2 h (CAD/CAM design, preparation of electrode and workpiece, process parameters setup);
- Operator's wage was equal to 25€/h;
- The operator monitored the machine only partially during the processing (e.g. 33%).

Figure 5.19 shows the total cost estimated for each pocket and the average value estimated considering the three repetitions performed for each combination of workpiece material and pulse type. The main aspect highlighted by this plot is the great increment of the costs for the machining performed by pulse type C. This increment in production cost related to the different pulse type can be correlated to the great differences in the machining duration; in fact, the labour cost is the most important component in the total cost evaluation representing in all cases the greater

part of the costs (Figure 5.20). In general, the differences in cost obtained are justified by the industries, since in this case, the higher machining time is related to the low energy transferred by a single discharge and this means higher surface finishing.

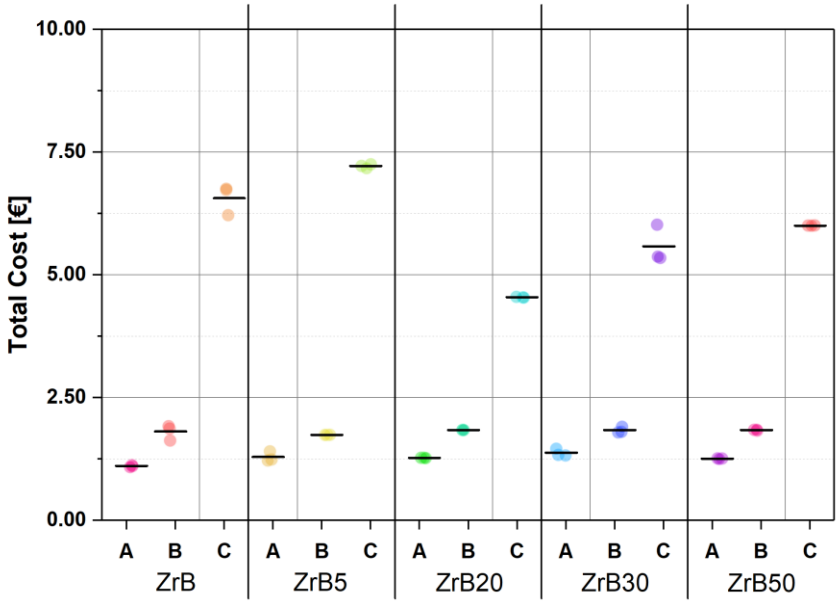

Figure 5.19. Total costs obtained for each pocket and average values.

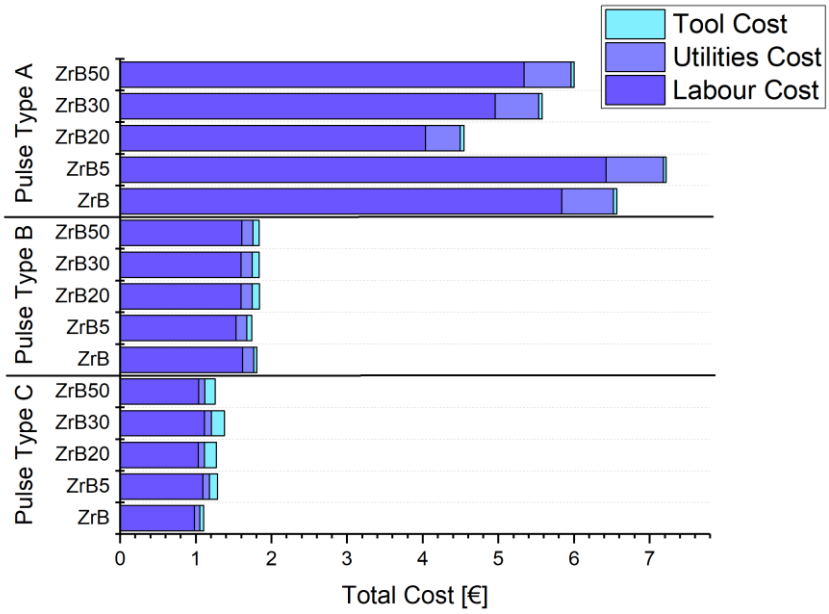

Figure 5.20. Total cost divided into its components.

5.5 Conclusions

An evaluation of the machinability of new advanced ceramic materials composed by ZrB_2 base matrix hot-pressed with different fractions of nonreactive additive (SiC) was performed in this work. The aim was to evaluate the stability and repeatability of the μEDM process to identify if the value of the additive fraction influences the process. The analysis was carried out on the performances, geometrical and surface finishing point of view.

A discharge characterization was performed to feature the different pulse type used during the machining.

In general, the discharge characterization and the performances indicators define a stable and repeatable process for all the samples; in particular, for short (C) and intermediate (B) pulses. Machining performed by pulse type "A" is characterized, in some cases, by a slight variability.

The evaluation of removed material and Sa complete the analysis showing a correlation between these indicators and the relative density of the materials themselves. In fact, the samples with high relative density generate better surface finishing and the dimensions of micro-slots, in terms of volume, resulted to be close to the nominal value.

The application of model cost shows great influence of the machining time, and in general, the costs are quite similar for all additive fractions. The only exception is represented by the ZrB20 machined by pulse type C which results to be (at the same machining condition) the cheapest.

Based on these results it is possible to asses that the addition of SiC may improve the mechanical properties, as demonstrated in the literature, and may affect the investigated aspects of the electrical discharge process. In particular, the present investigation shows that the specimens having a 20% vol. of additive resulted to be the best solution in terms of machinability by EDM process, not in terms of process performances indicators, but in terms of nominal/effective volume ratio and surface finishing.

CHAPTER 6

Conclusions

μEDM is an attractive solution for the micro-manufacturing and for the machining of advanced materials difficult to cut by conventional technologies. In order to improve its characteristics and increase the application of this kind of technology is very important to increase not only the process performance but also investigate the economic aspects and the process behaviour during the machining of new materials.

The economic evaluation of a process is very important for the industries, because it allows to allocate in the best way the resources, but it is equally important to optimize the process parameters to obtain the best performances in terms of process and product characteristics. The correlation of these aspects allows to optimized both aspects at the same time, without generating a loss in one of the two fields.

In the first part of this work, the economic aspects were taken into account to carry out a model and then a cost index, first to estimate the cost of the product machining and then to develop a method to correlate the economic and the technological aspects mainly involved in this process. The model cost, developed in Chapter 3, and the cost index developed in Chapter 4, are generic enough to be applied to every set of data collected during the experimentation.

In the second part of the work, the main issue is represented by the machinability of a ZrB_2-based composite doped with a different fraction of SiC. Their applications involve many disciplines, in particular, critical environment characterized by high oxidation rate and high temperature, for this reason, in the last years, the pursuit against this sort of material increase and the optimization and definition of processes suitable for their machining became one of the primary topics. The development of UHTCs materials is very important not only for the

critical environments but also for the such as a possible substitute of metal parts since ceramics materials are, in some cases, more sustainable than the traditional metal alloys. The investigation about the application of μEDM to these particular materials does not exclude the evaluation of costs.

Results propose a method for the evaluation of production costs in EDM as a function of the depth reached during the machining and then an algorithm for the optimization of cost and process performances as a function of the process parameters. These two models are applied to different experimental campaigns to verify their capability and are developed in a general way in order to be applied in almost every condition only with small modification of the equation. In this way, two methodologies for the evaluation and implementation of economic sustainability of μEDM were developed. Then the focus was moved toward the sustainability of the materials. Specifically, a stable and repeatable μEDM process of UHTCs sample demonstrates that it could be a proper choice for machining components of this technology. To find a suitable technology for difficult to cut materials is very important for the development of new advanced materials, in this way their application fields can increase reducing, in the long period, the use of metal components. Moreover, the evaluation of production costs shows that the milling process has a higher economic impact, not only because the single machining is longer, but it is important to remember that for the milling process of micro-components the design phase is necessary both to design the parts and to define the tool path.

This is only a starting point for a complete study about the application of μEDM process to UHTCs materials, but the results seem to be very attractive. Future steps are going to involve a wide range of materials and the deep comprehension about the material removal mechanism; in fact, as it was shown in chapter 5, since in some cases the additive is non-conductive, it is important to understand how these parts of the workpiece are removed from the surface. Several hypotheses have been formulated about this mechanism, but the actual phenomenon that occurs is still under investigation.

1. Masuzawa, T. State of the Art of Micromachining. *Ann. CIRP* **49,** 473–488 (2000).

2. Masuzawa, T. & Tönshoff, H. K. Three-Dimensional Micromachining by Machine Tools. *CIRP Ann. - Manuf. Technol.* **46,** 621–628 (1997).

3. NEXUS Microsystems | NEXUS – a European Network for Microsystems / MEMS related Activities. Available at: http://nexus-mems.com/. (Accessed: 20th August 2018)

4. Masuzawa, T. State of the Art of Micromachining. in *CIRP Annals - Manufacturing Technology* **49,** 473–488 (2000).

5. Corbett, J., McKeown, R. A., Peggs, G. N. & Whatmore, R. Nanotechnology: International developments and emerging products. *CIRP Ann. - Manuf. Technol.* **49,** 523–545 (2000).

6. Geiger, M., Kleiner, M., Eckstein, R., Tiesler, N. & Engel, U. Microforming. *CIRP Annals - Manufacturing Technology* **50,** 445–462 (2001).

7. Van Brussel, H. *et al.* Assembly of Microsystems. in *CIRP Annals - Manufacturing Technology* 499–514 (2001).

8. MacGeough, J. A., Leu, M. C., Rajurkar, K. P., De Silva, A. K. M. & Liu, Q. Electroforming process and application to micro/macro manufacturing. *CIRP Ann. - Manuf. Technol.* **50,** 499–514 (2001).

9. Kunieda, M., Lauwers, B., Rajurkar, K. P. & Schumacher, B. M. Advancing EDM through Fundamental Insight into the Process. *CIRP Ann. - Manuf. Technol.* **54,** 64–87 (2005).

10. Kadirvel, A., Hariharan, P. & Gowri, S. A review on various research trends in micro-EDM. *Int. J. Mechatronics Manuf. Syst.* **5,** 361 (2012).

11. Mohd Abbas, N., Solomon, D. G. & Fuad Bahari, M. A review on current research trends in electrical discharge machining (EDM). *Int. J. Mach. Tools Manuf.* **47,** 1214–1228 (2007).

12. Uhlmann, E., Piltz, S. & Doll, U. Machining of micro/miniature dies and moulds by electrical discharge machining - Recent development. *J. Mater. Process. Technol.* **167,** 488–493 (2005).

13. Rajurkar, K. P. *et al.* Micro and nano machining by electro-physical and chemical processes. *CIRP Ann. - Manuf. Technol.* **55,** 643–666 (2006).

14. Schumacher, B. M. After 60 years of EDM the discharge process remains still disputed. in *Journal of Materials Processing Technology* **149,** 376–381 (2004).

15. Raju, L. & Hiremath, S. S. A State-of-the-art Review on Micro Electro-discharge Machining. *Procedia Technol.* **25,** 1281–1288 (2016).

16. Rajurkar, K. P. & Pandit, S. M. Formation and Ejection of EDM Debris. *J. Eng. Ind.* **108,** 22 (1986).

17. Wang, J. & Han, F. Simulation model of debris and bubble movement in electrode jump of electrical discharge machining. *Int. J. Adv. Manuf. Technol.* **74,** 591–598 (2014).

18. Yanatori, K. & Kunieda, M. Study on Debris Movement in EDM Gap. *J. Japan Soc. Electr. Mach. Eng.* **29,** 19–27 (1995).

19. Kansal, H. K., Singh, S. & Kumar, P. Technology and research developments in powder mixed electric discharge machining (PMEDM). *J. Mater. Process. Technol.* **184,** 32–41 (2007).

20. Das, S., Klotz, M. & Klocke, F. EDM simulation: Finite element-based calculation of deformation, microstructure and residual stresses. *J. Mater. Process. Technol.* **142,** 434–451 (2003).

21. Kojima, A., Natsu, W. & Kunieda, M. Spectroscopic measurement of arc plasma diameter in EDM. *CIRP Ann. - Manuf. Technol.* **57,** 203–207 (2008).

22. Zahiruddin, M. & Kunieda, M. Comparison of energy and removal efficiencies between micro and macro EDM. *CIRP Ann. - Manuf. Technol.* **61,** 187–190 (2012).

23. Ho, K. H. & Newman, S. T. State of the art electrical discharge machining (EDM). *Int. J. Mach. Tools Manuf.* **43,** 1287–1300 (2003).

24. Heeren, P. H. s. *et al.* Microstructuring of silicon by electro-discharge machining (edm) -part ii: Applications. *Sensors Actuators, A Phys.* **61,** 379–386 (1997).

25. Ho, K. H., Newman, S. T., Rahimifard, S. & Allen, R. D. State of the art in wire electrical discharge machining (WEDM). *Int. J. Mach. Tools Manuf.* **44,** 1247–1259 (2004).

26. Maradia, U. *et al.* Die-sink EDM in meso-micro machining. in *Procedia CIRP* **1,** 166–171 (2012).

27. Yu, Z. Y., Rajurkar, K. P. & Shen, H. High aspect ratio and complex shaped blind micro holes by micro EDM. *CIRP Ann. - Manuf. Technol.* **51,** 359–362 (2002).

28. Yu, Z. Y., Masuzawa, T. & Fujino, M. Micro-EDM for Three-Dimensional Cavities - Development of Uniform Wear Method -. *CIRP Ann.* **47,** 169–172 (1998).

29. Kaneko, T. & Tsuchiya, M. Three-dimensional numerically controlled contouring by electric discharge machining with compensation for the

deformation of cylindrical tool electrodes. *Precis. Eng.* **10,** 157–163 (1988).

30. Pham, D. T., Dimov, S. S., Bigot, S., Ivanov, A. & Popov, K. Micro-EDM - Recent developments and research issues. *J. Mater. Process. Technol.* **149,** 50–57 (2004).

31. Rajurkar, K. P. & Yu, Z. Y. 3D micro-EDM using CAD/CAM. *CIRP Ann. - Manuf. Technol.* **49,** 127–130 (2000).

32. Masuzawa, T., Fujino, M., Kobayashi, K., Suzuki, T. & Kinoshita, N. Wire Electro-Discharge Grinding for Micro-Machining. *CIRP Ann. - Manuf. Technol.* **34,** 431–434 (1985).

33. Masuzawa, T., Kuo, C. L. & Fujino, M. A Combined Electrical Machining Process for Micronozzle Fabrication. *CIRP Ann. - Manuf. Technol.* **43,** 189–192 (1994).

34. Yeo, S. H. & Yap, G. G. A Feasibility Study on the Micro Electro-Discharge Machining Process for Photomask Fabrication. *Int J Adv Manuf Technol* **18,** 7–11 (2001).

35. Pandey, A. & Singh, S. Current research trends in variants of Electrical Discharge Machining : A review. *Int. J. Eng. Sci. Technol.* **2,** 2172–2191 (2010).

36. Mohan, B., Rajadurai, A. & Satyanarayana, K. G. Electric discharge machining of Al-SiC metal matrix composites using rotary tube electrode. *J. Mater. Process. Technol.* **153–154,** 978–985 (2004).

37. Son, S., Lim, H., Kumar, A. S. & Rahman, M. Influences of pulsed power condition on the machining properties in micro EDM. *J. Mater. Process. Technol.* **190,** 73–76 (2007).

38. Sundaram, M. M., Pavalarajan, G. B. & Rajurkar, K. P. A study on process parameters of ultrasonic assisted micro EDM based on Taguchi method. in

Journal of Materials Engineering and Performance **17,** 210–215 (2008).

39. Jahan, M. P., Wong, Y. S. & Rahman, M. A study on the fine-finish die-sinking micro-EDM of tungsten carbide using different electrode materials. *J. Mater. Process. Technol.* **209,** 3956–3967 (2009).

40. Jahan, M. P., Wong, Y. S. & Rahman, M. A comparative experimental investigation of deep-hole micro-EDM drilling capability for cemented carbide (WC-Co) against austenitic stainless steel (SUS 304). *Int. J. Adv. Manuf. Technol.* **46,** 1145–1160 (2010).

41. Yu, Z. Y., Rajurkar, K. P. & Tandon, A. Study of 3D Micro-Ultrasonic Machining. *J. Manuf. Sci. Eng.* **126,** 727 (2004).

42. Uhlmann, E. & Roehner, M. Investigations on reduction of tool electrode wear in micro-EDM using novel electrode materials. *CIRP J. Manuf. Sci. Technol.* **1,** 92–96 (2008).

43. Pham, D. T., Ivanov, A., Bigot, S., Popov, K. & Dimov, S. A study of micro-electro discharge machining electrode wear. *Proc. Inst. Mech. Eng. Part C J. Mech. Eng. Sci.* **221,** 605–612 (2007).

44. Bissacco, G., Hansen, H. N., Tristo, G. & Valentincic, J. Feasibility of wear compensation in micro EDM milling based on discharge counting and discharge population characterization. *CIRP Ann. - Manuf. Technol.* **60,** 231–234 (2011).

45. Surleraux, A., Pernot, J. P. & Bigot, S. A comparative study between NURBS surfaces and voxels to simulate the wear phenomenon in micro-EDM. *Computer-Aided Design and Applications* **13,** 1–7 (2016).

46. Tsai, Y. Y. & Masuzawa, T. An index to evaluate the wear resistance of the electrode in micro-EDM. *J. Mater. Process. Technol.* **149,** 304–309 (2004).

47. D'Urso, G. & Ravasio, C. Material-Technology Index to evaluate micro-

EDM drilling process. *J. Manuf. Process.* **26,** 13–21 (2017).

48. Aligiri, E., Yeo, S. H. & Tan, P. C. A new tool wear compensation method based on real-time estimation of material removal volume in micro-EDM. *J. Mater. Process. Technol.* **210,** 2292–2303 (2010).

49. Bleys, P., Kruth, J. P. & Lauwers, B. Sensing and compensation of tool wear in milling EDM. in *Journal of Materials Processing Technology* **149,** 139–146 (2004).

50. Puthumana, G., Bissacco, G. & Hansen, H. N. Modeling of the effect of tool wear per discharge estimation error on the depth of machined cavities in micro-EDM milling. *Int. J. Adv. Manuf. Technol.* **92,** 3253–3264 (2017).

51. *Uni en iso 4172:2004*. 9119–9119 (2004).

52. Bhushan, B. Surface Roughness Analysis and Measurement Techniques. in *Revista clínica española* **5,** 49–119 (2000).

53. Kurnia, W., Tan, P. C., Yeo, S. H. & Tan, Q. P. Surface roughness model for micro electrical discharge machining. *Proc. Inst. Mech. Eng. Part B J. Eng. Manuf.* **223,** 279–287 (2009).

54. Krishna Kiran, M. P. S. & Joshi, S. S. Modeling of Surface Roughness and the Role of Debris in Micro-EDM. *J. Manuf. Sci. Eng.* **129,** 265 (2007).

55. Jahan, M. P., Rahman, M. & Wong, Y. S. A review on the conventional and micro-electrodischarge machining of tungsten carbide. *Int. J. Mach. Tools Manuf.* **51,** 837–858 (2011).

56. D'Urso, G., Giardini, C. & Quarto, M. Characterization of surfaces obtained by micro-EDM milling on steel and ceramic components. *Int. J. Adv. Manuf. Technol.* **97,** 2077–2085 (2018).

57. Salonitis, K., Stournaras, A., Stavropoulos, P. & Chryssolouris, G. Thermal

modeling of the material removal rate and surface roughness for die-sinking EDM. *Int. J. Adv. Manuf. Technol.* **40,** 316–323 (2009).

58. Patel, K. M., Pandey, P. M. & Venkateswara Rao, P. Determination of an optimum parametric combination using a surface roughness prediction model for EDM of Al2O3/SiCw/TiC ceramic composite. *Mater. Manuf. Process.* **24,** 675–682 (2009).

59. Niazi, A., Dai, J. S., Balabani, S. & Seneviratne, L. Product Cost Estimation: Technique Classification and Methodology Review. *J. Manuf. Sci. Eng.* **128,** 563 (2006).

60. Shehab, E. & Abdalla, H. An intelligent knowledge-based system for product cost modelling. *Int. J. Adv. Manuf. Technol.* **19,** 49–65 (2002).

61. Shehab, E. M. & Abdalla, H. S. Manufacturing cost modelling for concurrent product development. *Robot. Comput. Integr. Manuf.* **17,** 341–353 (2001).

62. Shehab, E. M. & Abdalla, H. S. A design to cost system for innovative product development. *Proc. Inst. Mech. Eng. Part B J. Eng. Manuf.* **216,** 999–1019 (2002).

63. Zhang, Y. F., Fuh, J. Y. H. & Chan, W. T. Feature-based cost estimation for packaging products using neural networks. *Comput. Ind.* **32,** 95–113 (1996).

64. Ben-Arieh, D. & Qian, L. Activity-based cost management for design and development stage. *Int. J. Prod. Econ.* **83,** 169–183 (2003).

65. Luong, L. H. S. & Spedding, T. An integrated system for process planning and cost estimation in hole making. *Int. J. Adv. Manuf. Technol.* **10,** 411–415 (1995).

66. Rehman, S. & Guenov, M. D. A methodology for modelling manufacturing costs at conceptual design. *Comput. Ind. Eng.* **35,** 623–626 (1998).

67. Marafona, J. & Wykes, C. New method of optimising material removal rate using EDM with copper-tungsten electrodes. *Int. J. Mach. Tools Manuf.* **40,** 153–164 (2000).

68. Lin, J. L., Wang, K. S., Yan, B. H. & Tarng, Y. S. Optimization of the electrical discharge machining process based on the Taguchi method with fuzzy logics. *J. Mater. Process. Technol.* **102,** 48–55 (2000).

69. Simon, D. Biogeography-based optimization. *IEEE Trans. Evol. Comput.* **12,** 702–713 (2008).

70. Somashekhar, K. P., Ramachandran, N. & Mathew, J. Optimization of material removal rate in micro-EDM using artificial neural network and genetic algorithms. *Mater. Manuf. Process.* **25,** 467–475 (2010).

71. Panda, D. K. Modelling and optimization of multiple process attributes of electrodischarge machining process by using a new hybrid approach of neuro-grey modeling. *Mater. Manuf. Process.* **25,** 450–461 (2010).

72. Assarzadeh, S. & Ghoreishi, M. Neural-network-based modeling and optimization of the electro-discharge machining process. *Int. J. Adv. Manuf. Technol.* **39,** 488–500 (2008).

73. Chiang, K.-T. Modeling and analysis of the effects of machining parameters on the performance characteristics in the EDM process of Al2O3+TiC mixed ceramic. *Int. J. Adv. Manuf. Technol.* **37,** 523–533 (2008).

74. Çaydaş, U. & Hasçalik, A. Modeling and analysis of electrode wear and white layer thickness in die-sinking EDM process through response surface methodology. *Int. J. Adv. Manuf. Technol.* **38,** 1148–1156 (2008).

75. Mukherjee, R. & Chakraborty, S. Selection of EDM process parameters using biogeography-based optimization algorithm. *Mater. Manuf. Process.* **27,** 954–962 (2012).

76. D'Urso, G., Quarto, M. & Ravasio, C. A model to predict manufacturing cost for micro-EDM drilling. *Int. J. Adv. Manuf. Technol.* **91,** 2843–2853 (2017).

77. Yeo, S. H., Ngoi, B. K. A., Poh, L. S. & Hang, C. Cost-tolerance relationships for non-traditional machining processes. *Int. J. Adv. Manuf. Technol.* **13,** 35–41 (1997).

78. Scatteia, L., Onteverde, F. M., Lfano, D. A. & Antoni, S. C. Advances in Ultra High Temperature Ceramics For Hot Structures. *Trans. JSASS Sp. Tech.* **7,** 73–78 (2009).

79. Upadhya, K., Yang, J.-M. & Hoffman, W. P. Materials for ultrahigh temperature structural applications. *Am. Ceram. Soc. Bull.* **76,** 51–56 (1997).

80. Levine, S. R. *et al.* Evaluation of ultra-high temperature ceramics for aeropropulsion use. *J. Eur. Ceram. Soc.* **22,** 2757–2767 (2002).

81. Wuchina, E. *et al.* Designing for ultrahigh-temperature applications: The mechanical and thermal properties of HfB2, HfCx, HfNxand αHf(N). *J. Mater. Sci.* **39,** 5939–5949 (2004).

82. Silvestroni, L., Kleebe, H. J., Fahrenholtz, W. G. & Watts, J. Super-strong materials for temperatures exceeding 2000 °c. *Sci. Rep.* **7,** (2017).

83. Saccone, G., Gardi, R., Alfano, D., Ferrigno, A. & Del Vecchio, A. Laboratory, on-ground and in-flight investigation of ultra high temperature ceramic composite materials. *Aerosp. Sci. Technol.* **58,** 490–497 (2016).

84. Pierrat, B., Balat-Pichelin, M., Silvestroni, L. & Sciti, D. High temperature oxidation of ZrC-20%MoSi2in air for future solar receivers. *Sol. Energy Mater. Sol. Cells* **95,** 2228–2237 (2011).

85. Justin, J. F. & Jankowiak, A. Ultra High Temperature Ceramics: Densification, Properties and Thermal Stability. *AerospaceLab J.* **3,** AL3-08 (2011).

86. Opeka, M. M., Talmy, I. G. & Zaykoski, J. A. Oxidation-based materials selection for 2000°C + hypersonic aerosurfaces: Theoretical considerations and historical experience. *J. Mater. Sci.* **39,** 5887–5904 (2004).

87. Opeka, M. M., Talmy, I. G., Wuchina, E. J., Zaykoski, J. A. & Causey, S. J. *Mechanical, Thermal, and Oxidation Properties of Refractory Hafnium and zirconium Compounds*. *Journal of the European Ceramic Society* **19,** (1999).

88. Monteverde, F., Guicciardi, S. & Bellosi, A. *Advances in microstructure and mechanical properties of zirconium diboride based ceramics*. *Materials Science & Engineering A* **346,** (2003).

89. Tripp, W. C. & Graham, H. C. Thermogravimetric study of the oxidation of ZrB2 in the temperature range of 800C to 1500C. *J. Electrochem. Soc. J. Electrochem. Soc.* **118 No.7,** 1195–1199 (1971).

90. Fahrenholtz, W. G., Hilmas, G. E., Talmy, I. G. & Zaykoski, J. A. Refractory diborides of zirconium and hafnium. *J. Am. Ceram. Soc.* **90,** 1347–1364 (2007).

91. Bellosi, A. & Monteverde, F. Ultra-High Temperature ceramics: Microstructures control and properties improvement related to materials design and processing procedures. *Eur. Sp. Agency* 8 (2006).

92. Silvestroni, L., Landi, E., Bejtka, K., Chiodoni, A. & Sciti, D. Oxidation behavior and kinetics of ZrB2containing SiC chopped fibers. *J. Eur. Ceram. Soc.* **35,** 4377–4387 (2015).

93. Silvestroni, L., Failla, S., Neshpor, I. & Grigoriev, O. Method to improve the oxidation resistance of ZrB2-based ceramics for reusable space systems. *J. Eur. Ceram. Soc.* **38,** 2467–2476 (2018).

94. Chamberlain, A. L., Fahrenholtz, W. G., Hilmas, G. E. & Ellerby, D. T. High-strength zirconium diboride-based ceramics. *J. Am. Ceram. Soc.* **87,**

1170–1172 (2004).

95. Hwang, S. S., Vasiliev, A. L. & Padture, N. P. Improved processing and oxidation-resistance of ZrB2ultra-high temperature ceramics containing SiC nanodispersoids. *Mater. Sci. Eng. A* **464,** 216–224 (2007).

96. Rezaie, A., Fahrenholtz, W. G. & Hilmas, G. E. The effect of a graphite addition on oxidation of ZrB2-SiC in air at 1500°C. *J. Eur. Ceram. Soc.* **33,** 413–421 (2013).

97. Zhang, X. *et al.* Densification and ablation behavior of ZrB2ceramic with SiC and/or Fe additives fabricated at 1600 and 1800 °C. *Ceram. Int.* **42,** 17074–17080 (2016).

98. Zhang, L. & Kurokawa, K. Effect of SiC Addition on Oxidation Behavior of ZrB2at 1273 K and 1473 K. *Oxid. Met.* **85,** 311–320 (2016).

99. Gadow, R., Landfried, R. & Kern, F. Proceedings of the III Advanced Ceramics and Applications Conference. in *Proceedings of the III Advanced Ceramics and Applications Conference* 25–32 (2016). doi:10.2991/978-94-6239-157-4

100. Lauwers, B. *et al.* Investigation of material removal mechanisms in EDM of composite ceramic materials. *J. Mater. Process. Technol.* **149,** 347–352 (2004).

101. D'Urso, G., Maccarini, G. & Merla, C. The Downsizing Effects in EDM Drilling of Micro Holes. *Key Eng. Mater.* **549,** 503–510 (2013).

102. GELINAS, T. O. M. Cost of ownership. *Fleet Equip.* **39,** 38–42 (2013).

103. D???Urso, G., Maccarini, G., Quarto, M. & Ravasio, C. Investigation on power discharge in micro-EDM stainless steel drilling using different electrodes. *J. Mech. Sci. Technol.* **29,** 4341–4349 (2015).

104. D'Urso, G., Maccarini, G. & Ravasio, C. Influence of electrode material in micro-EDM drilling of stainless steel and tungsten carbide. *Int. J. Adv. Manuf. Technol.* **85,** 2013–2025 (2016).

105. Raji, A. O. & Ahemen, S. A. Engineering properties of Tacca involucrata tubers. in *Journal of Food Process Engineering* **34,** 267–280 (2011).

106. Ferraris, E. *et al.* Shaping of engineering ceramics by electro, chemical and physical processes. *CIRP Ann. - Manuf. Technol.* **65,** 761–784 (2016).

107. Silvestroni, L., Sciti, D., Melandri, C. & Guicciardi, S. Toughened ZrB2-based ceramics through SiC whisker or SiC chopped fiber additions. *J. Eur. Ceram. Soc.* **30,** 2155–2164 (2010).

108. Sciti, D., Guicciardi, S. & Silvestroni, L. SiC chopped fibers reinforced ZrB2: Effect of the sintering aid. *Scr. Mater.* **64,** 769–772 (2011).

109. Monteverde, F. & Silvestroni, L. Combined effects of WC and SiC on densification and thermo-mechanical stability of ZrB2ceramics. *Mater. Des.* **109,** 396–407 (2016).